U. S. Department of Commerce
National Oceanic and Atmospheric Administration
National Weather Service
National Centers for Environmental Prediction
5200 Auth Road Room 207
Camp Springs, MD 20746

Technical Note

Optimum Discrete Interaction Approximations for wind waves. Part 2: Convergence of model integration.[†]

Hendrik L. Tolman [‡]
SAIC-GSO at
Environmental Modeling Center
Marine Modeling and Analysis Branch

June 2005

[†] MMAB Contribution No. 247.

[‡] e-mail: Hendrik.Tolman@NOAA.gov

This page is intentionally left blank.

Abstract

This study represents a second part of a study into the potential of the Discrete Interaction Approximation (DIA) for nonlinear interactions in wind waves. After a brief review of the results of the first part of his study, reasons for instability in the model integration of some DIAs are assessed, and a phenomenological explanation is given. Effects of sampling of spectral space are analyzed, and finally, a variety of DIAs is optimized in the context of full model integration tests. Based on this 'holistic' optimization, it is shown that a multiple DIA with a more complex definition of the quadruplet can indeed lead to much more accurate model integrations, when compared to the results obtained with an 'exact' interaction algorithm. Finally, suggested work for part three of this study is discussed.

Acknowledgments. The author thanks Henrique Alves and Gerbrant van Vledder for comments on early drafts of this manuscript. The present study was supported by funding from the Office of Naval Research (ONR) through grant N00014-00-F-0332.

This report is available as a pdf file from

http://polar.ncep.noaa.gov/waves

Contents

This page is intentionally left blank.

This page is intentionally left blank.

1 Introduction

This study represents the second part of a study into the potential of the Discrete Interaction Approximation (DIA) for the exact nonlinear interactions in a spectral wind wave model. For a justification of this study and the for underlaying theory, reference is made to Tolman (2003, henceforth denoted as Part 1) and to Tolman (2004). Only a short review of the actual DIA will be presented here in section 2.2.

In Part 1 a review is given of previously suggested versions of the DIA. Furthermore, some new modifications have been suggested. A set of tests was then performed to determine the critical aspects of the DIA required to give an accurate representation of the exact interactions. It was found that it is essential to extend the flexibility of the original quadruplet layout, and that optimal results are found with approximately four representative quadruplets. This method as identified as the Multiple DIA (MDIA). An alternative method where free parameters in the DIA are allowed to vary with the spectral frequency f was also found to show promising results. The latter approach is less accurate, but more economical. This approach is called the Variable DIA (VDIA).

The study in Part 1 focuses mostly on the representation of the nonlinear interaction source term S_{nl} for a given spectrum F. It is, however, well known that this source term is very sensitive to details of the spectral shape. Furthermore, due to the strong nonlinearity, a good representation of an instantaneous source term is no guarantee that a model based on such a source term results in model integrations that converge with the corresponding results obtained with the exact interaction. One good example of this is that the original DIA (Hasselmann et al., 1985) represents the instantaneous interactions poorly, yet results in unexpectedly good model results with respect to growth behavior in homogeneous conditions. Conversely the VDIA shows much better representation of instantaneous interactions S_{nl} than the DIA, yet (surprisingly) results in unstable model integration behavior (see Part 1 and the present section 3).

The purpose of the present study is to analyze why the VDIA does not result in convergent model integration, and, more generally, to assess the convergence of model integration for different approaches. The layout of this report is as follows. In section 2, a brief review of relevant aspect of wave models is given, with an emphasis on the nonlinear interactions and the DIA. Because a detailed review of the interactions is given in Part 1, only relevant details are presented here. Because the present study represents a feasibility study, it is sufficient to address deep water conditions only (as in Part 1). Generalization for application in arbitrary wave model conditions will be the subject of the third part of this study.

Section 3 takes off where Part 1 ended; problems with the integration convergence of particularly the VDIA are illustrated and a phenomenological explanation is given for this behavior. Based on these observations, a strategy is

developed for further research. In section 4, the impact of quadruplet layout and sampling of spectral space is considered. It appears that some quadruplet layouts are more likely to result in stable model integration. Such quadruplets are constructed in Section 5. In Sections 6 and 7 an attempt is made to optimize several types of DIAs, using time and fetch limited wave growth calculations based on the exact interactions as a benchmark. The main difference with previous studies is that the optimization is performed on results of model integration, and is thus not limited to individual interactions for individual spectra. Finally, a discussion and conclusions are presented in Section 8.

2 Modeling wind waves

2.1 Wave model equations

The present study focuses on the feasibility of several DIAs to represent wave growth when implemented in numerical wave models. Being a feasibility study, it is sufficient to consider idealized conditions of deep water without currents. In such conditions, the evolution of the spectrum $F(f,\theta)$ as a function of the spectral frequency f and direction θ can be written as (e.g., Hasselmann, 1960)

$$\frac{\partial F(f,\theta)}{\partial t} + \boldsymbol{c}_g \cdot \nabla F(f,\theta) = S_{in}(f,\theta) + S_{nl}(f,\theta) + S_{ds}(f,\theta) \quad , \tag{2.1}$$

where the right side of the equation represents the sources and sinks, consisting of wind input (S_{in}), nonlinear interactions (S_{nl}) and dissipation (S_{ds}) source terms. In the present study, this equation will be solved using an experimental version of the WAVEWATCH III model (Tolman, 2002b). For the present study, this model version is identical to the latest release (version 2.22), with the exception of the necessary modifications to include alternative parameterizations for the nonlinear interactions S_{nl}. The main attention is focused on the nonlinear interactions, which will be discussed in section 2.2. For input and dissipation the standard options of this model are used (Tolman and Chalikov, 1996). Because these are not the subject of interest in the present study, the equations are not reproduced here. Relevant numerical aspects of this model will be discussed briefly in section 2.3.

2.2 Nonlinear interactions

For a given wave spectrum $F(f,\theta)$, contributions to the nonlinear interaction source term S_{nl} occur only for sets of four wave components (quadruplets) with frequencies $\sigma_1 = 2\pi f_1$ through σ_4 and corresponding wave number vectors $\boldsymbol{k}_1$ through $\boldsymbol{k}_4$ which satisfy the resonance conditions

$$\boldsymbol{k}_1 + \boldsymbol{k}_2 = \boldsymbol{k}_3 + \boldsymbol{k}_4 \quad , \tag{2.2}$$

$$\sigma_1 + \sigma_2 = \sigma_3 + \sigma_4 \quad . \tag{2.3}$$

The calculation of the source term formally requires the evaluation of a six-dimensional Boltzmann integral, as discussed in Part 1. In the present study the Webb-Resio-Tracy (WRT) method is used as the benchmark representing the exact nonlinear interactions (Webb, 1978; Tracy and Resio, 1982; Resio and Perrie, 1991). Calculations are performed with the portable package developed by Van Vledder (2002b)[1].

[1] Model version 5.04 used here.

Table 2.1: Quadruplet definitions according to Eqs. (2.2) through (2.4) as used in this study. $\boldsymbol{k}_d$ represents the discrete spectral wavenumber used to sample spectral space. σ as in Eq. (2.4). If $\Delta\theta$ is not given, it is uniquely defined by $\boldsymbol{k}_d$ and a_1 through a_4, but varies with them. DIA according to Hasselmann et al. (1985). VVDIA according to Van Vledder (2001). The modified definitions (mod) are used in Sections 4 and 5, respectively.

	$\boldsymbol{k}_d$	σ	$\Delta\theta$	a_1	a_2	a_3	a_4
DIA	$\boldsymbol{k}_1$	σ_1	0	1	1	$1+\lambda$	$1-\lambda$
Part 1	$\frac{1}{2}(\boldsymbol{k}_1+\boldsymbol{k}_2)$	$\frac{1}{2}(\sigma_1+\sigma_2)$		$1+\mu$	$1-\mu$	$1+\lambda$	$1-\lambda$
(mod)	$\boldsymbol{k}_n$	σ_n		$1+\mu$	$1-\mu$	$1+\lambda$	$1-\lambda$
VVDIA	$\boldsymbol{k}_1$	σ_1	$\Delta\theta$	1	$1+\mu'$	$1+\lambda'$	$1-\lambda'+\mu'$
(mod)	Eq. (5.3)	σ_d	$\Delta\theta$	$1+\mu$	$1-\mu$	$1+\lambda$	$1-\lambda$

In a DIA only a small number of representative quadruplets is considered for each discrete wavenumber $\boldsymbol{k}_d$ in spectral space. Each representative quadruplet is defined by the above resonance conditions and by

$$\left.\begin{array}{rcl} \sigma_1 &=& a_1\sigma \\ \sigma_2 &=& a_2\sigma \\ \sigma_3 &=& a_3\sigma \\ \sigma_4 &=& a_4\sigma \\ \theta_2 &=& \theta_1 \pm \Delta\theta \end{array}\right\} \quad , \tag{2.4}$$

where $a_1 + a_2 = a_3 + a_4$ to satisfy Eq. (2.3) and where the necessity to explicitly define $\Delta\theta$ depends on the actual definition of σ and a_1 through a_4, and on the relation between $\boldsymbol{k}_1$ through $\boldsymbol{k}_4$ and $\boldsymbol{k}_d$. The latter relation also defines the actual sampling of the spectral space by the representative quadruplet. A selection of practical quadruplets is presented in Table 2.1.

For each representative quadruplet, the contributions $\delta S_{nl,i}$ to the source term are calculated as

$$\begin{pmatrix} \delta S_{nl,1} \\ \delta S_{nl,2} \\ \delta S_{nl,3} \\ \delta S_{nl,4} \end{pmatrix} = \frac{1}{2} \begin{pmatrix} -1 \\ -1 \\ 1 \\ 1 \end{pmatrix} C\, g^{-4} f_d^{11} \times \left[\frac{F_1 F_2}{(a_1 a_2)^4} \left(\frac{F_3}{a_3^4} + \frac{F_4}{a_4^4} \right) - \frac{F_3 F_4}{(a_3 a_4)^4} \left(\frac{F_1}{a_1^4} + \frac{F_2}{a_2^4} \right) \right] , \tag{2.5}$$

where C is a proportionality constant, f_d is the frequency corresponding to $\boldsymbol{k}_d$, and $F_i = F(f_i, \theta_i)$, with i identifying the four components of the quadruplet. The

full source term contribution for each representative quadruplet is obtained by summation the contributions $\delta S_{nl,i}$ for all discrete spectral grid points (that is, all $\boldsymbol{k}_d$), as well as for components at higher frequencies with contributions inside the discrete spectral space. Note that this expression for contributions in the DIA implies deep water and an exponential frequency grid as described in the following section. Note, furthermore, that the factor 1/2 is introduced because the quadruplet definition (2.4) has four solutions, whereas the original quadruplet definition has only two solutions (see Part 1).

Because the four components of the quadruplet $\boldsymbol{k}_i$ generally do not coincide with the discrete spectral grid, F_i is estimated by bi-linear interpolation

$$F_i = \sum_{j=1}^{4} w_{i,j} F_{i,j} \quad , \tag{2.6}$$

where j is a counter for the four surrounding spectral grid points, $w_{i,j}$ are the corresponding bi-linear interpolation coefficients, and $F_{i,j}$ are corresponding discrete spectral energies. Similarly, source term contributions $\delta S_{nl,i}$ do not coincide with the discrete grid, and are distributed consistently with (2.6)

$$\delta S_{nl,i,j} = w_{i,j}\, \delta S_{nl,i} \quad , \tag{2.7}$$

where $S_{nl,i,j}$ are quadruplet contributions at actual discrete spectral grid points.

A multiple DIA is constructed by considering N separate quadruplet configurations. Defining $S_n(f,\theta)$ as the DIA according to quadruplet configuration $n \in [1,N]$, the multiple DIA (MDIA) becomes

$$S_{nl}(f,\theta) = \frac{1}{N} \sum_{n=1}^{N} S_n(f,\theta) \quad . \tag{2.8}$$

where N is the number of representative quadruplets. Note that each representative quadruplet has a unique value of the constant C in Eq. (2.5).

An alternative method suggested in Part 1 is the Variable DIA or VDIA, defined with $N = 1$, and with a quadruplet configuration that varies with f_d.

2.3 Numerical implementation

The wave model solves propagation and source terms in separate fractional steps. Propagation is calculated using either a simple first order scheme of the third order ULTIMATE QUICKEST scheme of Leonard (1979, 1991). Details of these schemes will not be discussed here. Source term integration is performed using a semi-implicit scheme where the discrete change of the spectrum $\Delta F(f,\theta)$ is calculated as

$$\Delta F(f,\theta) = \frac{S_{\rm tot}(f,\theta)\Delta t}{1-\alpha D(f,\theta)\Delta t} \quad , \tag{2.9}$$

where Δt is the time step, D is the diagonal term, defined as the diagonal contributions of $\partial S_{\rm tot}/\partial F$, and where α is a constant. This scheme was introduced in the WAM model (WAMDIG, 1988) with $\alpha = 0.5$. Recent refinements include the dynamic adjustment of the time step (Tolman, 1992) and the introduction of an off-center scheme with $\alpha = 1$ (Hargreaves and Annan, 1998, 2001). Both modifications are incorporated in WAVEWATCH III.

The wave model can use either spherical grids or Cartesian grids in physical space. The last option has been used here for fetch limited calculations. The spectral grid is regularly distributed over the entire 360° of directional space. The frequency grid is logarithmically spaced with

$$f_{m+1} = X_f f_m \quad , \tag{2.10}$$

where X_f is a constant.

The contributions of the DIA to diagonal term D in Equation (2.5) are governed by the partial derivatives of the term in square brackets (K), with respect to F_1 through F_4

$$K'_1 = \frac{\partial K}{\partial F_1} = \frac{F_2\, S_{34}}{(a_1 a_2)^4} - \frac{P_{34}}{a_1^4} \quad , \tag{2.11}$$

$$K'_2 = \frac{\partial K}{\partial F_2} = \frac{F_1\, S_{34}}{(a_1 a_2)^4} - \frac{P_{34}}{a_2^4} \quad , \tag{2.12}$$

$$K'_3 = \frac{\partial K}{\partial F_3} = \frac{P_{12}}{a_3^4} - \frac{F_4\, S_{12}}{(a_3 a_4)^4} \quad , \tag{2.13}$$

$$K'_4 = \frac{\partial K}{\partial F_4} = \frac{P_{12}}{a_4^4} - \frac{F_3\, S_{12}}{(a_3 a_4)^4} \quad , \tag{2.14}$$

where

$$S_{12} = \frac{F_1}{a_1^4} + \frac{F_2}{a_2^4} \quad , \quad S_{34} = \frac{F_3}{a_3^4} + \frac{F_4}{a_4^4} \quad ,$$
$$P_{12} = \frac{F_1 F_2}{(a_1 a_2)^4} \quad , \quad P_{34} = \frac{F_3 F_4}{(a_3 a_4)^4} \quad .$$

With this, the contributions to the diagonal D (δD_1 etc.) corresponding to Eq. (2.5) become

$$\begin{pmatrix} \delta D_1 \\ \delta D_2 \\ \delta D_3 \\ \delta D_4 \end{pmatrix} = \frac{1}{2} \begin{pmatrix} -K'_1 \\ -K'_2 \\ K'_3 \\ K'_4 \end{pmatrix} C g^{-4} f^{11} \quad , \tag{2.15}$$

These contributions also do not coincide with the discrete spectral grid. Applying (2.6) and (2.7), discrete spectral contributions $D_{i,j}$ to the diagonal term become

$$D_{i,j} = \frac{1}{2} w_{i,j}^2 \, (\pm K_i') \, C g^{-4} f^{11} \quad , \tag{2.16}$$

which again requires summation if multiple representative quadruplets are used, as in Eq. (2.8).

2.4 Set up of WAVEWATCH III

All calculations performed with WAVEWATCH III reported in this study are performed with the default model setup of model version 2.22 as described in Tolman (2002b). Only non-standard model setting will be discussed here.

For all computations the default physics settings of the model are used, with the exception of the parameterization of the nonlinear interactions. All computations are performed for deep mater, making the choice of the bottom friction parameterization moot.

In Sections 3 and 4 results from time limited, single point computations from Part 1 are reproduced. The wave field is assumed to be spatially homogeneous. In such conditions, Eq. (2.1) reduces to

$$\frac{\partial F(f,\theta)}{\partial t} = S_{in}(f,\theta) + S_{nl}(f,\theta) + S_{ds}(f,\theta) \quad . \tag{2.17}$$

In WAVEWATCH III this equation is invoked by setting the propagation flags in the file ww3_grid.inp to false (see Tolman, 2002b, for details). The four time steps in the file ww3_grid.inp are set to 900, 900, 900 and 5 s, respectively. A spectral grid is used with 36 directions ($\Delta\theta = 10^\circ$) and with 35 frequencies with and increment factor $X_f = 1.07$ and ranging from 0.0418 to 0.417 Hz. This spectral resolution has been adopted to assure sufficient resolution for the computations using the exact WRT algorithm. The wind speed at 10 m is kept constant at $U_{10} = 20\,\mathrm{ms}^{-1}$.

In the second part of this study (Section 6 and following), the entire growth behavior of a wave model with alternative interaction approximations will be considered, instead of interactions for selected spectra. As a baseline for such model behavior, a time limited and fetch limited test based on the WRT interactions are performed.

The time limited model setup is similar to the setup described above with some small changes. The stability correction for wave growth is not invoked, thus reproducing the results of (Tolman and Chalikov, 1996) for stable atmospheric stratification when the conventional DIA is used. The initial conditions consist of a JONSWAP spectrum with a peak frequency $f_p = 0.25$ Hz, $\gamma = 2$, and aligned with the wind direction (using a standard WAVEWATCH III initialization option). The integration is performed for 48 h. The overall model time step is

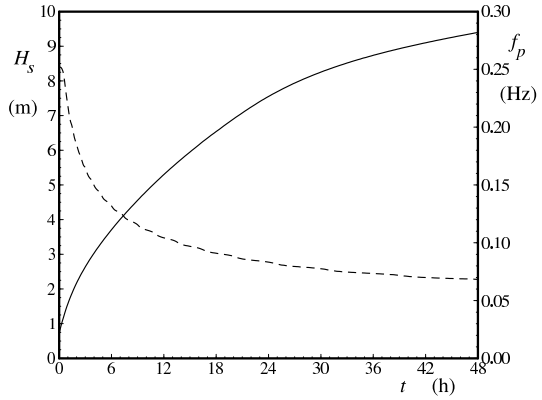

Fig. 2.1 : Wave height H_s (solid line) and peak frequency f_p (dashed line) of the time limited growth test used as baseline in Sections 6 through 7.

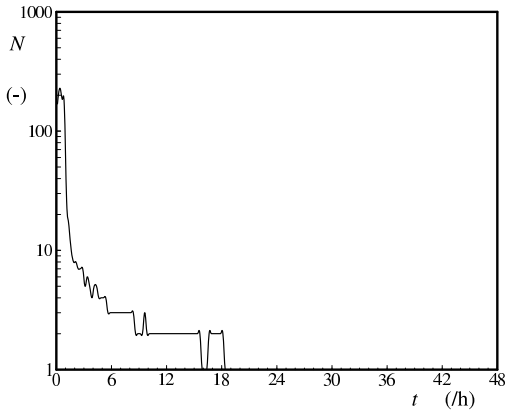

Fig. 2.2 : Number of source term integration time steps N per overall time step $\Delta t = 900$ s as a function of time corresponding to Fig. 2.1.

set to 900 s, and the minimum time step for source term integration is set to 1 s. As above, 36 directions are used with a directional increment of $\Delta\theta = 10°$, and the frequency increment factor is set to 1.07. However, to assure that the entire prognostic part of the spectrum is always resolved by the discrete frequency space, 45 discrete frequencies are now used ranging from 0.040 to 0.785 Hz. The resulting evolution of the wave height H_s and the peak frequency f_p are presented in Fig. 2.1.

Using a new option in a test version of WAVEWATCH III, each spectrum and corresponding source term S_{nl} is saved for this run. Because the internal time step is calculated dynamically, it can be much smaller than 900 s, particularly in the initial growth stages. This is illustrated in Fig. 2.2, which shows the number of time steps used in the source term integration to advance the solution over each overall time step $\Delta t = 900$ s. By saving each spectrum and source term, a total of 1111 tests spectra have been generated from this test, and the dynamic

time step in the initial stages of wave growth became as small as 3.2 s. Depending on the optimization considered, all of these test cases or a subset will be used. Additional relevant results of these computations will be addressed in Sections 6 through 7.

The second test scenario to be considered in the optimization is conventional fetch limited wave growth. Such a test generally considers homogeneous conditions in the y direction, with a straight coast line at $x = 0$. Wind is blowing offshore at a constant speed with a constant direction perpendicular to the coast. The steady state solution corresponding to such conditions can be calculated with the reduced balance equation

$$c_x \frac{\partial}{\partial x} F(f,\theta) = S_{in}(f,\theta) + S_{nl}(f,\theta) + S_{ds}(f,\theta) \quad , \tag{2.18}$$

where c_x is the advection velocity in the offshore (x) direction. Two complications occur when fetch-limited conditions are computed with a convectional wave model.

First, conventional wave models propagate the solution forward in time, based on Eq. (2.1). When this equation is reduced to Eq. (2.18), the equation becomes elliptic rather than hyperbolic, and requires fundamentally different solution techniques (see, for instance Booij et al., 1999). For a model like WAVEWATCH III, is is more convenient to solve the evolution of the wave field in time according to Eq. (2.1), until a (quasi-) steady solution is reached.

Second, assuming that conditions are homogeneous in y direction allows for wave components to travel along the coast indefinitely, and being turned back in upwind directions by the nonlinear interactions. This requires the area of interest to be much larger in y direction than in x (fetch) direction, which is not realistic. More realistic results are therefore expected with a finite size of the test area in y direction, while solving the full Eq. (2.1).

With this in mind the fetch limited test will consider an area of 500×500 km^2, resolved with $\Delta x = 10$ km and $\Delta y = 250$ km, taking fetch limited results from the perpendicular offshore line centered in the y direction. The overall and propagation time steps are set to 360 s, and the minimum source term time step is set to 1 s. It is well known that higher order propagation schemes when used in this idealized test result in oscillations in the solution before reaching the quasi-steady solution. This can be avoided by using the first order scheme, at a minor impact to the overall results (see Tolman, 1992). Thus, the general model setup in the fetch limited tests is identical to that in the time limited tests with the addition of the first order propagation scheme.

As in the time limited test, a constant offshore wind speed $U_{10} = 20$ ms^{-1} is applied. The WAVEWATCH III model is initialized with the same initial spectrum as used in the time limited case. Note that this choice has in principle no impact on the final fetch limited results, but makes it possible to assure

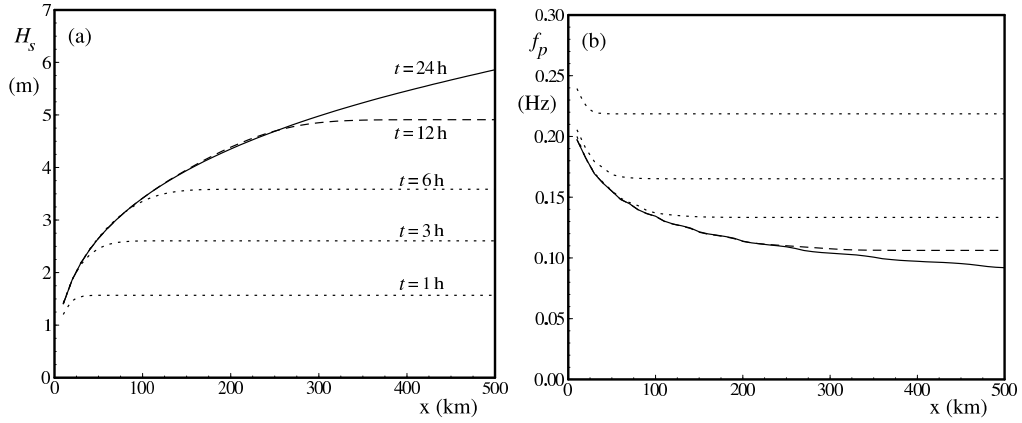

Fig. 2.3 : Wave height H_s (a) and peak frequencies f_p (b) for fetch limited test used as baseline in Sections 6 through 7.

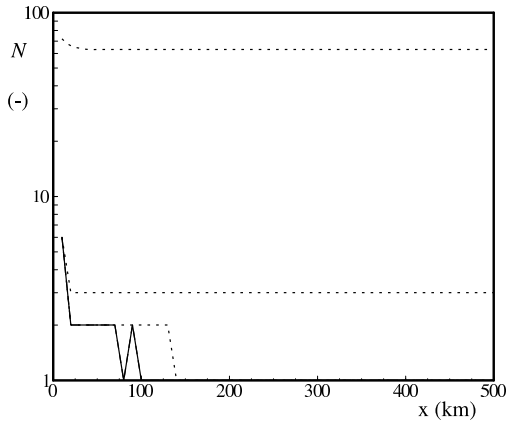

Fig. 2.4 : Number of source term integration time steps N per overall time step $\Delta t = 360$ s as a function of fetch x corresponding to Fig. 2.3.

that the entire spectrum is always properly resolved in the discrete frequency space. The spectral discretization of the time limited test is also adopted without changes. The model integration is performed for 24 h, at which time the model has practically reached the quasi-steady solution. The corresponding wave heights H_s and peak frequencies f_p after 1, 3, 6, 12 and 24 h of model integration are presented in Fig. 2.3. The corresponding number of source term integration time steps per 360 s model time step are presented in Fig. 2.4. Spectra and source terms for all grid points as valid at 30 min intervals have been saved to be used for the development of the DIA in the following sections.

3 Model integration in Part 1

The final sets of tests performed in Part 1 consider incorporation of the VDIA and MDIA in the WAVEWATCH III wave model (Tolman, 1991, 1992; Tolman and Chalikov, 1996; Tolman et al., 2002; Tolman, 2002b) using a duration limited test as described in section 2.4. The corresponding results were shown in Figs. 5.1 through 5.4 of Part 1. The final results after 6 hours of model integration are reproduced here in Fig. 3.1. In the present figure, the spectra are displayed in Cartesian representation, unlike the polar representation in Part 1, but are otherwise identical.

Figure 3.1a shows the spectrum obtained with the exact interactions, whereas Fig. 3.1d shows the conventional results obtained with the original DIA. Note that in WAVEWATCH III, the original DIA is rescaled to obtain better integration results (see Tolman and Chalikov, 1996). The results obtained with MDIA are presented in Fig. 3.1b. The MDIA shows consistent spectral growth with a realistic single-peaked spectrum, however, details of the spectrum differ clearly from both the exact and DIA solutions. Somewhat surprisingly, the VDIA (Fig. 3.1c) does not result in consistent spectral growth, in spite of the fairly accurate nonlinear interactions as calculated for individual spectra.

It is not necessarily surprising that the more accurate description of interactions for a single spectrum do not immediately translate into more accurate model integration. This is a typical aspect of nonlinear models. The opposite was already observed by Hasselmann et al. (1985); in spite of the fact that the original DIA does not do a particularly good job at representing individual interactions, it nevertheless resulted in acceptable behavior when first applied in the WAM model.

The observation in Fig. 3.1c that the fairly accurate[2] VDIA does not only give poor results, but cannot even reproduce consistent single-peaked wind sea spectra is nevertheless somewhat surprising. Many previous authors presenting modified DIAs have not tested their parameterizations by incorporating them in a practical wave model. The implicit assumption seems to have been that all DIAs would automatically result in stable model integration. Figure 3.1c clearly proves such an assumption to be wrong.

An important feature of the nonlinear interactions is their ability to stabilize the spectral shape. Local perturbations, in particular for frequencies above the spectral peak frequency, are rapidly smoothed out by a process that resembles diffusion (e.g., Resio and Perrie, 1991; Young and Van Vledder, 1993). Because Eq. (2.5) retains the diffusive character of the exact interactions (compare, for instance, with Webb, 1978), it might be expected than any DIA has the proper diffusive character to stabilize the spectral shape. This, in turn, would support the suggestion that a DIA in principle should be able to stabilize the spectral

[2] Accurate with respect to representation of interactions for individual spectra.

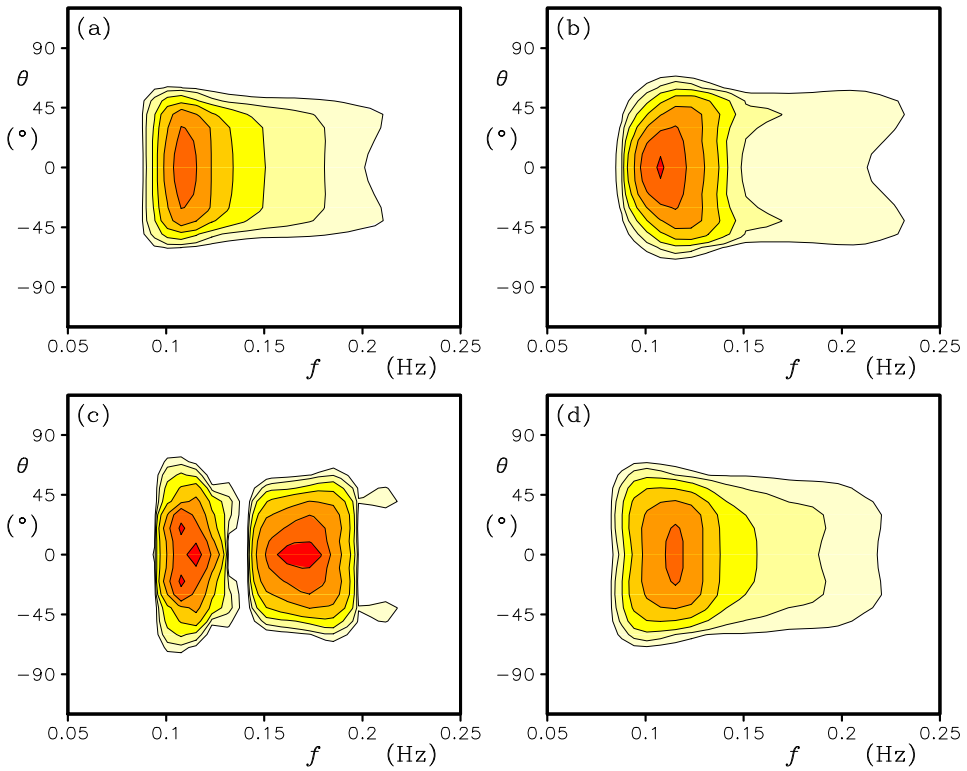

Fig. 3.1 : Spectra $F(f,\theta)$ from six hour model integration test from Part 1, for models with different parameterizations for S_{nl}. (a) Exact interactions (WRT). (b) frozen MDIA. (c) frozen VDIA. (d) rescaled DIA. Contours at factor 2 increment, with lowest contour level at 1 m^2s^{-1}. See also Figs. 5.1 through 5.4 in Part 1.

shape, and hence result in stable and/or convergent model integration.

Close inspection of the results presented in Fig. 3.1c, or in Fig. 5.3 in Part 1 suggest that the disintegration of the spectrum is not necessarily related to the lack of diffusive behavior of the VDIA at high frequencies. In fact, the problems appear to start close to the spectral peak early in the integration. It is furthermore observed that the disintegration occurs in frequency space first. This suggests that the sampling of the spectrum in frequency space may be one of the reasons for the disintegration to occur. To assess if this could be an explanation for the integration behavior of in particular the VDIA, contributions to S_{nl} for a single discrete frequency are presented in Fig. 3.2 for the DIA, the VDIA and the MDIA, using the initial conditions of the integration tests of Fig. 3.1 with a peak frequency $f_p = 0.15$ Hz, and looking at the contributions for discrete frequency bin 20, with $f_{20} = 0.151$ Hz. Similar results for $f_{25} = 0.212$ Hz are presented in Fig. 3.3.

Two observations can be made from these figures. First, the DIA contribu-

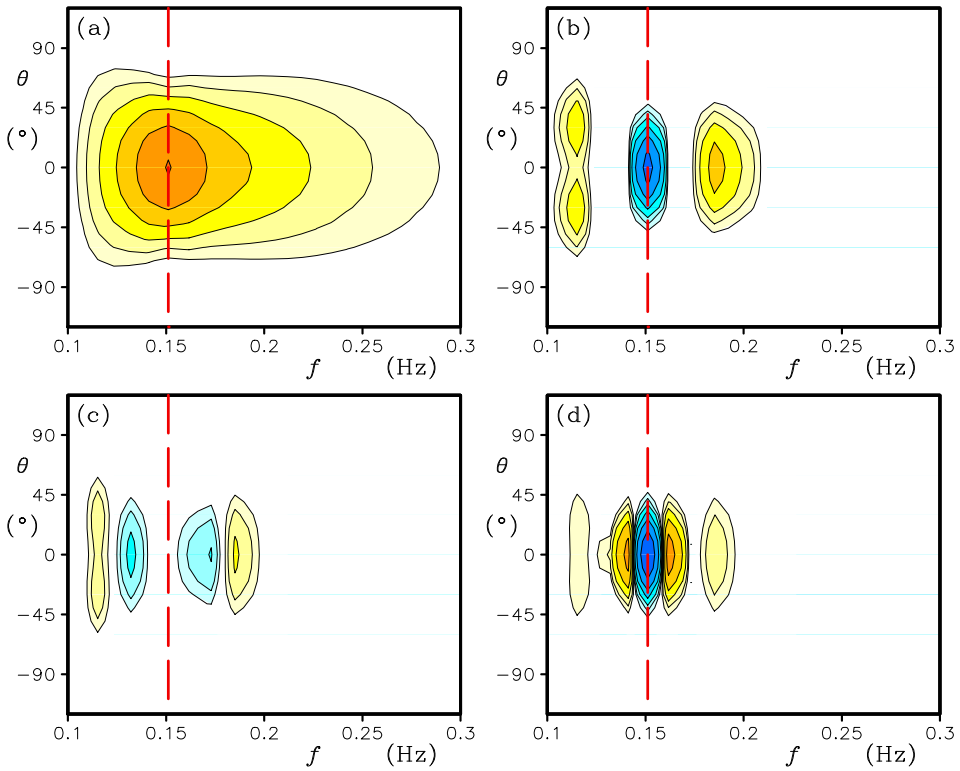

Fig. 3.2 : Contribution to the nonlinear interaction for a given discrete frequency $f_d = 0.151$ Hz only (red dashed line) for the initial conditions used in the time integration test. (a) Spectrum. (b) DIA. (c) VDIA. (d) MDIA. Contours at factor 2 increments starting at 10^{-1} m^2s^{-1} (spectrum) or $\pm 10^{-6}$ (source terms). Blue identifies negative values.

tion *for a single frequency* (panels b in both figures) by definition has a three-lobe structure with either a -/+/- or a +/-/+ signature. The VDIA contributions *for a single frequency* (panels c), however, have a four-lobe structure, whereas similar MDIA contributions (panels d) have a more complex and variable structure. Tentatively, it could be expected that the four-lobe structure of the VDIA contribution for a given frequency requires a rather sensitive balance of contributions of different frequencies to obtain an overall three-lobe structure of $S_{nl}(f)$. The much more complicated and variable structure of the MDIA could be expected to be more versatile in this respect, whereas the three-lobe structure of the DIA for a single frequency could be expected to more naturally result in a three-lobe overall structure if a small number of frequencies dominate the contributions to S_{nl}.

Secondly, the VDIA by definition does not contribute to the nonlinear interaction at the discrete frequency f_d (unless $1 + \lambda$ or $1 + \mu$ are smaller than the increment factor in the discrete frequency grid). In other numerical model prob-

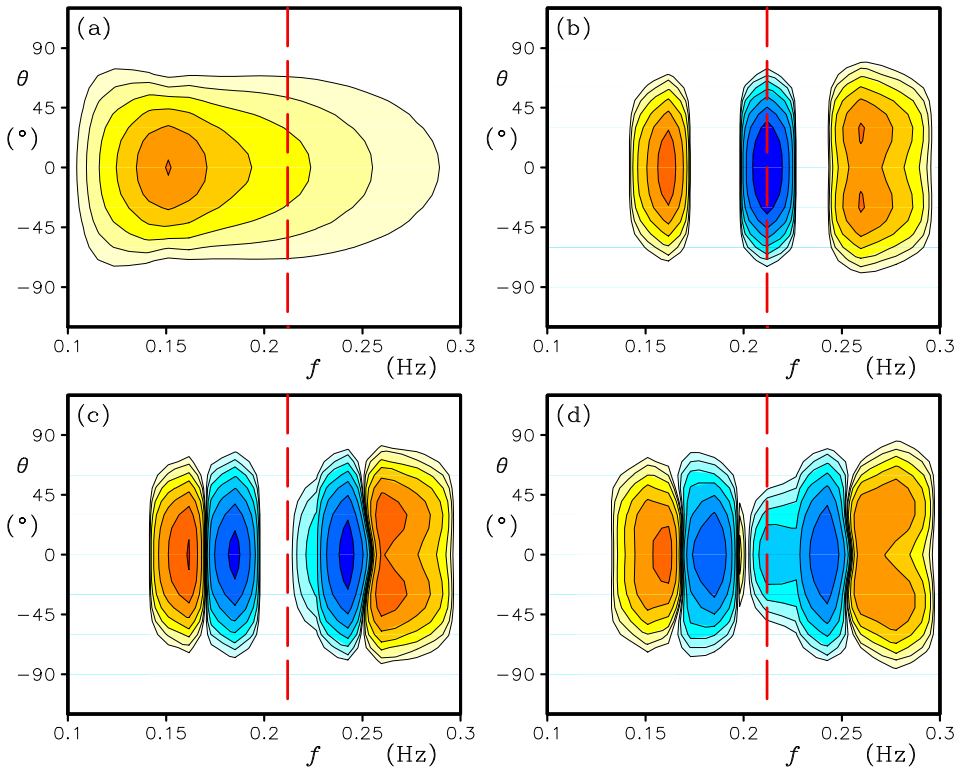

Fig. 3.3 : Like Fig. 3.2 with contributions of the discrete frequency $f_d = f_{25} = 0.212$ *Hz only.*

lems such a disconnect is known to result occasional decoupled grid solution, for instance with a so-called Leap-Frog numerical propagation scheme (e.g., Fletcher, 1988).

These two observations by no means explain in full why the VDIA as suggested in Part 1 results in a disintegration of the spectrum when applied in a wave model. However, it does indicate that the layout of the quadruplet and the way in which the quadruplet is used to sample the spectral space is deserving further attention. This will therefore be the subject of the following section.

4 Quadruplet layout and the sampling of spectral space

The present section will address the effects of the quadruplet layout, and the way in which this quadruplet is used to sample spectral space. This is most easily investigated using a single component VDIA or MDIA. Because the disintegration of the model spectrum in Part 1 appeared to be related to the general quadruplet layout, and not to the fact the the quadruplet layout varied in spectral space, it is sufficient here to address single component DIAs with uniform quadruplet layout throughout spectral space (i.e., the single component MDIA from Part 1). In the following subsection, spectral shape and spectral sampling are discussed first (Section 4.1). After this, the effects of spectral sampling on source terms for selected spectra and on model integration are investigated (Section 4.2). Intermediate conclusions are presented in Section 4.3, leading into the subjects of investigation in the following sections.

4.1 Quadruplet shape and sampling

Quadruplets, whether used in the exact interactions or in a DIA, need to satisfy Eqs. (2.2) and (2.3). There are two ways in which the quadruplet layout can be visualized. The first is by means of drawing the vectors $\boldsymbol{k}_1 + \boldsymbol{k}_2$ and $\boldsymbol{k}_3 + \boldsymbol{k}_4$ either as vectors, or as loci of connection points between $\boldsymbol{k}_1$ and $\boldsymbol{k}_2$ or between $\boldsymbol{k}_3$ and $\boldsymbol{k}_4$ (e.g., Phillips, 1977, Fig. 3.7). A second way to display the layout of the quadruplet is to identify the location of the quadruplet components $\boldsymbol{k}_1$ through $\boldsymbol{k}_4$ for a given discrete spectral component $\boldsymbol{k}_d$ in the discrete spectral space (e.g., Van Vledder, 1990, Fig. 3.2). The latter display is typically adapted to the actual description of spectral space in the model, that is $(k,\theta)_{n,d}$ or $(f,\theta)_{n,d}$. These two ways of displaying the quadruplet are utilized in Figs. 4.1 and 4.2, respectively.

Figures. 4.1a and 4.2a show the quadruplet of the original DIA ($\lambda = 0.25$). Because $\boldsymbol{k}_d = \boldsymbol{k}_1 = \boldsymbol{k}_2$ ($\square$ and $\bullet$ in Fig. 4.2a), a major contribution of a DIA using such a quadruplet will be at the discrete wavenumber $\boldsymbol{k}_d$ that is considered. This guarantees a strong coupling between the local spectral density ($F(\boldsymbol{k}_d)$) and the corresponding source term ($S_{nl}(\boldsymbol{k}_d)$). Close inspection of Eq. (2.5) as applied to this quadruplet, in combination with the quadruplet layout of Fig. 4.2a also makes it clear that each individual contribution to the DIA will always have a -/+/- or +/-/+ signature in both the frequency (f) and direction (θ) space. These attributes of the original DIA quadruplet can tentatively be expected to contribute to the success of the original DIA, although they by no means fully explain it.

Figures. 4.1b and 4.2b show the extended quadruplet as used in Part 1, with $\lambda = 0.248$ and $\mu = 0.127$. In this configuration, $\boldsymbol{k}_3$ and $\boldsymbol{k}_4$ remain essentially unchanged compared to the original DIA setup (compare dashed vectors in Fig. 4.1a

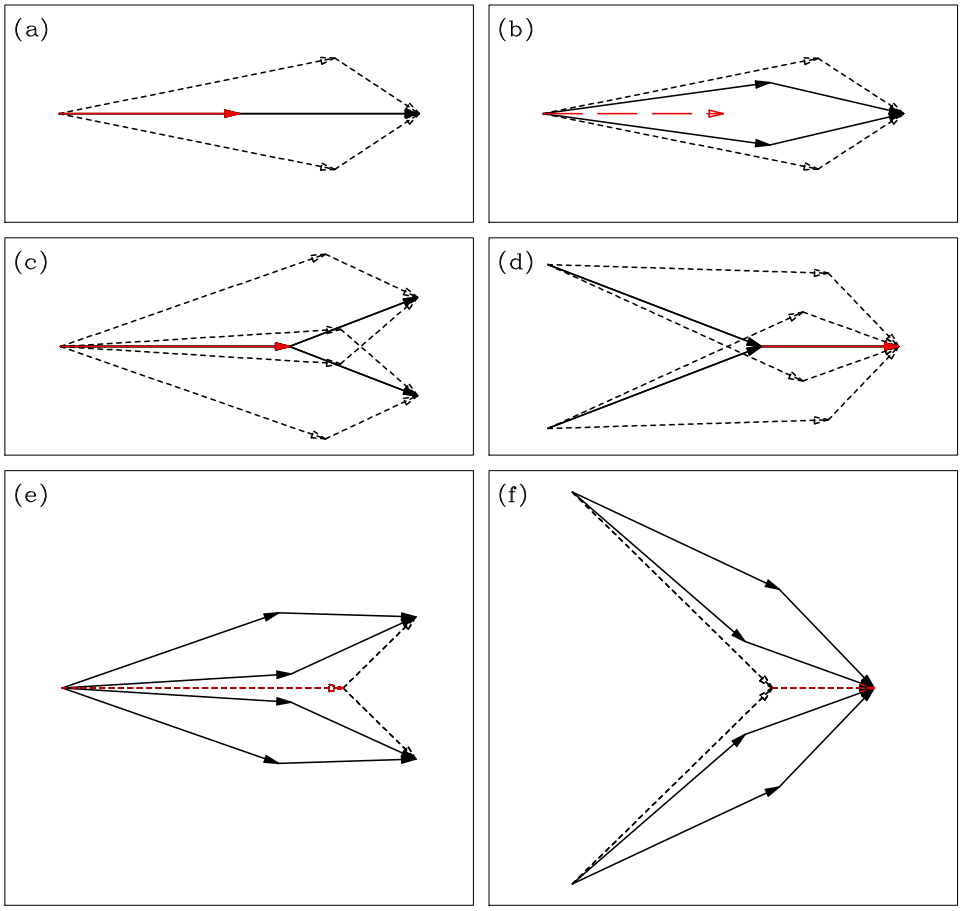

Fig. 4.1 : Quadruplet layout in terms of vectors $\boldsymbol{k}$ *for different quadruplet definitions and for different sampling methods. (a) Original DIA quadruplet with* $\lambda = 0.25$*. (b-f) Quadruplet of Part 1 with* $\lambda = 0.248$ *and* $\mu = 0.127$*. (b)* $\boldsymbol{k}_d = 0.5(\boldsymbol{k}_1 + \boldsymbol{k}_2)$ *as in Part 1. (c-f)* $\boldsymbol{k}_d = \boldsymbol{k}_1$ *through* $\boldsymbol{k}_4$*. Solid vectors* $\boldsymbol{k}_1 + \boldsymbol{k}_2$*. Dashed vectors* $\boldsymbol{k}_3 + \boldsymbol{k}_4$*. Red vector identifies* $\boldsymbol{k}_d$*, which in turn determines the actual sampling of spectral space.* $\boldsymbol{k}_d$ *is part of the quadruplet in all panels except for (b).*

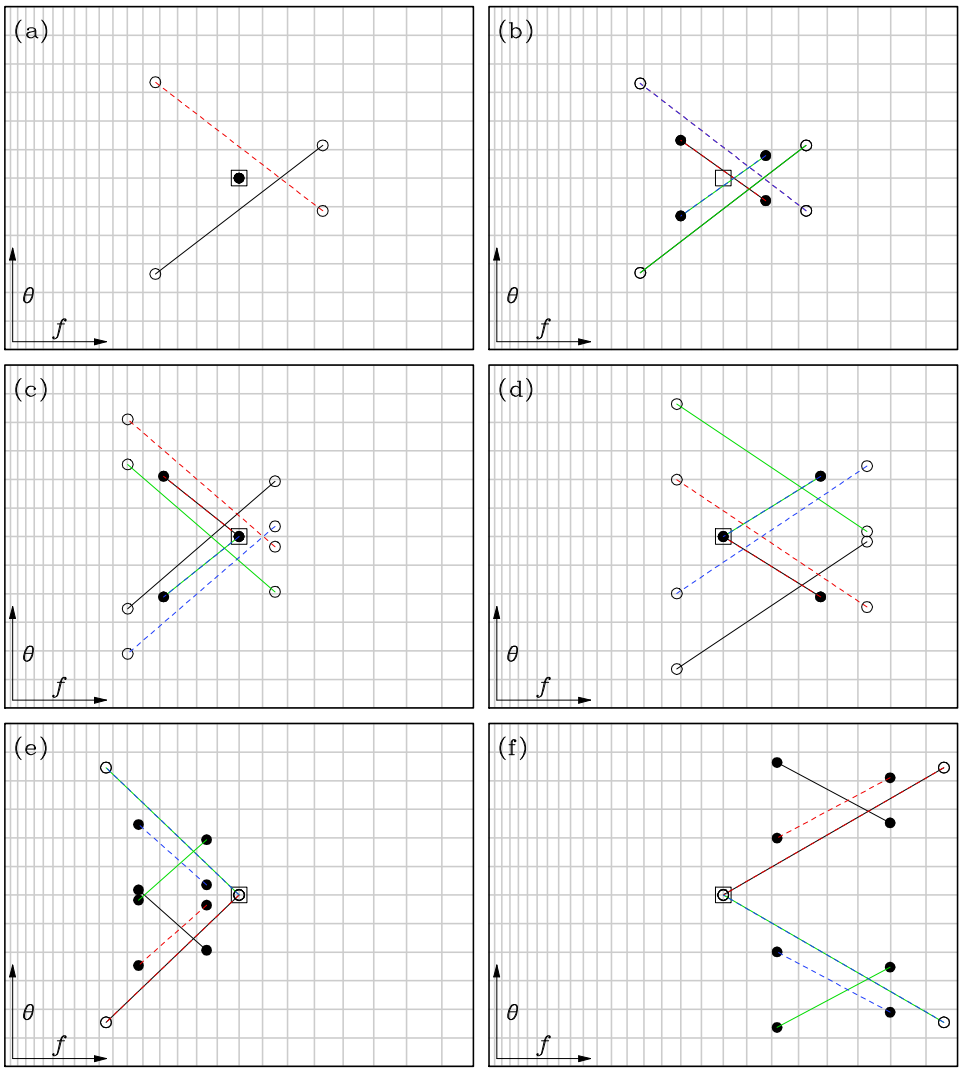

Fig. 4.2 : Quadruplet layouts in (f, θ) space for the six quadruplets and sampling patters as in Fig. 4.1. □: Discrete spectral component $(f, \theta)_d$. •: $(f, \theta)_1$, $(f, \theta)_2$. ∘: $(f, \theta)_3$, $(f, \theta)_4$. Connecting lines identify individual quadruplets. The gray lines identify the discrete spectral grid with a frequency increment factor 1.07 and a directional increment $\Delta\theta = 10°$.

and b, and $\circ$ in Fig. 4.2a and b). However, $\boldsymbol{k}_1$ and $\boldsymbol{k}_2$ (solid vectors or $\bullet$) are now defined differently, and no longer coincide with the discrete spectral frequency (red vector or $\square$). Figure 4.2b identifies two major differences between this quadruplet definition, and the original definition as used in the DIA (panel a). First, when calculating contributions for $\boldsymbol{k}_d$, the corresponding contributions to the interactions $\delta S_{nl}(\boldsymbol{k}_d) = 0$. This may suggest some decoupling of the interactions from the spectrum. However, since contributions of the interactions are always redistributed to all spectral grid points from which spectral densities are used to compute the contributions, such a decoupling cannot be complete. As will be shown below, this apparent decoupling in fact does not exist. Second, close inspection of Eq. (2.5) and Fig. 4.2b shows that individual contributions δS_{nl} for this quadruplet will always have a four-peaked structure in f space, with a -/+/+/- or +/-/-/+ structure. Both the potential decoupling, and the four-peak structure of individual contributions are potentially detrimental to the integration properties of the DIA with the new quadruplet layout as suggested in Part 1.

Figures. 4.1 and 4.2 panels c through f show quadruplet layouts and sampling patterns for the new quadruplet with $\lambda = 0.248$ and $\mu = 0.127$, but with a different definition of $\boldsymbol{k}_d$. These figures show that for a given layout (λ, μ) of the quadruplet, the sampling of spectral space (definition of $\boldsymbol{k}_d$) has a major impact on layout of quadruplets considered for $\boldsymbol{k}_d$, and on the sampling pattern in (f, θ) space. Several observations can be made from these figures. First, coupling between $F(\boldsymbol{k}_d)$ and $S_{nl}(\boldsymbol{k}_d)$ is restored at the level of individual contributions δS_{nl}. Second, a four-peak structure for individual contributions $S_{nl}(\boldsymbol{k}_d)$ remains in f space, independent of the sampling. Third, the layout of the sampling pattern for each of the four possible quadruplets remains essentially the same, with a shift in directional space, and a factor multiplication of the frequencies of the components of the quadruplet. The four individual quadruplets, however, are generally shifted farther apart in (f, θ) space, creating a sampling of a larger area in this space.

On first inspection, Fig. 4.2 may suggest that different definitions of $\boldsymbol{k}_d$ will result in completely different interactions. This is not the case, however, because a large number of $\boldsymbol{k}_d$ values supply contributions to the interactions at any given frequency and direction, resulting in analytically identical interactions, irrespective of the actual choice of $\boldsymbol{k}_d$ in the quadruplet. This is illustrated in Fig. 4.3 using a degenerated quadruplet from Part 1 with $\lambda = \mu = 0.2$. Note that only one independent quadruplet satisfies this choice of λ and μ is used here. Figure 4.3a shows the corresponding sampling pattern for this quadruplet in (f, θ) space, using the original definition of $\boldsymbol{k}_d$. Only four spectral components are included in this quadruplet. For simplicity ignoring the redistribution of contributions δS_{nl} in Eq, (2.7) (i.e., assuming continuous spectral space), only four quadruplets contribute to the interactions for a given spectral component. These

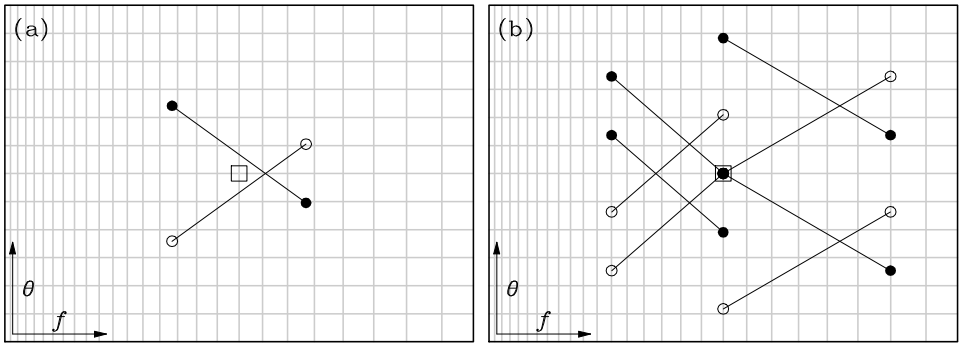

Fig. 4.3 : (a) Quadruplet layout in (f, θ) space for quadruplet from Part 1 with $\lambda = \mu = 0.2$. (b) All quadruplets contributing to discrete spectral grid point $\square$, assuming continuous spectral space. Legend as in Fig. 4.2.

four quadruplets are displayed in Fig. 4.3b. It is obvious from this figure that the contributing quadruplets for a given spectral component are independent of the choice of $\boldsymbol{k}_d$ in the calculation of individual contributions. The same is obviously true for more complicated quadruplets. However, the discrete spectral space will have some impact on the necessary interpolations and redistributions of contributions per component. Tentatively, this is expected to be a second order effect, with small or negligible impact on the resulting interactions. However, due to the highly nonlinear nature of the problem considered here, a practical test of this assumption is appropriate. Such a test is provided in the following section.

4.2 Impact on interactions and model integration

To assess the impact of the sampling pattern for a given quadruplet, consider a single component MDIA with a two parameter quadruplet defined as $\lambda = 0.248$, $\mu = 0.127$ and $C = 1.81\,10^7$. This represents the optimized quadruplet from Part 1 (see Table 3.1 in Part 1). This quadruplet is applied to the 6 h integration test of Part 1, using different ways of sampling the spectral space with this quadruplet. Considered are all five sampling patterns for this quadruplet as analyzed in Figs. 4.1 and 4.2, panels (b) through (f).

Modifying the sampling patterns in a quadruplet has two impacts in the computation of S_{nl}. Typically, the change of the discrete frequency can be expressed in terms of a multiplication factor for the discrete frequency relative to the original sampling pattern. This factor will be denoted as X_d, with $\sigma_{d,\mathrm{new}} = X_d \sigma_{d,\mathrm{old}}$. Effectively this shifts the quadruplet by a factor X_d in frequency space. This modifies the factors a_n in Eq. (2.4) by a factor X_d, and hence modifies the contributions to the interactions in Eq. (2.5) by a factor X_d^{-12}. An additional correction factor is introduced because of the dependency of Eq. (2.5) on f_d. This corre-

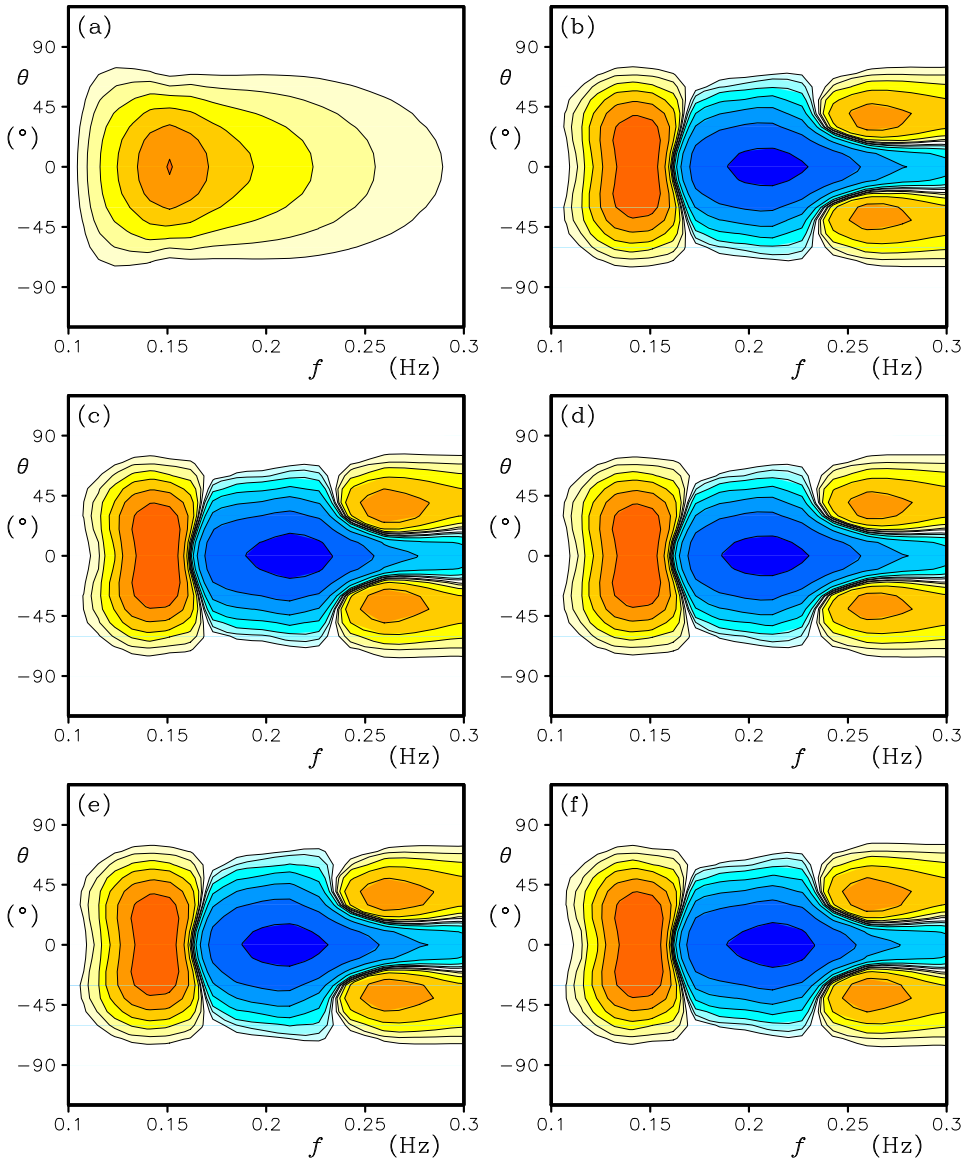

Fig. 4.4 : Spectrum (a) and corresponding source term for single component DIA with $\lambda = 0.248$, $\mu = 0.127$ and $C = 1.81\,10^7$. (b) $\boldsymbol{k}_d = 0.5(\boldsymbol{k}_1 + \boldsymbol{k}_2)$, (c) $\boldsymbol{k}_d = \boldsymbol{k}_1$, (d) $\boldsymbol{k}_d = \boldsymbol{k}_2$, (e) $\boldsymbol{k}_d = \boldsymbol{k}_3$, (f) $\boldsymbol{k}_d = \boldsymbol{k}_4$. Legend as in Fig. 3.2.

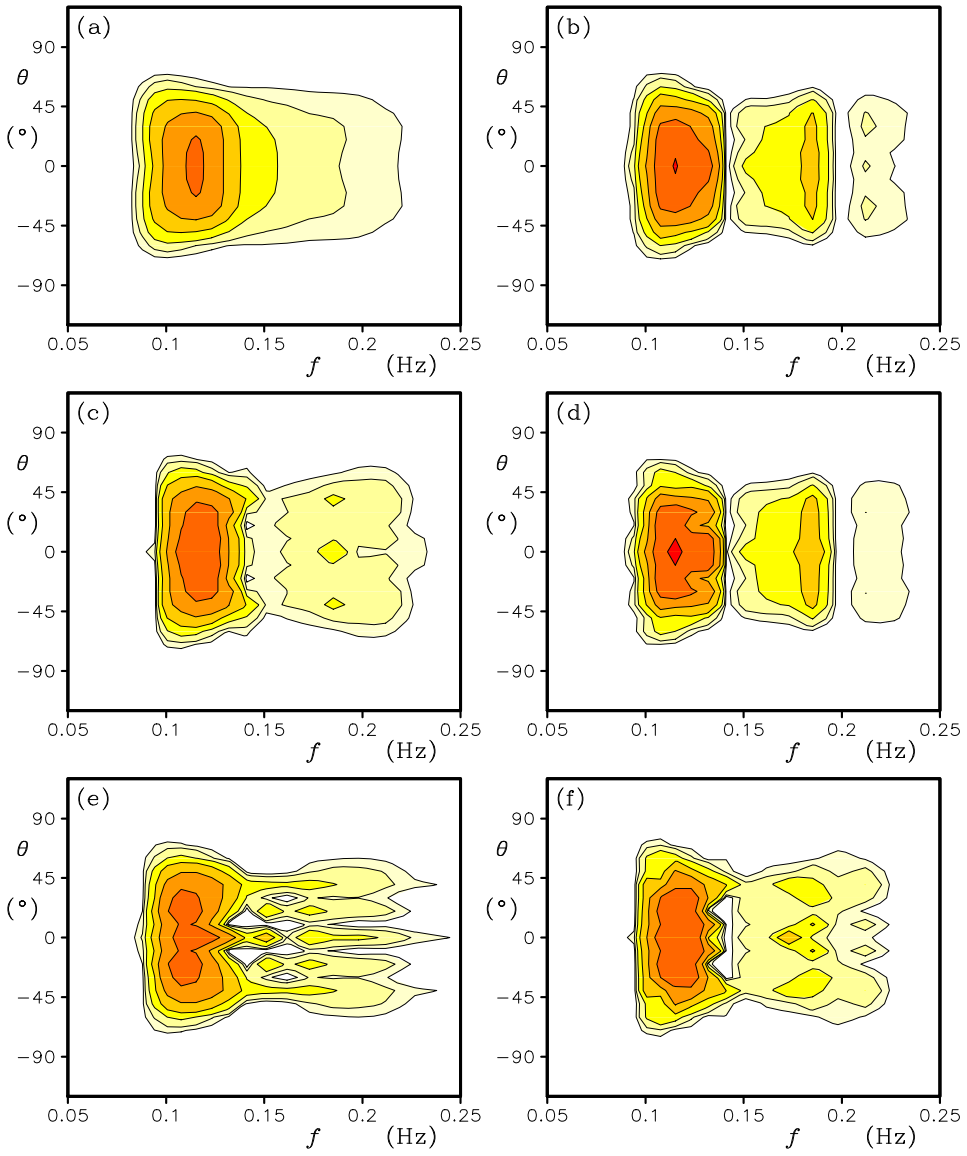

Fig. 4.5 : Spectra after 6 h of model integration as in Part 1, from initial conditions in Fig. 4.4. (a) Conventional DIA with $\lambda = 0.25$ *and* $C = 110^7$ *(b-f) Single component DIA as in Part 1 wit* $\lambda = 0.248$, $\mu = 0.127$ *and* $C = 1.81\ 10^7$. *(b)* $\boldsymbol{k}_d = 0.5(\boldsymbol{k}_1 + \boldsymbol{k}_2)$, *(c)* $\boldsymbol{k}_d = \boldsymbol{k}_1$, *(d)* $\boldsymbol{k}_d = \boldsymbol{k}_2$, *(e)* $\boldsymbol{k}_d = \boldsymbol{k}_3$, *(f)* $\boldsymbol{k}_d = \boldsymbol{k}_4$. *Legend as in Fig. 3.1.*

sponds to an additional correction factor of X_d^{-11}, bringing the total correction factor to X_d^{-23}.

Figure 4.4 shows the initial conditions for the model integration in panel (a), and the corresponding source term S_{nl} for the different sampling patterns of spectral space in panel (b) through (f). As expected, S_{nl} is fairly insensitive to the choice of $\boldsymbol{k}_d$, with only minor differences in the details of S_{nl} in panels (b) through (f).

Figure 4.5 shows the corresponding model results after 6 hours of model integration, with panel (a) showing the results of the standard WAVEWATCH III model as a reference ($\lambda = 0.25$, $\mu = 0$, $C = 1\,10^7$). Differences between model results in panels (b) through (f) are much bigger than might be expected from differences in the source terms in Fig. 4.4. However, as discussed above, this might have been expected due to the highly nonlinear nature of the problem considered. In spite of the differences between the results, all sampling versions result in spectra with similar deficiencies. It should also be noted that the results from alternative sampling patters (panels c through f) result in somewhat more noisy spectra. This may be due to the fact that this quadruplet was optimized for the sampling pattern in panel (b).

Note that the corresponding experiments with the frozen MDIA of Part 1 lead to similar conclusions, and will therefore not be reported here.

4.3 Conclusions

The experiments with the different sampling pattens performed in this section have lead to the following conclusions.

1) The quadruplet layout with two free parameters as introduced in Part 1 results in four-peaked individual contribution to the interactions for an isolated frequency. Tentatively, this makes it more difficult to reproduce a three-peaked overall structure of the interactions. For the original DIA, the basic contribution for a given frequency mimics the overall structure of the total interactions.

2) For a given quadruplet layout, the sampling method used for the quadruplet only has a minor impact on the instantaneous interactions.

3) Due to the nonlinearity of the problem, the impact in model integration is larger. However, the basic characteristics of the model do not appear to be influenced significantly by the sampling technique.

4) Alternate sampling patterns for a given quadruplet seem to add some noise to the model integration, which tentatively might be attributed to the fact that the quadruplet was optimized for the original sampling pattern.

The last three points suggest that the sampling pattern (choice of $\boldsymbol{k}_d$) for a quadruplet can be chosen purely based on economic considerations.

Figure 4.2 shows that one quadruplet of the original DIA (panel a) requires information from 5 wavenumbers $\boldsymbol{k}$ in the spectral space for the quadruplet to be evaluated. Similarly the contributions of such a quadruplets are redistributed to 5 wavenumbers $\boldsymbol{k}$. For the new quadruplet with the original sampling pattern (Fig. 4.2b), the number of wavenumbers involved in a quadruplet is 8, whereas for all alternative sampling patterns (Figs. 4.2c through f) the number is 11. Considering that the gathering and scattering of the information in the spectral space represents a major part of the computation effort required for a DIA, it can be expected that the original layout of the two parameter quadruplet from Part 1 (Fig. 4.2) is potentially more economical than the alternative layouts, and therefore is preferable, and will be used in the following sections.

The first conclusion indicates that the new quadruplet layout introduced in Part 1 is not suitable for single component DIAs, due to the basic signature it generates in spectral space, particularly in spectral frequency (f) space. Further research into the DIA should consider quadruplet configurations that at least tentatively are able to produce basic shape of the DIA. It is possible to design a quadruplet layout that has a three-peaked layout in at least frequency space. Such quadruplets will be considered in Section 5.

This page is intentionally left blank.

5 Quadruplets with a three-peak signature

In this section alternative quadruplets with three-peaked signatures in the frequency space will be investigated. Only single component DIAs will be considered in this section. In Section 5.1, possible quadruplet layouts are considered. In Section 5.2, such quadruplets are applied in the WAVEWATCH III model. Conclusions and an introduction to the remainder of the report are presented in Section 5.3.

5.1 Quadruplet layouts

In order to investigate the possibility of creating quadruplets with a three-peak structure of its elementary contributions in frequency space, it is prudent to start with the most versatile quadruplet available. This is the quadruplet defined by Van Vledder (2001), and in Table 2.1 and Eqs. (2.2), (2.3) and (2.4). An example of the layout of such a quadruplet with $\lambda' = 0.136$, $\mu' = -0.182$ (corresponding to $\lambda = 0.25$, $\mu = 0.10$, as will be shown below) and $\Delta\theta = 15°$ is presented in Figs. 5.1a and 5.2a. Comparison of these figures with Figs. 4.1 and 4.2 indicates that this quadruplet lacks the symmetry and compactness of the quadruplet introduced in Part 1. This symmetry can be introduced in the quadruplet by modifying the sampling method in spectral space. First, however, the layout of the quadruplet will be made equivalent to the quadruplet of Part 1. Substitution of

$$\mu' = \frac{2\mu}{1+\mu} \quad , \quad \lambda' = \frac{\lambda - \mu}{1+\mu} \quad . \tag{5.1}$$

results in the quadruplet definition on the bottom line of Table 2.1, which is similar to the quadruplet definition introduced in Part 1. The only difference in these quadruplets is the definition of σ in Eq. (2.4). For the quadruplet of Part 1, it is assumed that $\boldsymbol{k}_d = \frac{1}{2}(\boldsymbol{k}_1 + \boldsymbol{k}_2)$ and $\sigma_d = \frac{1}{2}(\sigma_1 + \sigma_2)$ satisfy the dispersion relation. This uniquely defines $\Delta\theta$. In the Van Vledder quadruplet, this assumption is not made. Instead, $\Delta\theta$ is defined explicitly to uniquely define the quadruplet.

To reproduce the symmetry of the quadruplet from Part 1, a proper sampling quadruplet needs to be selected. It is easily verified that the symmetry of the quadruplet is achieved for any $\boldsymbol{k}_d$ satisfying

$$\boldsymbol{k}_d = \alpha\,(\boldsymbol{k}_1 + \boldsymbol{k}_2) \quad . \tag{5.2}$$

where α is an arbitrary constant. An analogy with the Part 1 quadruplet suggest that $\alpha = 0.5$. A marginally more elegant definition is obtained with

$$\boldsymbol{k}_d = \frac{||\boldsymbol{k}_1||}{||\boldsymbol{k}_1 + \boldsymbol{k}_2||}\,(\boldsymbol{k}_1 + \boldsymbol{k}_2) \quad , \tag{5.3}$$

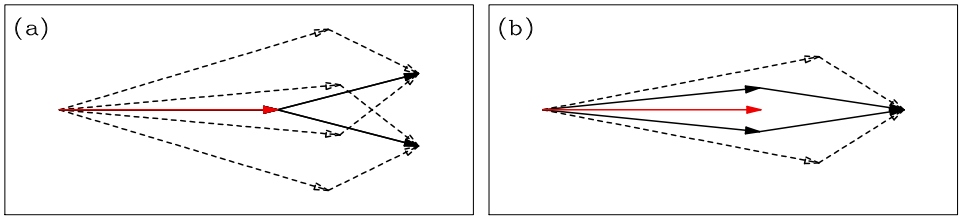

Fig. 5.1 : Like Fig. 4.1 for the quadruplet layout of Van Vledder (2001) with $\lambda = 0.25$, $\mu = 0.10$ and $\Delta\theta = 15°$ (corresponding to $\lambda' = 0.136$, $\mu' = -0.182$). (a) Original definition of $\boldsymbol{k}_d$. (b) Modified definition of $\boldsymbol{k}_d$ of Eq. (5.3).

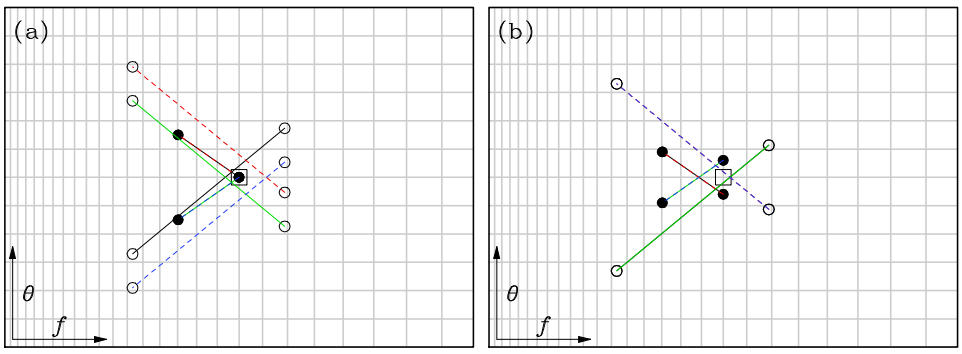

Fig. 5.2 : Like Fig. 4.2 for the quadruplets displayed in Fig. 5.1.

which guarantees that at least one of the components of the quadruplet (σ_1) always coincides with the spectral frequency grid. This layout is particularly elegant for cases with $\mu = 0$ and $\Delta\theta \neq 0$, in which case $\sigma_1 = \sigma_2 = \sigma_d$. This modified Van Vledder quadruplet defined as in Table 2.1 and Eq. (5.3) is visualized in Figs. 5.1b and 5.2b, and will be used as the generic quadruplet in the remainder of this study.

Equation 2.4 indicates that a quadruplet with a three-peak signature of contribution in the frequency space will require that exactly two of the factors a_1 through a_4 are identical. This requires that either $\lambda = 0$ or $\mu = 0$ in the generic quadruplet definition. The sampling patterns in (f, θ) space for such quadruplets are illustrated in Fig. 5.3 for $\Delta\theta = 15°$, and λ and μ alternately 0 or 0.25. These two quadruplets are essentially identical, with only a shift in frequency space for the sampling pattern. In the remainder of this section, the quadruplet will be defined as $\mu \equiv 0$, $\lambda \neq 0$ and $\Delta\theta \neq 0$.

It should be noted that a special situation occurs when $\lambda = \mu$, in which case there are only two frequencies at which each quadruplet generates contributions. In this case, only two quadruplets give non-zero contributions. Because this quadruplet does not result in a three-peaked elementary contribution, it will not

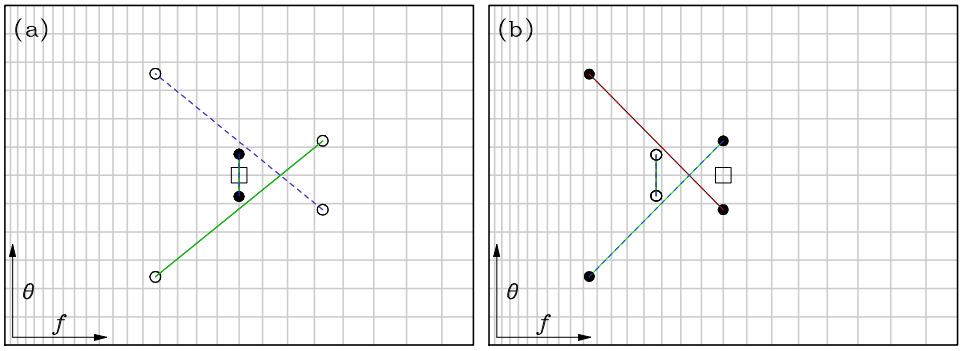

Fig. 5.3 : Like Fig. 5.2 for the generic quadruplet with (a) $\lambda = 0.25$, $\mu = 0$ and $\Delta\theta = 15°$, or (b) $\lambda = 0$, $\mu = 0.25$ and $\Delta\theta = 15°$.

be considered here.

5.2 Mapping and integration

The remainder of this section can be considered as an extension to Part 1. The test case and optimization techniques from Part 1 are therefore adopted without further documentation. After a quadruplet has been defined, it will be tested in model integration as in Part 1. The goal in this section is only to show that an alternative single quadruplet as developed in Section 5.1 can indeed result in reasonable model integration. In this context, a VDIA based on this new quadruplet will not yet be considered here.

Considering the present context, a detailed optimization for selected test spectra is not relevant. Based on some simple tests, the new three parameter quadruplet will be defined with $\lambda = 0.2$, $\Delta\theta = 15°$ and $C = 1\ 10^7$. A more detailed optimization of this quadruplet will be provided in the following sections. This quadruplet has been applied in the model integration test from Section 5 of Part 1, and the results are presented here in Fig. 5.4. It is obvious that the model spectra are generally well behaved, and that this quadruplet layout does not result in the disintegration of the spectrum associated with the new quadruplet as defined in Part 1. The three parameter quadruplet defined in this section can thus be the basis for further optimization in the remainder of this report, particularly for single component DIAs and VDIAs.

5.3 Conclusions

In the beginning of this section, the general quadruplet layout of (Van Vledder, 2001) is modified to make it symmetrical, without altering any of its features. From this general quadruplet, an alternative three-peaked quadruplet is defined where λ and $\Delta\theta$ are variable, and where $\mu \equiv 0$. Application of this quadruplet

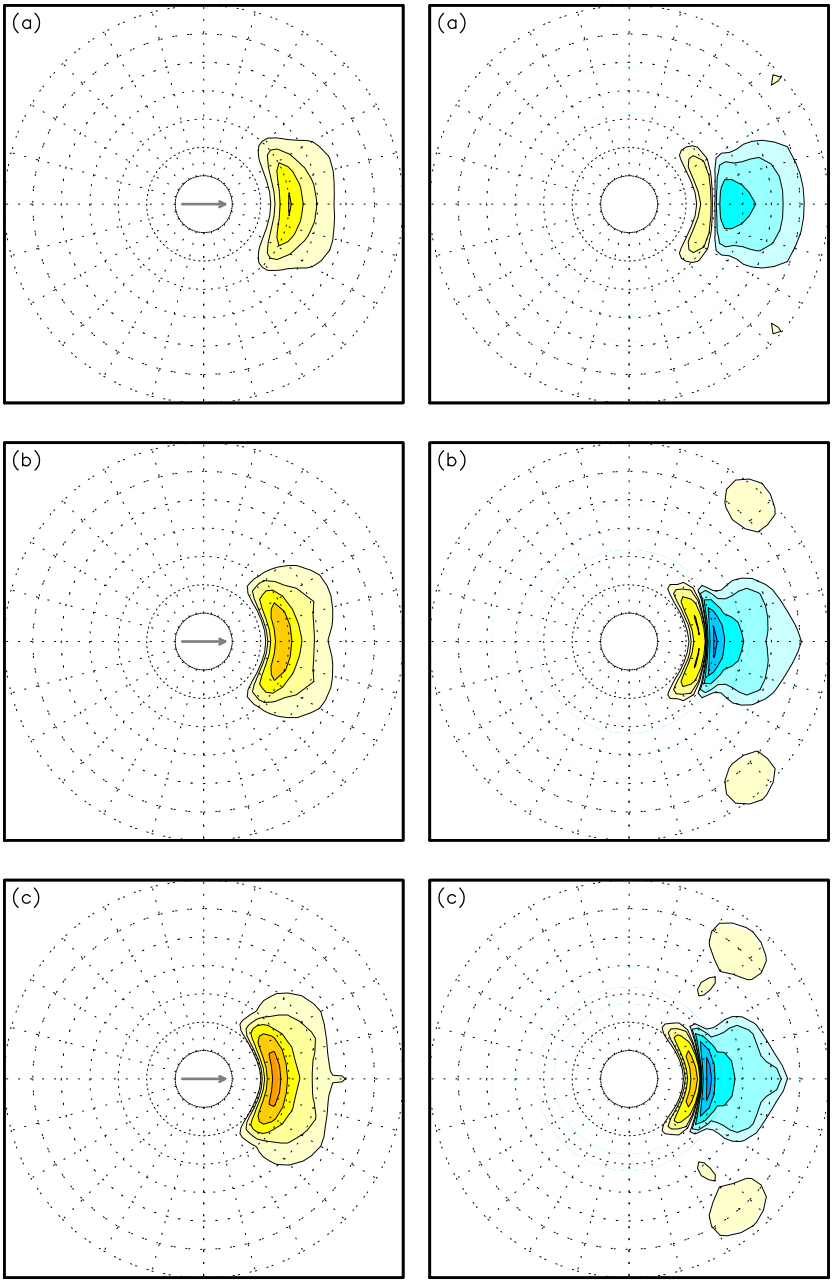

Fig. 5.4 : Like Figs. 5.1 through 5.4 from Part 1 for the new three parameter quadruplet layout with $\lambda = 0.20$, $\Delta\theta = 15^\circ$ *and* $C = 1\ 10^7$.

in the WAVEWATCH III model indicates that such a quadruplet indeed results in stable model integration. This supports the theorem that the new quadruplet from Part 1 results in non-stable model integration due to the four peaked structure in frequency space of its basic contributions.

In the remainder of this report, several DIAs will be optimized in several ways. First the optimum parameter settings of the DIAs for the previously defined growth curves obtained with the WRT method will be considered using inverse modeling techniques as defined in Part 1. Although Part 1 and the present study show the limitation of such an approach, it is nevertheless useful to identify the expected or needed variability of the corresponding quadruplet layouts of the DIAs. The present study expands on this 'classical' approach, by optimizing both integral and detailed aspects of the growth curve computation as a function of the free parameters in the DIA. Details of this optimization are discussed in Appendix B. Section 6 starts with the simplest approaches possible; single component DIAs with constant coefficients and quadruplet layouts form the original DIA (λ, C), or as defined in the present section $(\lambda, \Delta\theta, C)$.

This page is intentionally left blank.

6 Single component DIA optimization

The general strategy for testing single component DIAs is already outlined in the previous section. First, the free parameters in the two DIAs considered here are optimized for individual spectra from the time and fetch limited test cases. Second, these parameters are separately optimized using results of model integrations.

6.1 Optimization for individual spectra.

To investigate the potential of DIAs with either λ and C, or λ $\Delta\theta$ and C as free parameters, such parameters are estimated as in Part 1 for all spectra from the time limited test and for the results after 24h for the fetch limited growth.

Results for the most simple DIA (λ and C optimized) are presented in Fig. 6.1. The optimization for each spectrum and corresponding exact source term are initialized with $\lambda = 0.25$ and the corresponding optimal C. Solid lines represent the optimum estimate for λ, dotted lines represent the corresponding estimate for C. Several observations can be made from Fig. 6.1.

First, in spite of the dramatic evolution of the spectra with time or fetch, the optimum values of λ and C are remarkably well behaved. This implies implicitly that spectra from the model are well behaved, and evolve systematically rather than randomly. It also explains some of the success of the original DIA, because the DIA appears similarly representative throughout time and fetch limited wave field evolution. Neither of these observations are new.

Second, the optimum parameters appear to display bifurcation behavior, with preferred values of λ of approximately 0.16 and 0.20. To the knowledge of the present author, such behavior has not been observed before in this context. At least two potential sources can be identified for this behavior. First, nonlinear optimization is typically more complicated than optimization for linear systems. The bifurcation behavior might well indicate that there are several local error minima, where the search process 'randomly' selects from these minima. Second, there may in fact be truly different solutions for different spectra due to the highly nonlinear nature of the interactions considered here.

Third, preferred values of λ of about 0.16 or 0.20 are systematically lower than previously used values in third generation wave models ($\lambda = 0.25$). These findings are nevertheless supported by previous Japanese results, where $\lambda = 0.19$ was found as the optimum value for a single DIA (see, e.g., Hashimoto and Kawaguchi, 2001).

Figure 6.1 does not address the quality of the fitted DIAs. In a quantitative sense, this will be addressed with full model integration in the following subsection. A qualitative assessment is presented with example spectra from the time and fetch limited tests is presented in Figs. 6.3 and 6.4. These figures present the

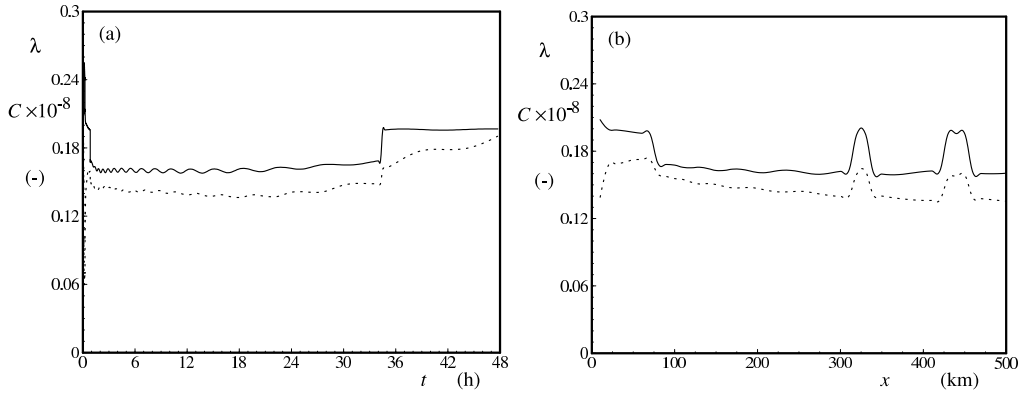

Fig. 6.1 : Optimized parameters for a DIA with a quadruplet defined by λ only for the idealized time (t) and fetch (x) limited tests (panels a and b, respectively). Solid lines: optimum λ. Dotted line: optimum C.

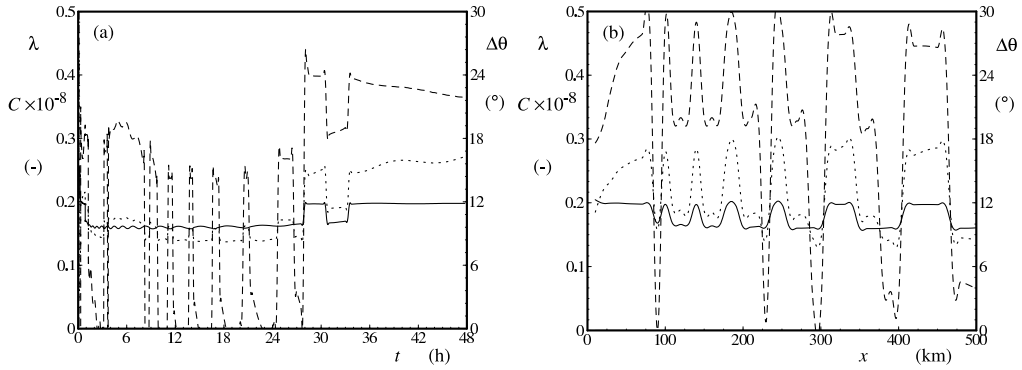

Fig. 6.2 : Like Fig. 6.1 for a DIA with a quadruplet defined by λ and $\Delta\theta$. Dashed lines: optimum $\Delta\theta$.

exact (WRT) solutions, the original DIA, and this DIA with optimized C, and the optimized DIA corresponding to Fig. 6.1.

A comparison of the different panels in Figs. 6.3 and 6.4 indicates that the optimization of λ and C simultaneously (panels e) results in a much better representation of S_{nl} for frequencies around or below the spectral peak than is obtained with the traditional setting of $\lambda = 0.25$ (panels c). Nevertheless, systematic errors in S_{nl} remain at frequencies above the spectral peak frequency. The most obvious shortcoming is the presence of a spurious positive peak just above the spectral peak frequency. Note that this does not necessarily imply that this DIA will result in unrealistic spectra. It will nevertheless be expected, that this will result in systematic errors in spectral shapes.

Similar optimization results for the DIA with two free parameters defining the quadruplet (λ, $\Delta\theta$) are presented in Fig. 6.2. Optimized values for λ and C follows the results of the more simple model presented above, in terms of

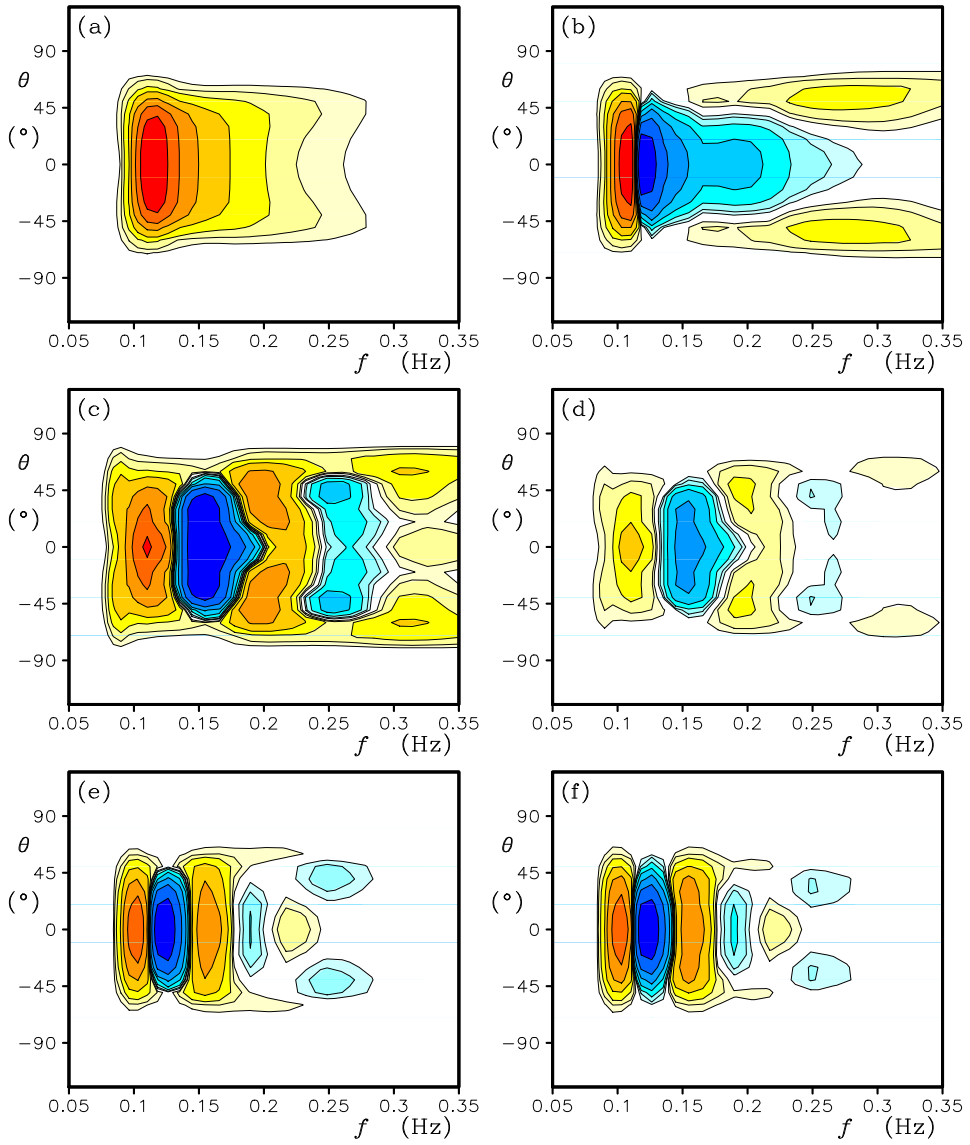

Fig. 6.3 : Example spectrum and source terms for time limited test at $t = 9h$. (a) Spectrum. (b) Exact interactions (WRT). (c) Original DIA. (d) DIA with optimized C. (e) DIA with optimized λ and C. (f) DIA with optimized λ, $\Delta\theta$ and C. Legend as in Fig. 3.1.

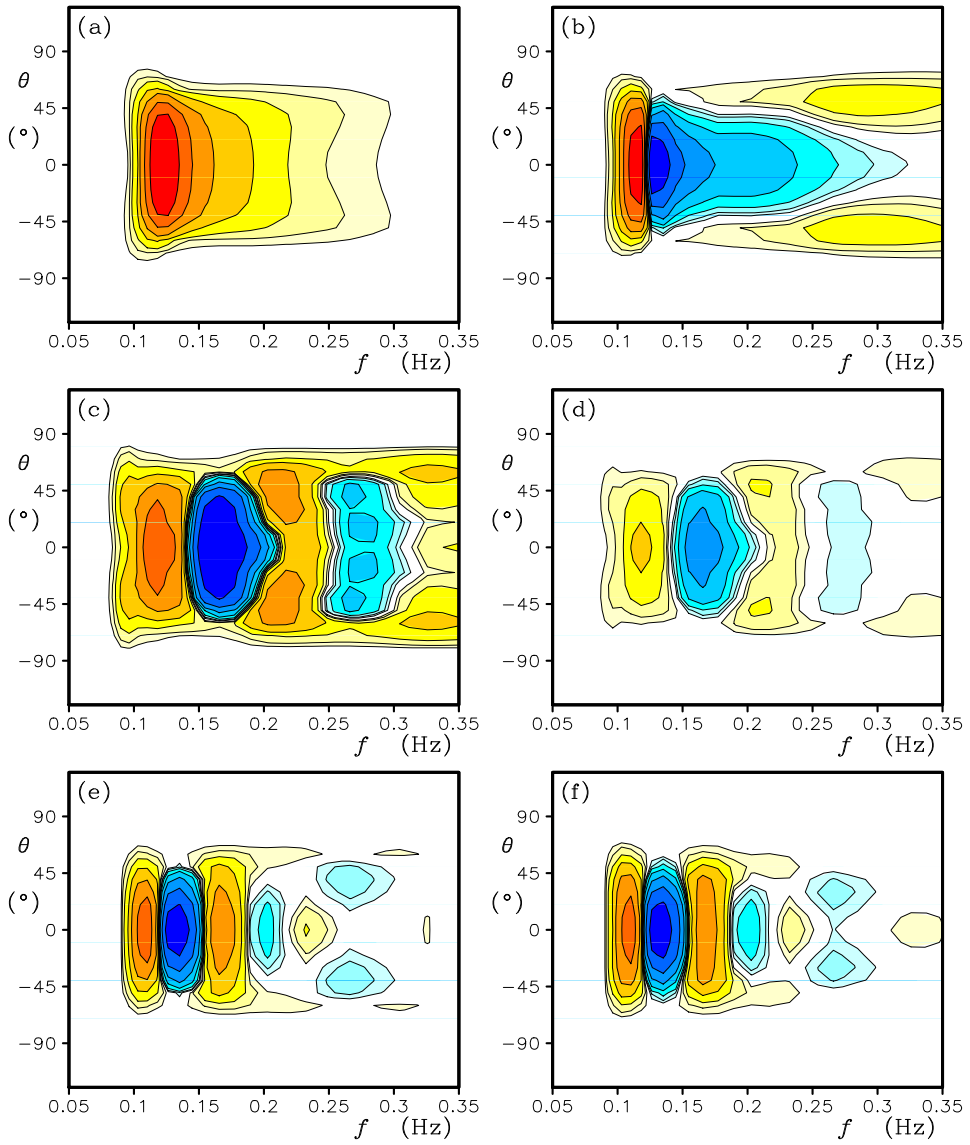

Fig. 6.4 : Like Fig. 6.3 for fetch limited tests at $x = 150km$.

the bifurcation behavior and optimum values. The directional gap $\Delta\theta$ shows a more complicated bifurcation behavior with several preferred directions. If is also noteworthy that the optimum values for $\Delta\theta$ between time and fetch limited cases are not fully consistent.

Unfortunately, the accuracy gained by adding the parameter $\Delta\theta$ to the optimizations has been very limited. For practical purposes, there is no difference, as is illustrated in Figs. 6.3 and 6.4. Due to the nonlinearity, this conclusion cannot be ported automatically to the complete wave model. For this reason, both the one and two parameter quadruplet layouts will be considered for full model optimization in the following subsection.

6.2 Full model optimization.

Full model optimization assesses the performance of DIA approaches in the time and fetch limited test cases as presented in Section 2.4. Considered will be 48 hourly spectra from the time limited wave growth test, starting with the spectrum after 1 h of model integration, and all 50 spectra at the ending time (24 h) of the fetch limited test case. Five error measures are considered, representing the wave height (ϵ_H), the one and two dimensional spectra (ϵ_{E1} and ϵ_{E2}), and the one and two dimensional steepness spectra (ϵ_{s1} and ϵ_{s2}). The steepness spectra S are defined as $S = k^2 E$, where E is the energy or variance spectrum. These error measures are internally normalized to give similar weight to conditions along the growth curve, and are presented in detail in Appendix B.

For the original two parameter DIA, it is feasible to map the errors in the DIA parameter (λ, C) space. Such an exercise is useful to identify the potential existence of multiple minima, and to address the general integration stability of such a DIA as a function of λ and C. This is achieved by computing all error measures for λ ranging from 0.12 to 0.30 at intervals of 0.005, and C ranging from $0.9\,10^7$ to $4.0\,10^7$ at intervals of $0.1\,10^7$. The resulting error distributions in the (λ, C)-space are presented in Figs. 6.5 and 6.6 for the time and fetch limited test, respectively.

Errors in both figures are presented as percentages. The wave height errors are internally normalized with the instantaneous and local reference wave height, and hence can be interpreted as an average relative wave height error for the test case considered. The spectral energy measures are similarly normalized. Hence, ideally all errors would be in the single digit percentage range. For the wave heights, such behavior can be achieved, with minimum errors for the time limited growth of the order of 5% (Fig. 6.5a), and for the fetch limited growth of less than 1% (Fig. 6.6a). For the spectral measures, however, relative errors are much larger, and are of the order of 100% for the energy spectra, and of the order of 30% for the steepness spectra, Note that one- and two dimensional spectral errors for either energy or steepness behave largely identical. The above indicates that

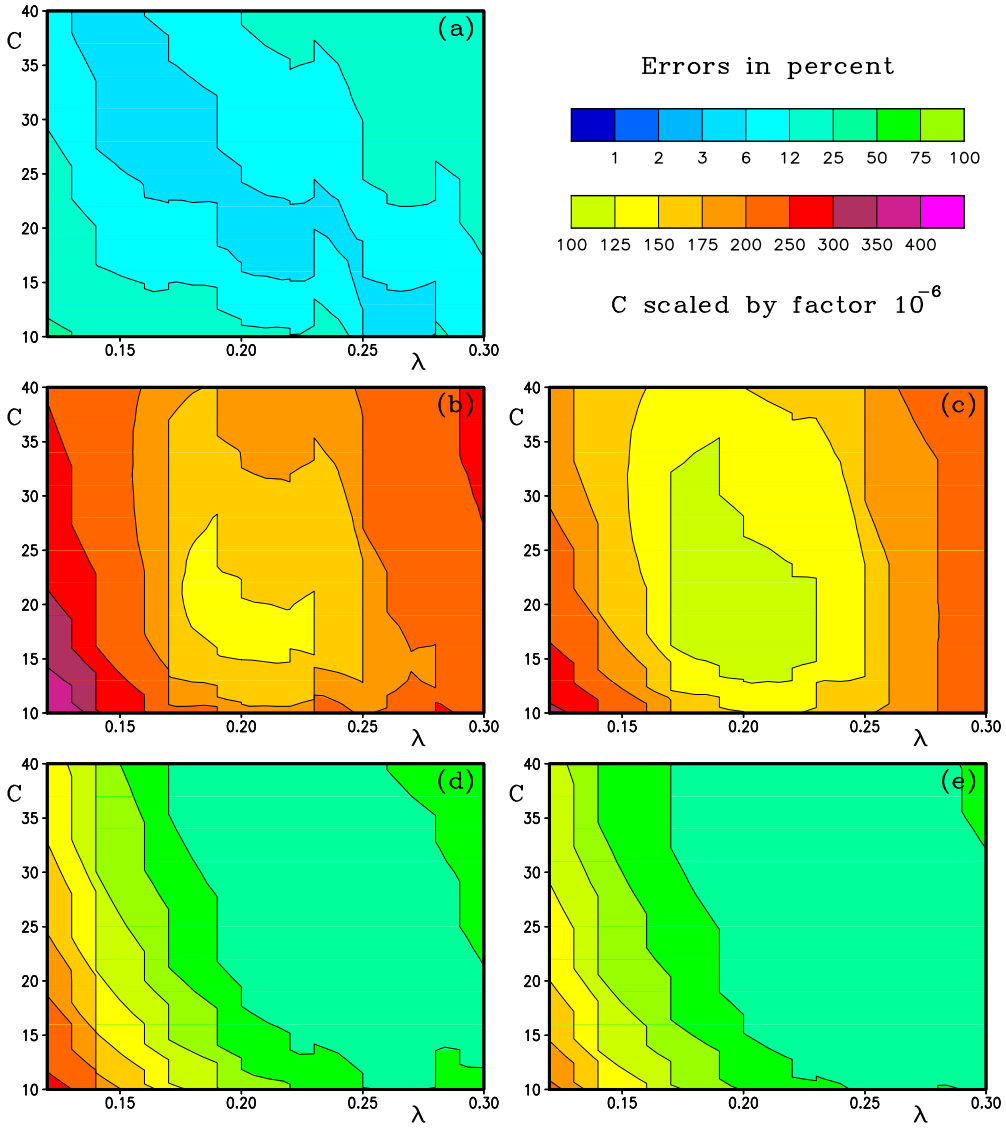

Fig. 6.5 : Model integrations errors for two parameter DIA (λ, C) for the time limited test case as a function of λ and C. (a) Wave height (ϵ_H). (b) 1-D spectrum (ϵ_{E1}). (c) 2-D spectrum (ϵ_{E2}). (d) 1-D steepness spectrum (ϵ_{s1}). (e) 2-D steepness spectrum (ϵ_{s2})

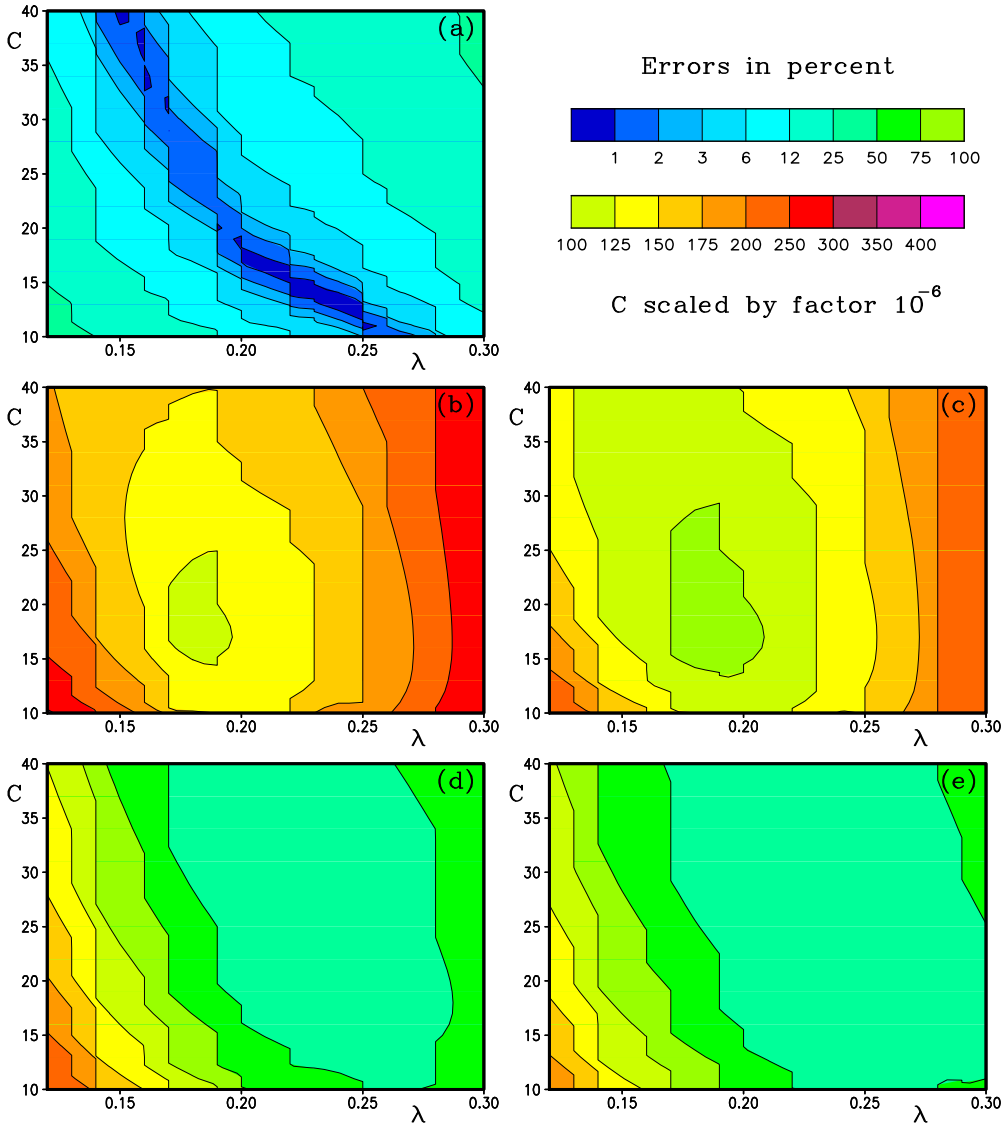

Fig. 6.6 : Like Fig. 6.5 for fetch limited test case.

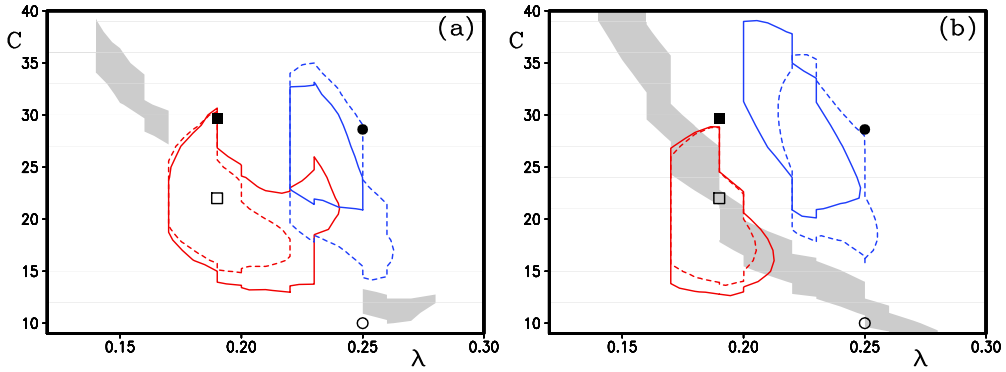

Fig. 6.7 : Composite of error measures for two parameter DIA as a function of λ and C. Areas in parameters space are shown where the model error is less that 1.1 times the minimum model error or 2% for the given parameter. Shaded area: wave heights. Solid lines: one dimensional spectra. Dashed lines: two dimensional spectra. Red: energy spectra. Blue: steepness spectra. (a) Time limited test. (b) Fetch limited test. 2% error threshold used for wave heights in panel (b) only. Symbols correspond to (λ, C) combinations from Table 6.1.

the traditional two-parameter DIA is capable of reproducing the integral spectral energy during wave growth accurate, but that this is accompanied by significant errors in the spectral shape.

Figures 6.5 and 6.6 indicate that there is a large area in (λ, C)-space for which near optimum wave heights can be obtained. This implies that optimization by search algorithms rather than be mapping of the full error space is likely to result in significantly different optimum parameter setting for different initializations of the search algorithm. It also is at least tentatively in accordance with the bifurcation behavior of the optimization for single interactions as identified above.

Another apparent feature of Figs. 6.5 and 6.6 is that the areas of near-optimum model behavior with respect to the different error measures do not coincide. This is illustrated more clearly in Fig. 6.7, which identifies areas in (λ, C)-space where the different error measures are less than 10% larger than their optimum value, or less than 2% in general. Optimal areas for the wave height and spectral spectral energy nearly coincide (gray areas and red lines). This indicates that the total energy and the energy distribution in general can be optimized simultaneously. The steepness spectra, however, (blue) lines show optimum behavior in a distinctly different part of parameter space. This implies that the high-frequency part of the spectrum, on which the steepness error measures focus, cannot be optimized simultaneously with the total energy or the spectral peak energy (on which the spectral energy error measures focus). This is furthermore illustrated in Table 6.1, which present resulting errors for several previously suggested pa-

Table 6.1: Model errors for DIA with setting according to Hasselmann et al. (1985, HHAB), Tolman and Chalikov (1996, TC), Hashimoto and Kawaguchi (2001, HK) and from present study. First line per entry represents errors of time limited test, second represents errors of fetch limited test.

Source	λ (-)	C (-)	ϵ_H %	ϵ_{E1} %	ϵ_{E2} %	ϵ_{s1} %	ϵ_{s2} %
HHAB	0.25	$3.00\,10^7$	12.9	193	165	33.6	34.0
			13.0	180	148	34.0	32.2
TC	0.25	$1.00\,10^7$	6.4	195	169	53.6	43.2
			2.2	182	152	50.9	41.7
HK	0.19	$2.97\,10^7$	6.1	158	120	42.0	42.2
			4.4	137	104	39.2	39.3
present	0.19	$2.20\,10^7$	5.1	145	110	54.9	49.4
			1.0	124	94	50.2	46.6

rameter settings for this DIA, as well an near-optimal choice for both wave heights and energy spectra as follows from the previous figures.

To illustrate the nature of the model errors introduced by the DIA, model results obtained with the parameter setting of Table 6.1 are compared to the reference (WRT) model results in Figs. 6.8 through 6.12.

Figure 6.8 present the resulting wave heights. For the HHAB parameter settings, the wave heights H_s are systematically underestimated. For the other three model setting, the resulting wave height represent the reference results excellently. Particularly interesting is the deviation of all DIA based wave heights from the reference wave height (solid line) after about 30 h of model integration in Fig. 6.8a. This appears to indicate that near full development of the wave spectrum, the dominant scales in the exact interaction change. Because the scales of the interactions in spectral space are fixed by the choice of λ the DIA in principle cannot reproduce this type of behavior. Note that in the fetch limited test such wave conditions may not yet have appeared at the largest fetch, and that the lack of this behavior in the fetch limited test is likely a result of limited fetches considered. Note furthermore, that this behavior might be alleviated by dynamically adjusting the parameter setting in the DIA as a function of the development stage of the spectrum. This refinement of the DIA will not be considered in the present study.

Figure 6.8 also leads to an interesting observation; if the interactions are made weaker by reducing C, the resulting wave heights become higher. This was confirmed with additional example computations, the result of which are not reproduced here. This may seem paradoxical, because weaker interaction result

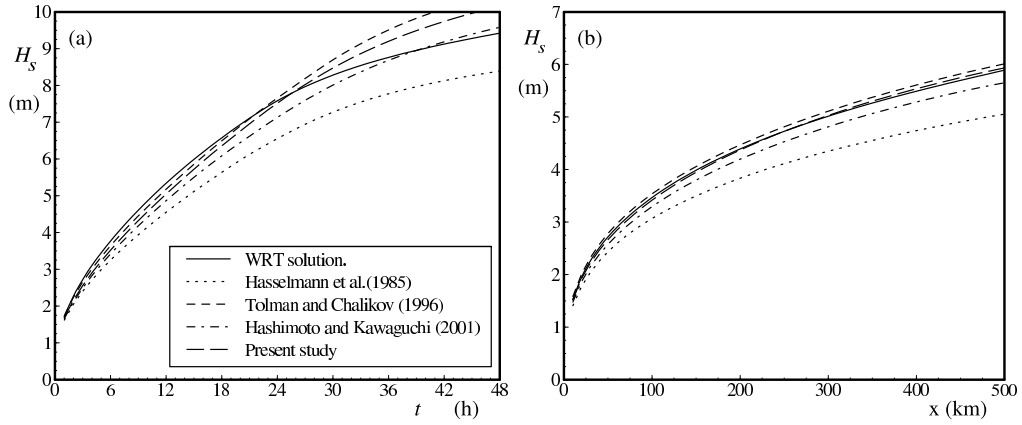

Fig. 6.8 : Wave height H_s for (a) time limited test as a function of time t and (b) for fetch limited test as a function of fetch x for the WRT model solution and various settings of the two parameter DIA as identified in the legend and in Table 6.1.

in a slower shift of energy to low frequencies. However, after initial energy shifts to lower frequencies, local wind input will become dominant. Stronger interactions, however, also includes a larger flux of wave energy to high frequencies, where this energy is dissipated. This at least qualitatively explains this somewhat paradoxical behavior.

Figures 6.9 and 6.10 present one dimensional energy and steepness spectra after 24 h in the time limited test and at 300 km in the fetch limited test, respectively. Inspection of all test spectra indicates that these selected spectra are representative for all spectra. This is illustrated here by the similar model behavior both figures.

All DIA based models systematically underestimate the peak energy density of the spectrum from the reference run (solid lines). The HHAB parameter settings combine this with a general underestimation of the wave energy and hence of the wave height in the previous figures. The other parameter settings compensate for the lack of energy at the spectral peak by overestimating the wave energy at high frequencies. The TC parameter settings (short dashed lines) furthermore spuriously shift the spectral peak frequency to higher frequencies, although energy at frequencies just below the spectral peak are well represented. The steepness spectra (right panels of figures) indicate that the selection of the parameter settings in the DIA has a large impact on the high-frequency energy.

Finally, Figs. 6.11 and 6.12 represent the two dimensional wave spectra corresponding to Figs 6.9 and 6.10. Again, the fetch and time limited results are very similar. All DIA approaches underestimate the spectral energy at the spectral peak. The HHAB model settings (panels b) combine this with a moderate underestimation at higher frequencies, whereas the other three overestimate wave en-

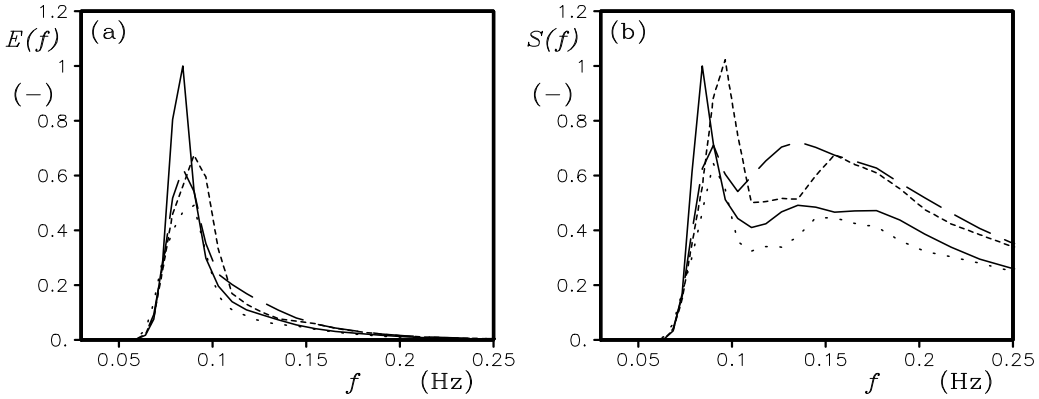

Fig. 6.9 : One dimensional spectrum $E(f)$ (panel a) and steepness spectrum $S(f) = k^2E(f)$ for the time limited test after 24 h. Legend as in Fig. 6.8. Spectra normalized with maximum value for WRT results. HK results not presented for clarity.

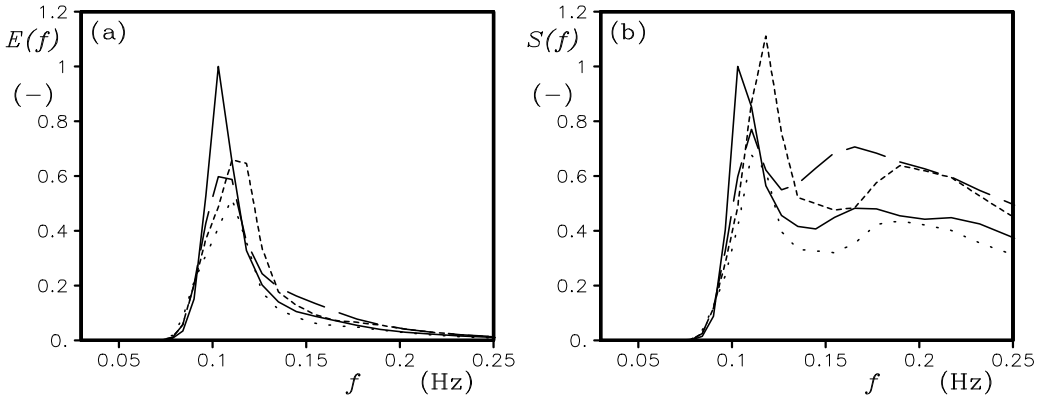

Fig. 6.10 : Like Fig. 6.9 for fetch limited test at 300 km.

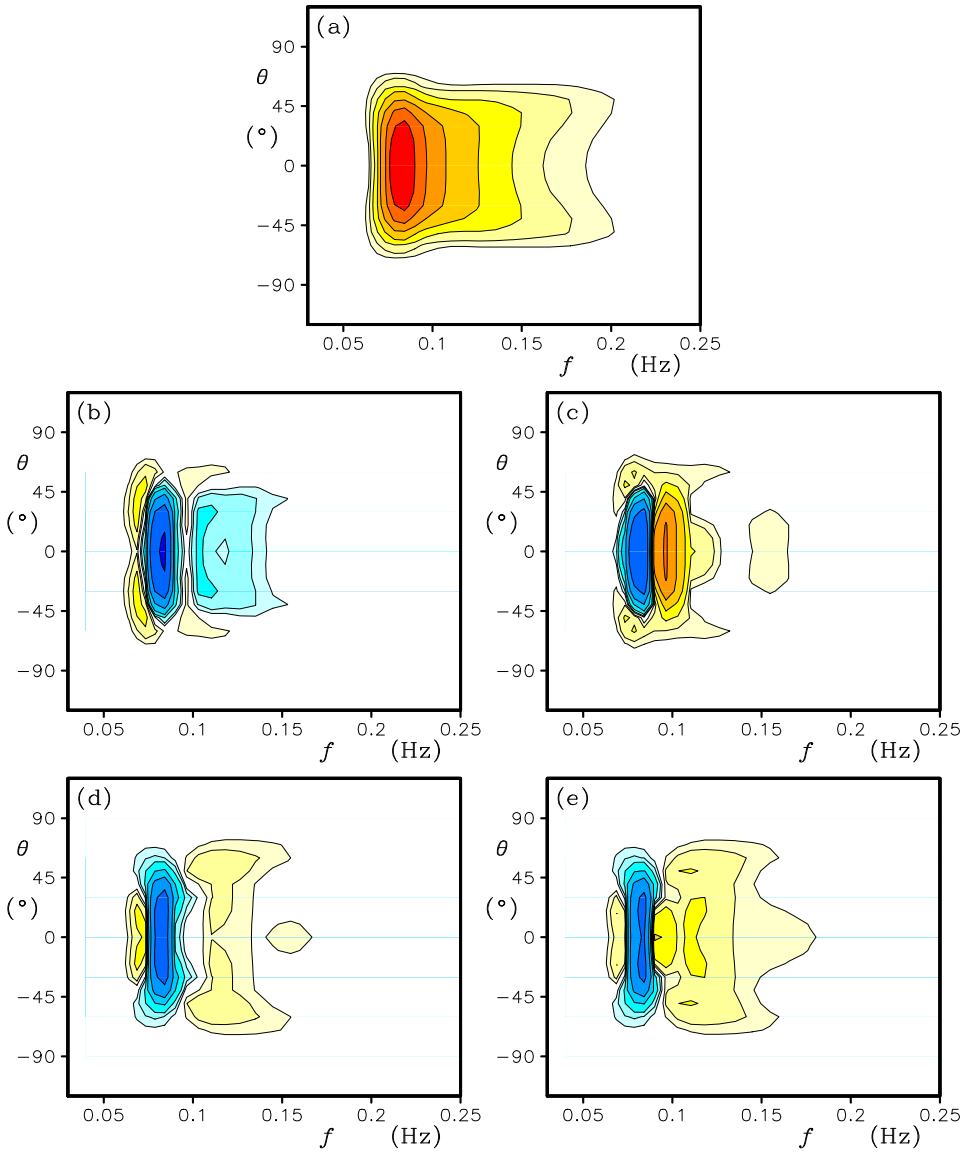

Fig. 6.11 : (a) Reference spectrum (WRT) after 24 from time limited test, and differences with results for (b) HHAB, (c) TC, (d) HK, and (e) 'present' model runs (see Table 6.1). Contours at factor 2 interval with highest contour at 0.5 times the maximum spectral energy density. Blue shading identifies negative differences. Differences defined as WRT - DIA results.

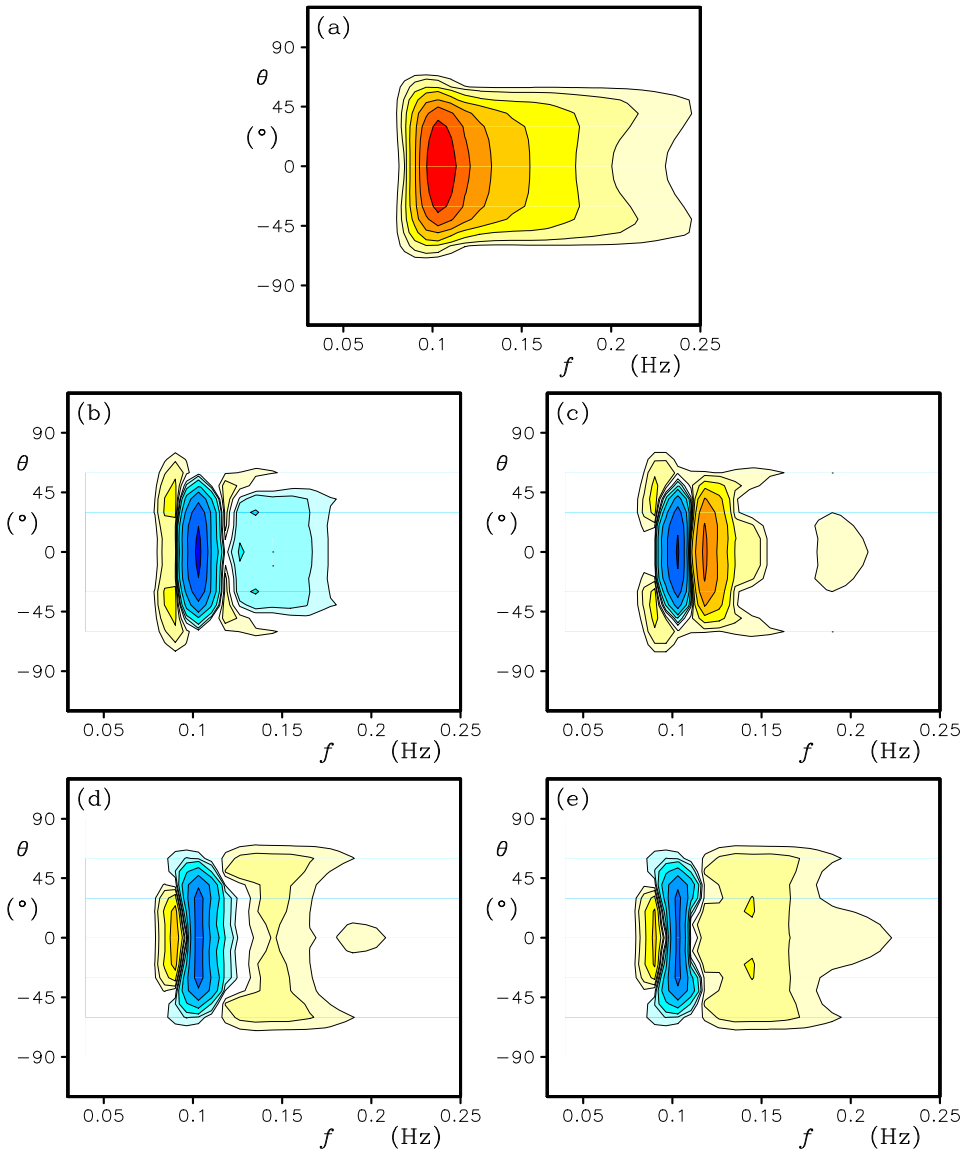

Fig. 6.12 : Like Fig. 6.11 for fetch limited test at 300 km.

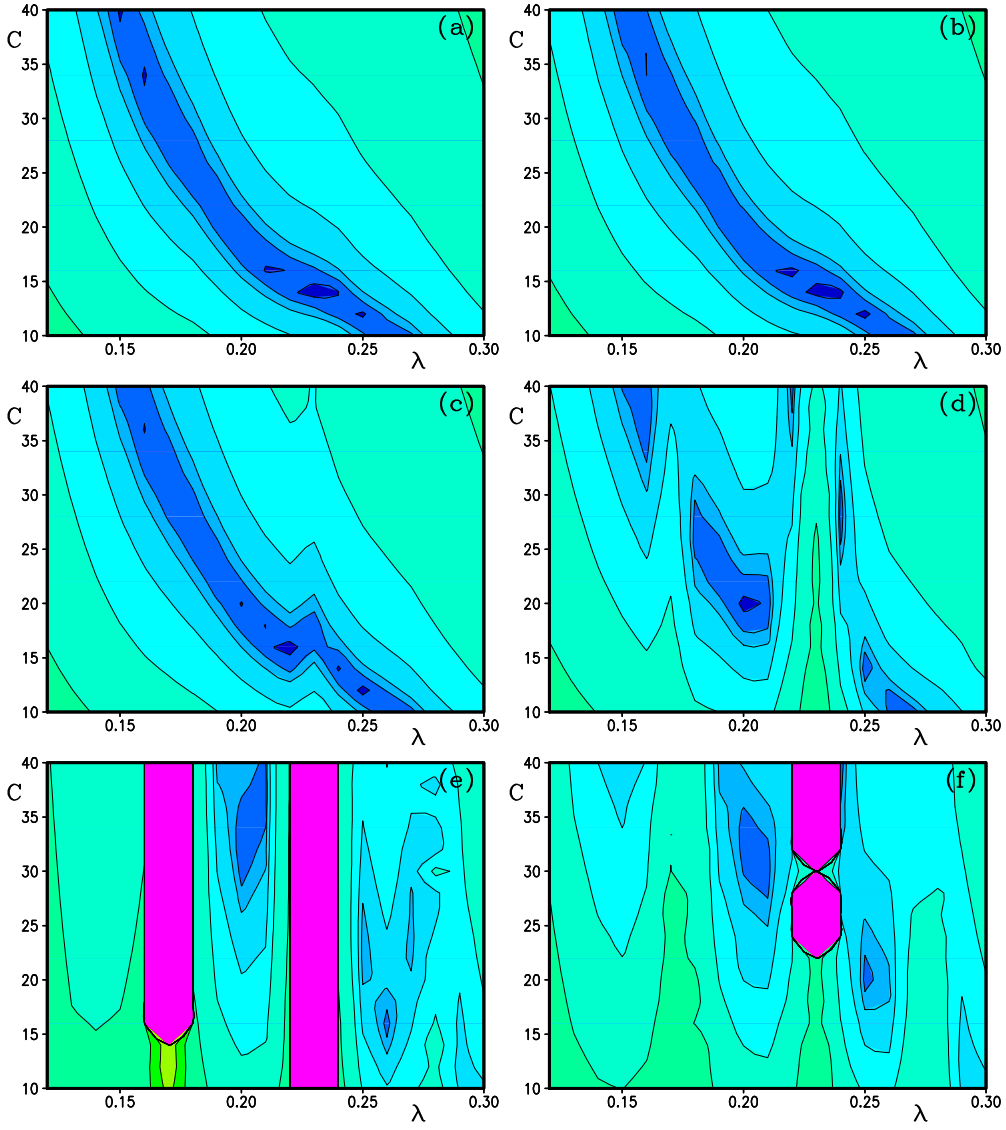

Fig. 6.13 : Wave height error ϵ_H for the fetch limited test for the three parameter DIA as a function of λ and C for (a) $\Delta\theta = 0°$, (b) $\Delta\theta = 2°$, (c) $\Delta\theta = 4°$, (d) $\Delta\theta = 6°$, (e) $\Delta\theta = 8°$, and (f) $\Delta\theta = 10°$. Legend as in Fig. 6.5. C multiplied by 10^{-6}.

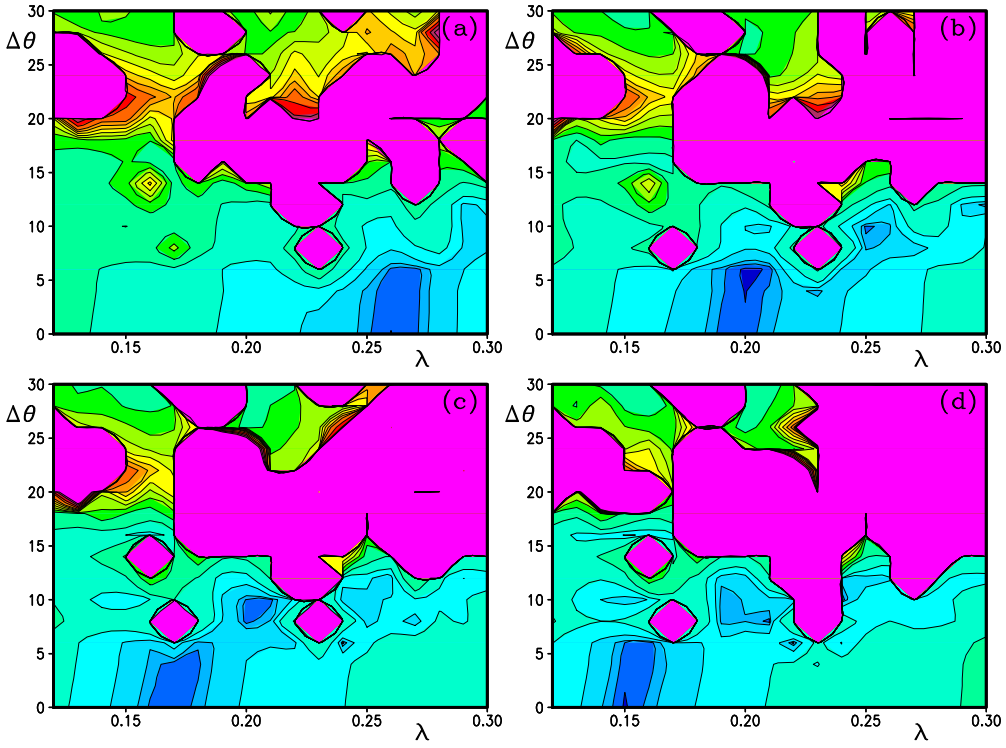

Fig. 6.14 : Like Fig. 6.13 as a function of λ and $\Delta\theta$ for (a) $C = 1\,10^7$, (a) $C = 2\,10^7$, (a) $C = 3\,10^7$, and (a) $C = 4\,10^7$.

ergy at higher frequencies. The TC model settings show a clear positive-negative signature near the spectral peak, indicating a spurious shift of the spectral peak to high frequencies.

For the three parameter DIA, the parameter space is also of sufficiently low dimensionality to attempt to map the errors in the $(\lambda, \Delta\theta, C)$ space. For economical reasons this is done on a coarser resolution than for the two parameter DIA. Error measures are computed for λ ranging from 0.12 to 0.30 at intervals of 0.01, $\Delta\theta$ ranging from 0° to 30° at intervals of 2°, and C ranging from $1.0\,10^7$ to $4.0\,10^7$ at intervals of $0.2\,10^7$. Some resulting error distributions for the wave height (ϵ_H) are presented in Figs. 6.13 and 6.14 for the fetch limited test.

Figure 6.13 shows the wave height error in the (λ, C) plane for the lowest 6 discrete values of $\Delta\theta$. Panel (a) corresponds to Fig. 6.6a. Differences between these two figures are solely due to the reduced discrete resolution in Fig. 6.13. With increasing $\Delta\theta$, extremely large wave height errors (purple) develop. These areas correspond to instability in the model integration. Thus, whereas the three parameter DIA suggested in this study can result in stable model integration, it lacks the robustness of the conventional two parameter DIA. This is furthermore

illustrated in Fig. 6.14, which shows error distributions in the $(\lambda, \Delta\theta)$ plane, for several values of C. This lack of robustness is generally unacceptable in practical model applications. This is particularly true because it is suspected that the robustness is sensitive to the discretization of the spectral domain, although this has not been tested in the present study.

6.3 Conclusions.

The holistic approach to optimizing interaction parameterizations has resulted in the following conclusions for the conventional two parameter (λ, C), single component DIA:

1) This type of DIA can reproduce idealized fetch and time limited wave heights accurately for a range of values of λ and C. It does, however, not capture the apparent transition to other dominant interaction scales near full development.

2) This type of DIA cannot accurately describe the spectral shape of either the two or one dimensional spectrum. A systematic problem appears to be the underestimation of the sharpness of the spectral peak.

3) The wave height and energy spectra can be optimized simultaneously. The steepness spectra, however, are optimally represented for values of λ and C where significant wave height and spectral errors occur.

4) The present DIA settings as used in WAVEWATCH III (Tolman and Chalikov, 1996) systematically shift the spectral peak to higher frequencies. Modeling impacts of this behavior will be discussed in Section 8.

The same optimization approach has been applied to the new three parameter DIA, where λ, $\Delta\theta$ and C are free parameters. Whereas this approach can be used successfully, it was shown to lack the desirable robustness. Similar conclusions were found for another three parameter DIA (λ, μ, C) in Part 1. With this in mind, it appears that more generalized single component DIAs as suggested by, for instance Van Vledder (2001, 2002a) and in previous parts of this study, are not viable in practical wave models.

In Part 1, a variable DIA was suggested. Considering that the results of Part 1 indicate that it is crucial to extend the DIA to a three parameter DIA to successfully improve interactions for individual spectra, it does not appear likely that a VDIA based on the traditional two parameter approach will result in a relevant improvement of the model results. Because, furthermore, the three parameter DIA appears unfeasible, the VDIA will not be investigated in more detail here. Consequently, the following section will immediately concentrate on the multiple DIA (MDIA).

7 MDIA optimization

The general strategy for testing and optimizing MDIAs in broad lines follows the approach for single component DIAs in the previous section. First, optimization of parameters for individual spectrum-source term pairs is considered to establish expected ranges of parameter values and general approaches. After that, the holistic approach, optimizing the overall model results, is employed. The latter optimization is more complicated than in the previous section, because the inherent number of free parameters in the MDIA prohibits brute-force mapping of errors in parameter space. The inability to map errors in the full parameter space, combined with the finding that not all DIAs result in stable model integration, requires that the stability of the optimized MDIAs has to be addressed explicitly.

7.1 Optimization for individual spectra.

As in the previous section, the behavior of an optimal MDIA is first assessed with the help of optimal parameter setting for individual spectra and the corresponding exact interactions. Again, the results for each grid point at the end of the fetch limited growth case are used. However, for the time limited test, only results at 15 min intervals are used. Optimization again is performed as in Part 1. Part 1 suggests that some MDIA approaches are less likely to be fruitful, for instance, an MDIA based on the traditional one parameter (λ) quadruplet layout. For several reasons, such an MDIA is nevertheless considered here also. First, only this MDIA appears to result in model stability for each of its possible components, and hence should be unconditionally stable too. Second, the convergence behavior of this DIA for the previous parametric spectra might not be representative for model spectra. Third, such an analysis is necessary for obtaining a complete picture of the potential of the MDIA in general.

With this in mind, an MDIA based on the traditional single parameter quadruplet is considered first. For all test spectra, optimum values of λ and C are estimated for each of the N components in the MDIA. The number of components N is increased systematically from 1 through 5. The resulting errors ϵ

$$\epsilon = \left[\int \int \{S(f,\theta) - X(f,\theta)\}^2 \; df \; d\theta \right]^{1/2} \quad , \tag{7.1}$$

where S is the estimated source term and X is the exact source term, are presented in Fig. 7.1. In this figure the errors ϵ decrease with increasing N. Thus the results are ordered naturally with N increasing from top to bottom.

Several observations can be made form this figure. First, most errors show a clear oscillation with either time or fetch. This appears to be related to the actual location of the peak of the spectrum in frequency space relative to the

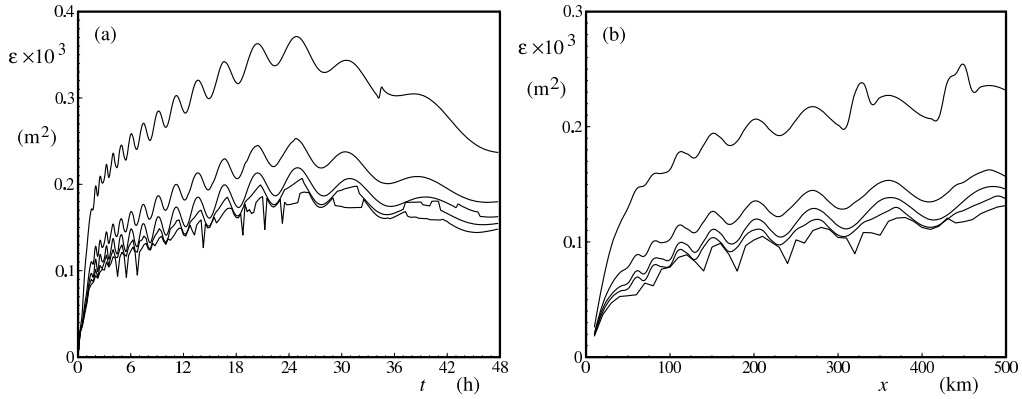

Fig. 7.1 : Error ϵ of optimum MDIA based on single parameter quadruplet (λ) with 1 through 5 components (top to bottom lines) for time limited test at 15 min intervals (panel a) and fetch limited test (panel b).

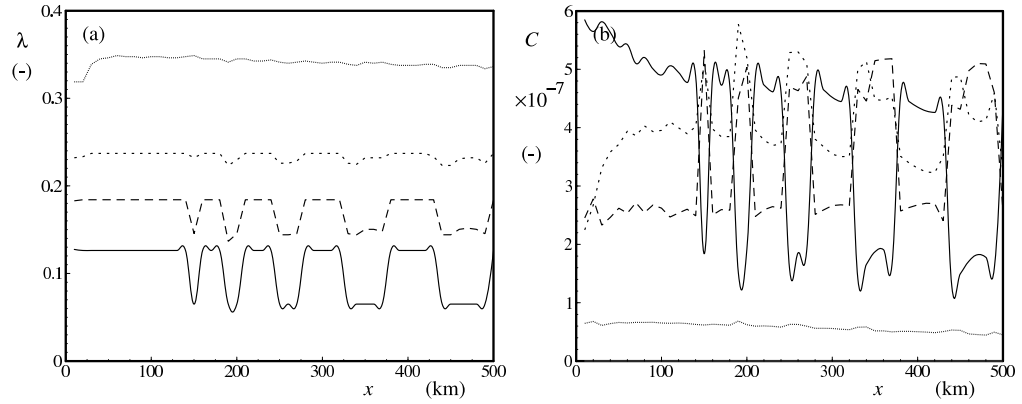

Fig. 7.2 : The optimum values of λ (panel a) and C (panel b) for the fetch limited test case for a four component DIA with a single parameter quadruplet definition (λ).

discrete spectral grid; each oscillation corresponds to the discrete spectral peak shifting by one discrete spectral frequency.

Second, while going from $N = 1$ (top lines in figure) to $N = 2$ (second lines from top) the resulting errors ϵ reduce significantly, typically by about 30 to 40%. Increasing the number components to $N = 3$ systematically reduces the errors by another 10 to 15%, but further increase of N has only small incremental impacts.

Third, for the largest number of components considered ($N = 5$, bottom lines), the oscillatory nature of the errors becomes more erratic, with occasionally significant reductions of the error ϵ.

For this MDIA with up to 4 components, the behavior of the optimum parameters show many similarities with the corresponding single component DIA discussed in the previous section. This is illustrated in Fig. 7.2 with the optimum

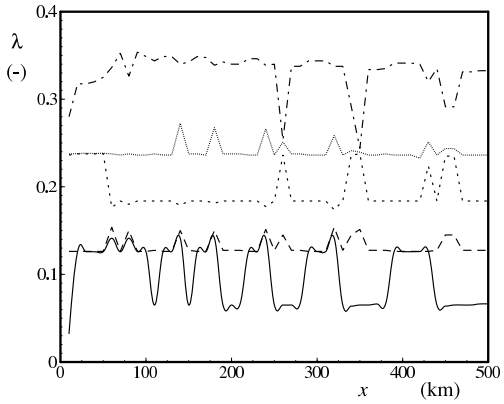

Fig. 7.3 : The optimum values of λ for the fetch limited test case for a five component DIA with a single parameter quadruplet definition (λ).

values of λ and C for this MDIA with $N = 4$. For individual components, λ and C show a bifurcation behavior, but are otherwise well behaved. Furthermore, the values of λ remain well separated, and the bifurcation behavior of individual components occurs simultaneously for λ and C.

When the number of components is increased to $N = 5$, the behavior of the optimum parameters for the MDIA changes systematically, with several components having nearly identical values of λ, as illustrated in Fig. 7.3. This behavior was also observed in Part 1, and is accompanied by values of C that are larger by one or two orders of magnitude, and with opposite signs (not illustrated here, see Part 1). This changing behavior is probably responsible for the changing behavior of the error ϵ (that is, the error behaving more erratic) when going from $N \leq 4$ to $N = 5$ in Fig. 7.1.

An example of the resulting interactions for this MDIA for the time limited growth after 9 h, and for the fetch limited growth at 150 km are presented in Figs. 7.4 and 7.5, respectively. These figures correspond to Figs. 6.3 and 6.4 in the previous section. The first two panels in these figures again present the spectrum and the exact (WRT) interactions. Panels (c) through (f) correspond to the optimum MDIA with the number of components N increasing from 1 to 4. In creasing the number of components from 1 to 2, or from 2 to 3 has a clear positive impact on the quality of the resulting MDIA. Increasing the number of components further to 4 has a minor impact, for both the time and fetch limited cases. Note that there remain clear deficiencies in the optimum MDIA with 3 or 4 components, particularly at frequencies well above the spectral peak frequency.

The logical next step is to address the error behavior and the corresponding optimum source terms for MDIAs with increasingly complex definitions of the quadruplet. The evolution of errors corresponding to Fig. 7.1 for the single component quadruplet are presented in Figs. 7.6 through 7.8 for the two parameters quadruplets $(\lambda, \Delta\theta)$ and (λ, μ), and for the three parameter quadruplet $(\lambda, \mu, \Delta\theta)$,

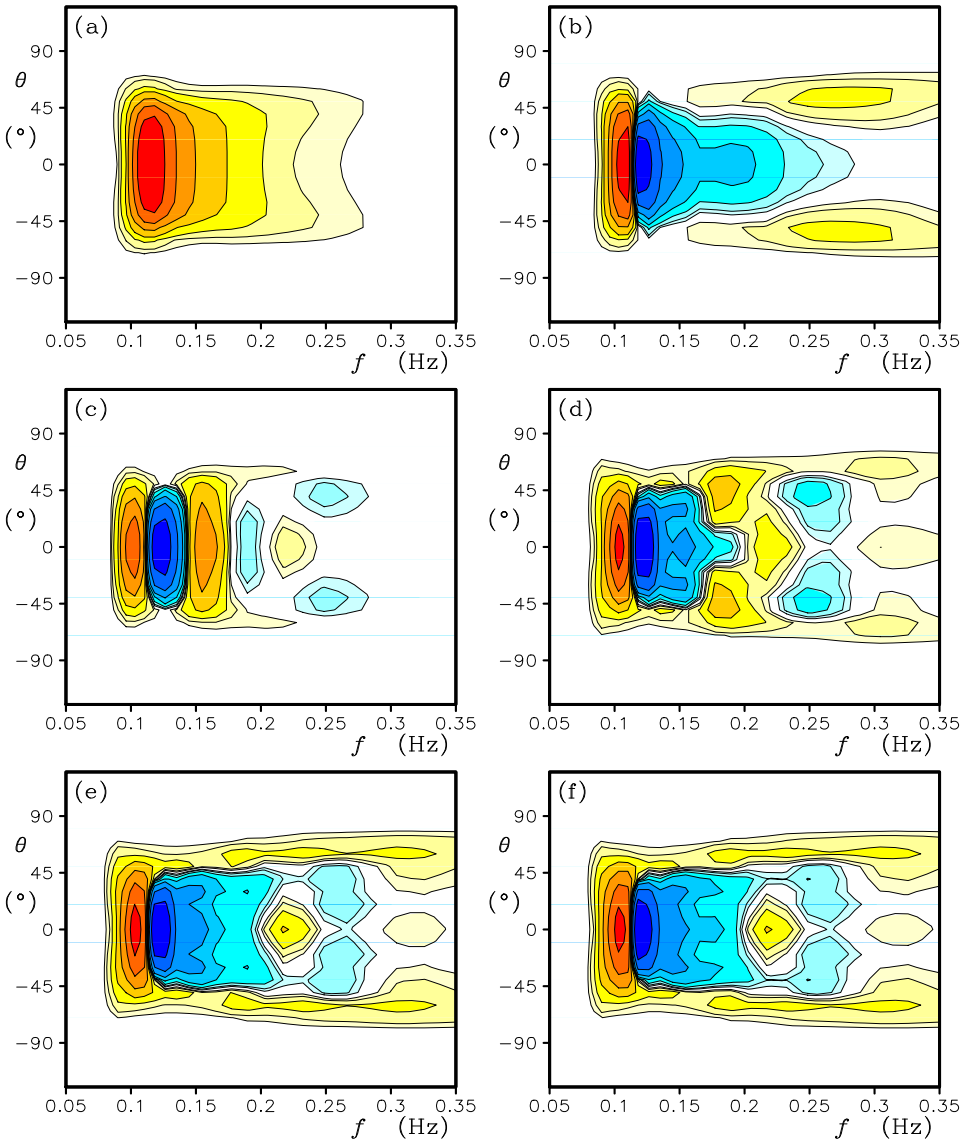

Fig. 7.4 : Example spectrum and source terms for time limited test at $t = 9h$. (a) Spectrum. (b) Exact interactions (WRT). (c-f) MDIA based on single parameter quadruplet (λ) with $N = 1$ through 4, respectively. Legend as in Fig. 3.1. Corresponds to Fig. 6.3.

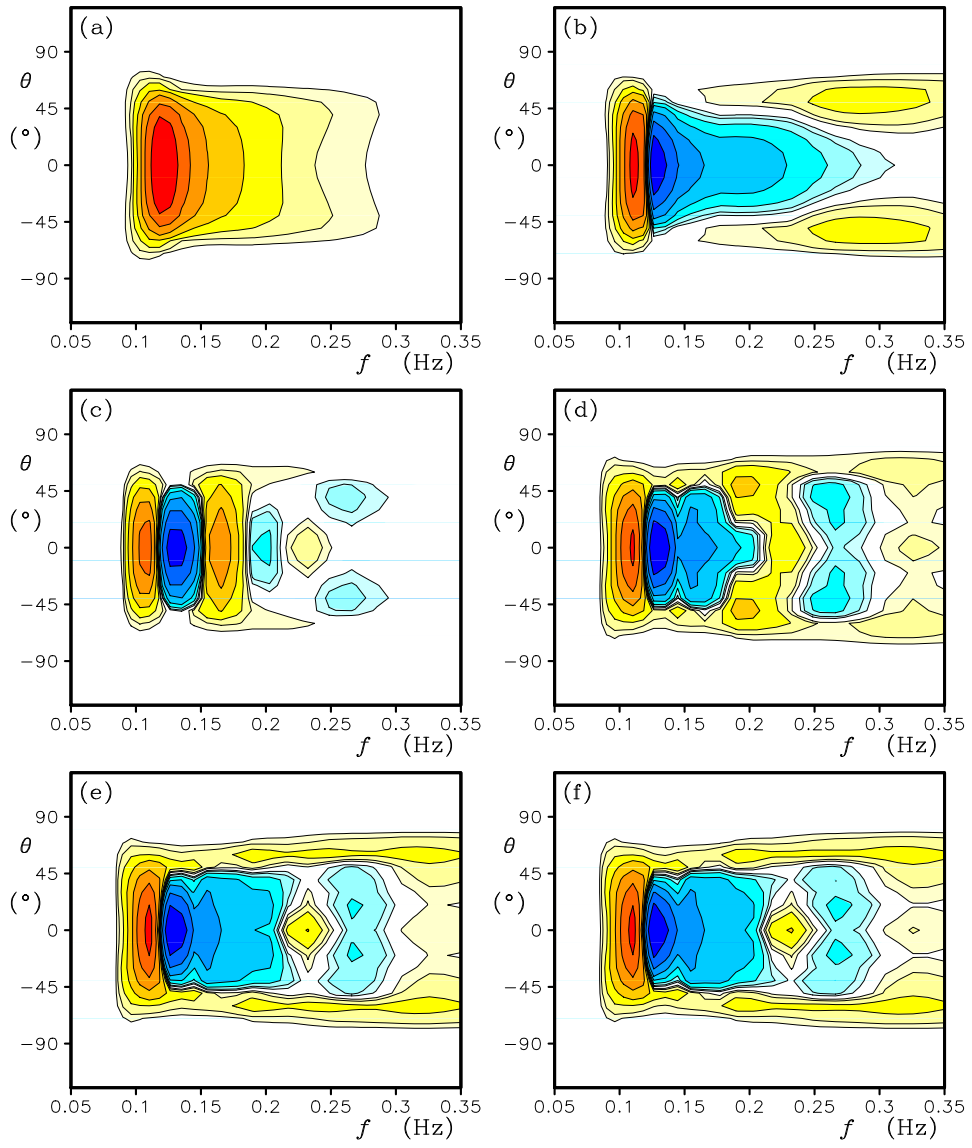

Fig. 7.5 : Like Fig. 7.4 for fetch limited tests at $x = 150$km. Corresponds to Fig. 6.4.

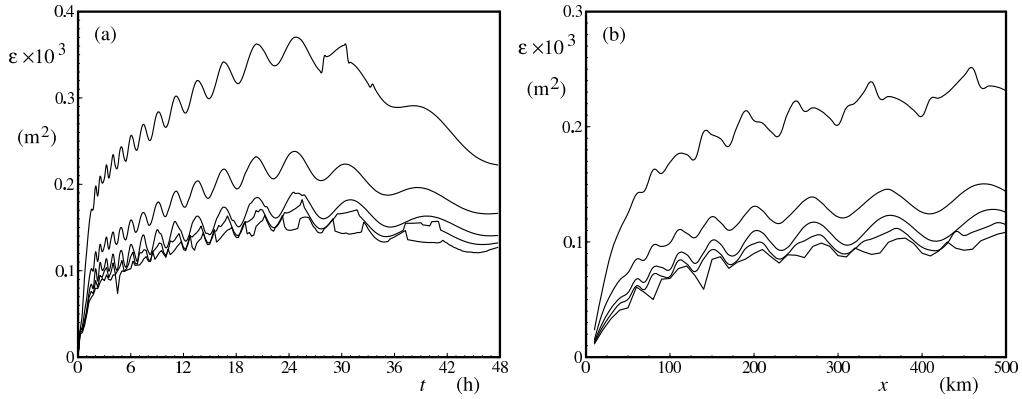

Fig. 7.6 : Like Fig. 7.1 for two parameter quadruplet ($\lambda, \Delta\theta$).

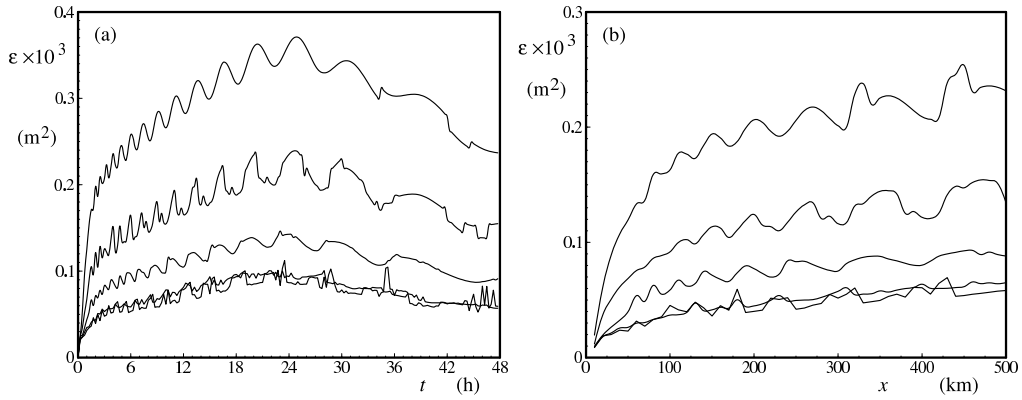

Fig. 7.7 : Like Fig. 7.1 for two parameter quadruplet (λ, μ).

respectively. Corresponding example optimum MDIAs for the time limited test case after 9 h of model integration are presented in Fig. 7.9 through 7.11.

Surprisingly, there is little difference in the resulting errors for all single component optimum MDIAs (top lines in Fig. 7.6 through 7.8, panels (b) in Figs. 7.9 and 7.10). However, the resulting errors for the MDIA with multiple components are clearly improved with the more complex quadruplet definition.

Going from a single parameter (λ) quadruplet (Figs. 7.1 and 7.4) to a two-parameter ($\lambda, \Delta\theta$) quadruplet (Figs. 7.6 and 7.9) has a limited impact. The optimum errors for large N reduce moderately by a approximately 15%. The error structure, as well as the qualitative deficiencies in the example spectra remain largely unchanged (Figs. 7.4 and 7.9).

Going from a single parameter (λ) quadruplet (Figs. 7.1 and 7.4) to a two-parameter (λ, μ) quadruplet (Figs. 7.7 and 7.10) has a more distinct impact. The optimum errors for large N reduce significantly by typically more than 50%. Unlike for previous quadruplet layouts, increasing the number of MDIA components

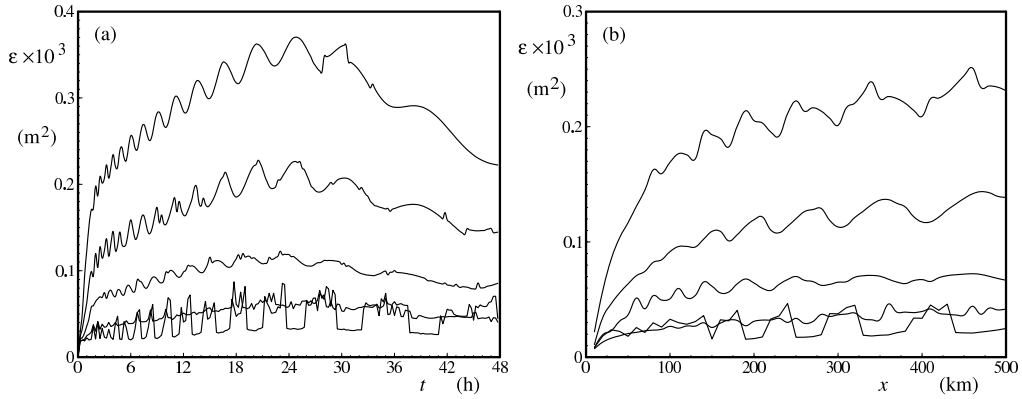

Fig. 7.8 : Like Fig. 7.1 for three parameter quadruplet $(\lambda, \mu, \Delta\theta)$.

to 4 now has a systematic positive impact. Qualitatively, this quadruplet layout improves the performance of the MDIA significantly at high frequencies, albeit at some deterioration of the qualitative behavior near the spectral peak (i.e., the mild reintroduction of the 'horseshoe shape' of the positive lobe as identified in Part 1, present Fig. 7.10).

Going from a single parameter (λ) quadruplet (Figs. 7.1 and 7.4) to a three-parameter $(\lambda, \mu, \Delta\theta)$ quadruplet (Figs. 7.8 and 7.11) improves the fit of the MDIA even more. For $N = 4$, the reduction of the error now is typically 70%, and for about half of the test spectra, $N = 5$ reduces the error by nearly 85%. Figure 7.11 represents one of the cases where using 5 components has a distinct advantage. Both the qualitative and quantitative improvement reached by this MDIA are impressive.

The above results give some direction to the the full model optimization to be performed in the following subsection. Starting with a MDIA based on the traditional single parameter (λ) quadruplet is prudent, considering the established stability of such an approach in model integration. For a two-parameter quadruplet layout, the (λ, μ) quadruplet as introduced in Part 1 appears to have significantly more potential than the $(\lambda, \Delta\theta)$ quadruplet introduced here. This makes the (λ, μ) quadruplet a logical quadruplet to be investigated next. The three parameter quadruplet $(\lambda, \mu, \Delta\theta)$ has even more potential. It should be noted that the expected cost of the implementation of this quadruplet is expected to be nearly identical to that of the (λ, μ) quadruplet, as both require the evaluation of the same number of discrete spectral densities. Thus, although the optimization of the three parameter quadruplet will be more complicated than the optimization of the two parameter quadruplet, it is nevertheless expected that they will result in similar model economies.

It should be noted that in the approach chosen here, the layout of individual

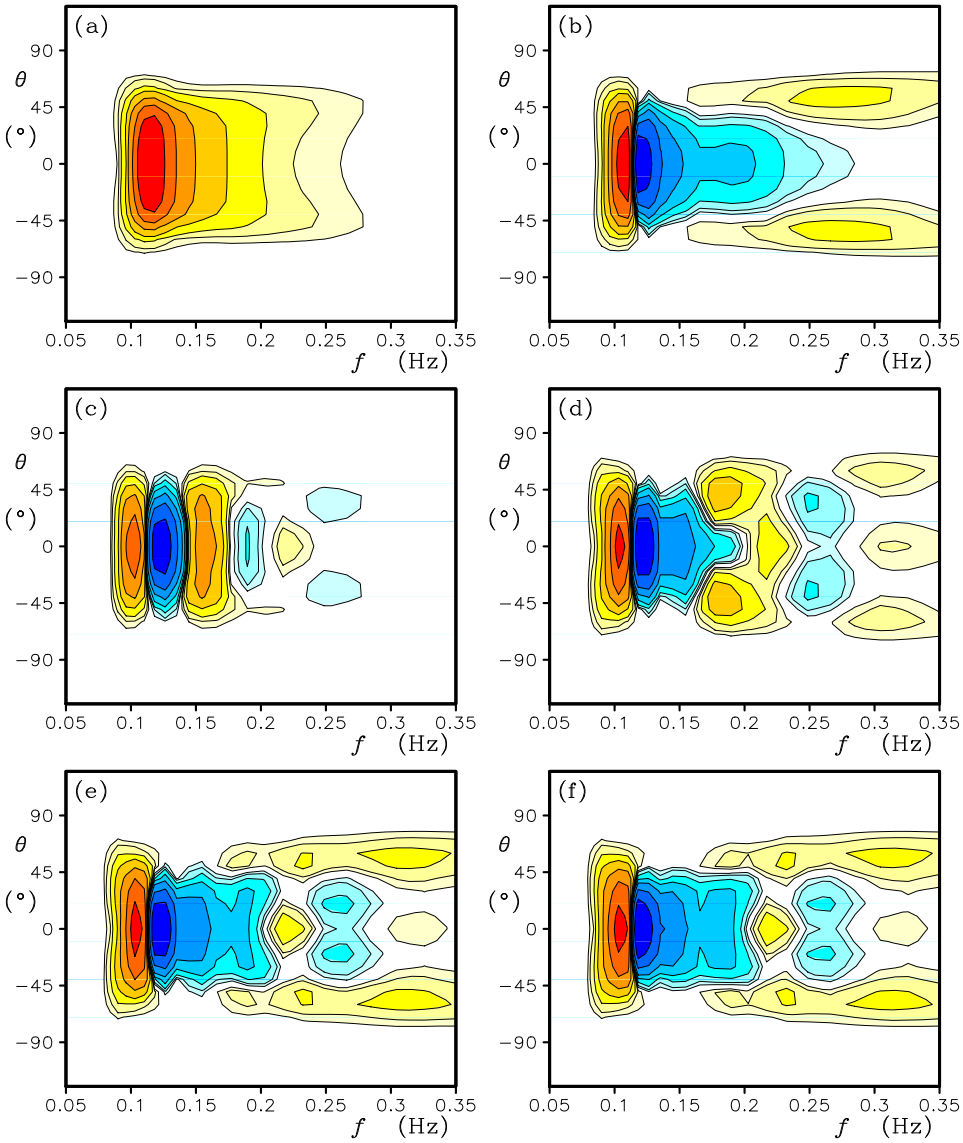

Fig. 7.9 : Like Fig. 7.4 for two parameter $(\lambda, \Delta\theta)$ quadruplet.

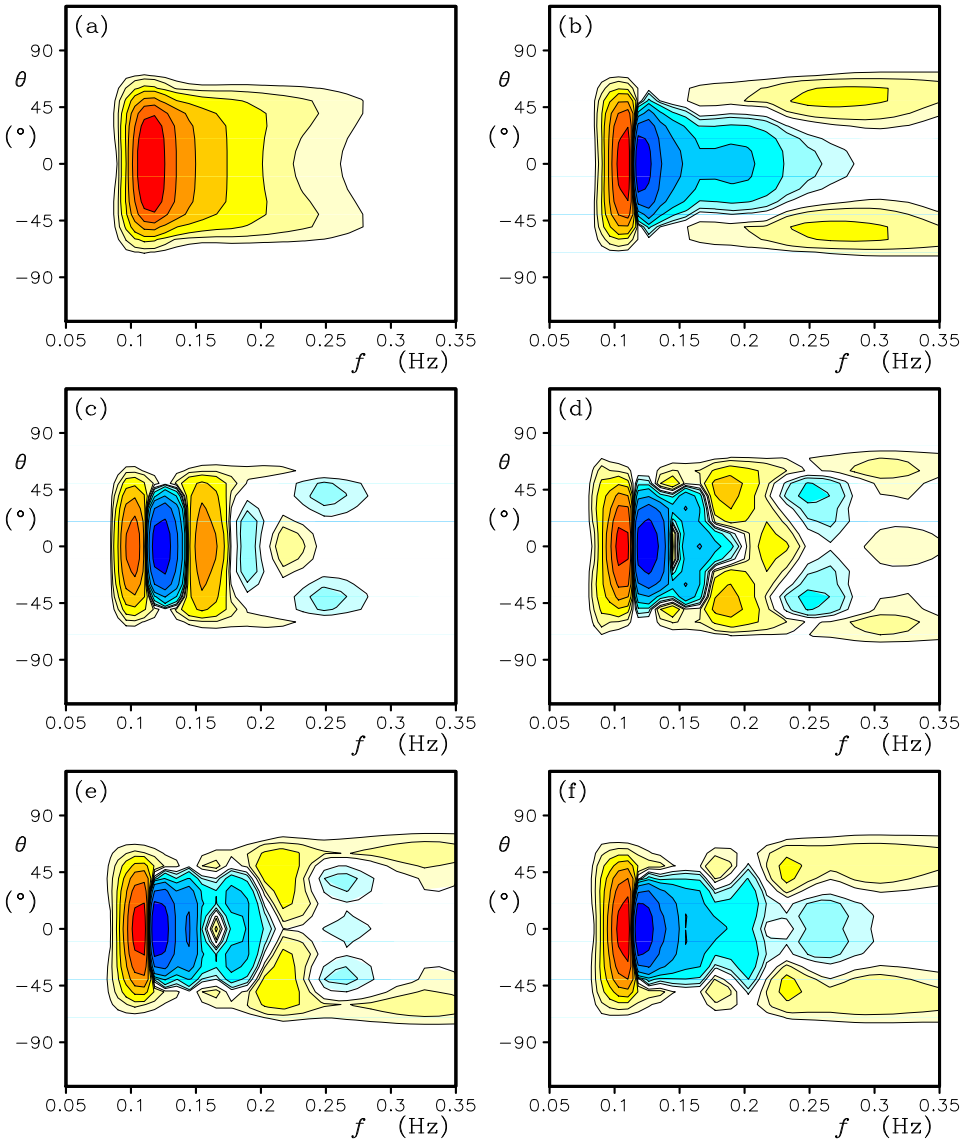

Fig. 7.10 : Like Fig. 7.4 for two parameter (λ, μ) quadruplet.

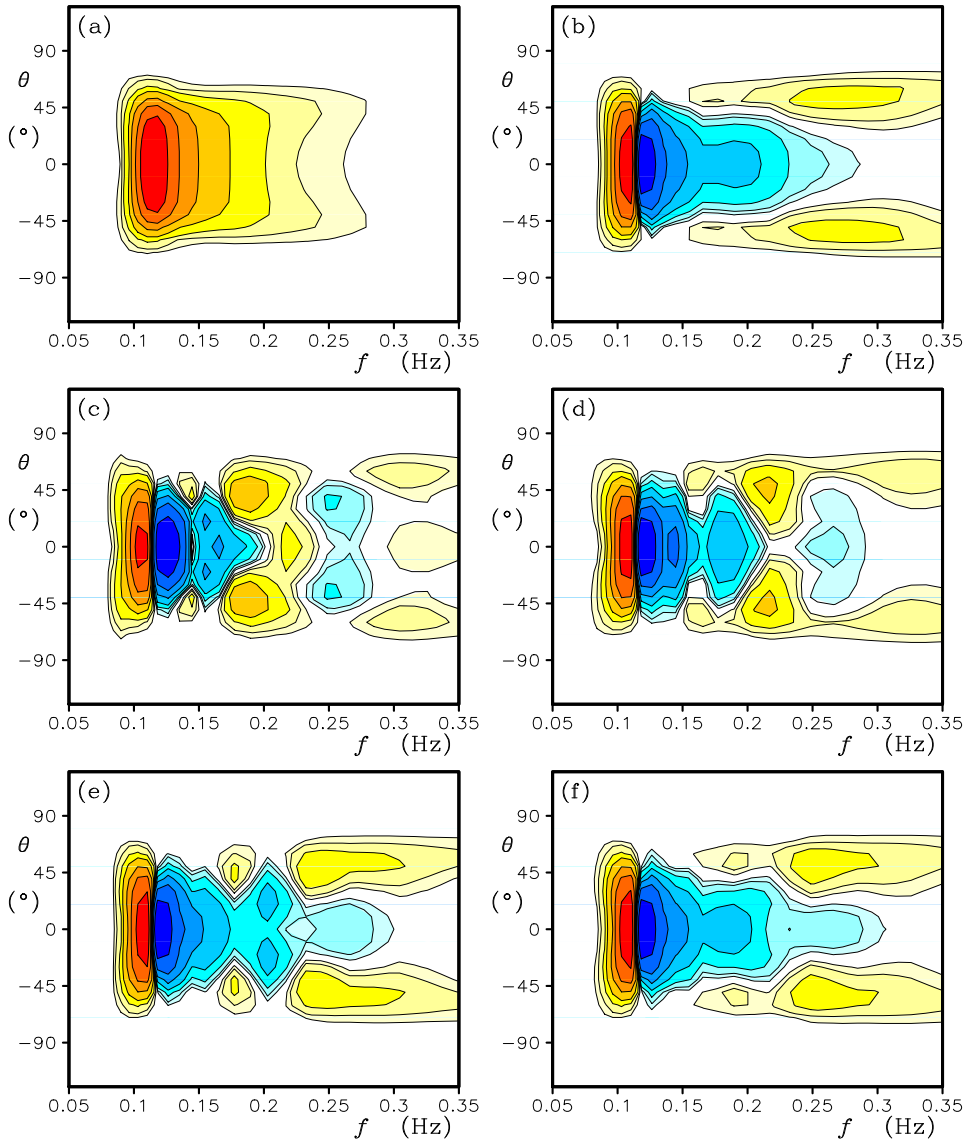

Fig. 7.11 : Like Fig. 7.4 for three parameter $(\lambda, \mu, \Delta\theta,)$ quadruplet. Number of components in panels (c-f) ranging from 2 to 5.

quadruplets are allowed to vary freely. Other methods could be contrived, for instance, with a fixed distribution of one of the parameters, and others freely varying. Although such approaches may be worthwhile to investigate, they are not considered here for practical reasons.

7.2 Full model optimization.

An MDIA in almost any configuration will have a significant number of free parameters that need to be optimized. Unlike for the single DIA as optimized in the previous section, it is therefore not economically feasible to map the error behavior in the full parameter space. Consequently, a search algorithm needs to be established. A first step in doing so, is to define a single cost function based on the five error measures for wave height and spectral shapes. This cost function ζ will be defined here as a weighted average of these five error measures

$$\zeta = \frac{a_H\epsilon_H + a_{E1}\epsilon_{E1} + a_{E2}\epsilon_{E2} + a_{s1}\epsilon_{s1} + a_{s2}\epsilon_{s2}}{a_H + a_{E1} + a_{E2} + a_{s1} + a_{s2}} \quad , \tag{7.2}$$

where the factors a represent the weight factors. The effects of these weight factors will be addressed here using the error maps derived in the previous section. In the following figures, maps of ζ will be based on the lower resolution error maps corresponding to Fig. 6.13.

To illustrate the behavior of the cost function ζ, it is displayed in Fig. 7.12 and 7.13 in the (λ, C) parameter space for the DIA considered in the previous section. The weight functions are chosen to properly emphasize different errors. First, the overall wave height error is of paramount importance, To assure that the cost function focuses on the wave height, a relatively large weight a_H is required. Figure 6.7 indicates that the wave height and the spectral energy measures can be optimized simultaneously. For this case an appropriate setting of the weights could be $a_h = 10$, and $a_{E1} = a_{S1} = 1$, whereas the spectral steepness measures are ignored by setting $a_{s2} = a_{s2} = 0$. The resulting cost function is presented in Fig. 7.12, and indeed appears to have minima near the subjectively chosen values of $\lambda = 0.19$ and $C = 2.2 10^7$ from Table 6.1. Adding the error measures for the steepness spectra will draw the optimum value of the parameters to higher λ and/or C. Considering that the error measures of the steepness spectra appeared smaller than those for the energy spectra in the previous section, a somewhat larger weight might be appropriate. However, because there appears to be no reason to favor accuracy of the former spectra over the latter, identical weights appear appropriate. A map of the cost function for $a_h = 10$, $a_{E1} = a_{S1} = a_{S2} = a_{S2} = 1$ is presented in Fig. 7.13. Indeed, the optimum values of λ and C now are moved to higher values. Note that for both examples, the cost function appears to have a well defined minimum, suggesting that most search procedures should result in general in the global minimum of the cost function, in spite of

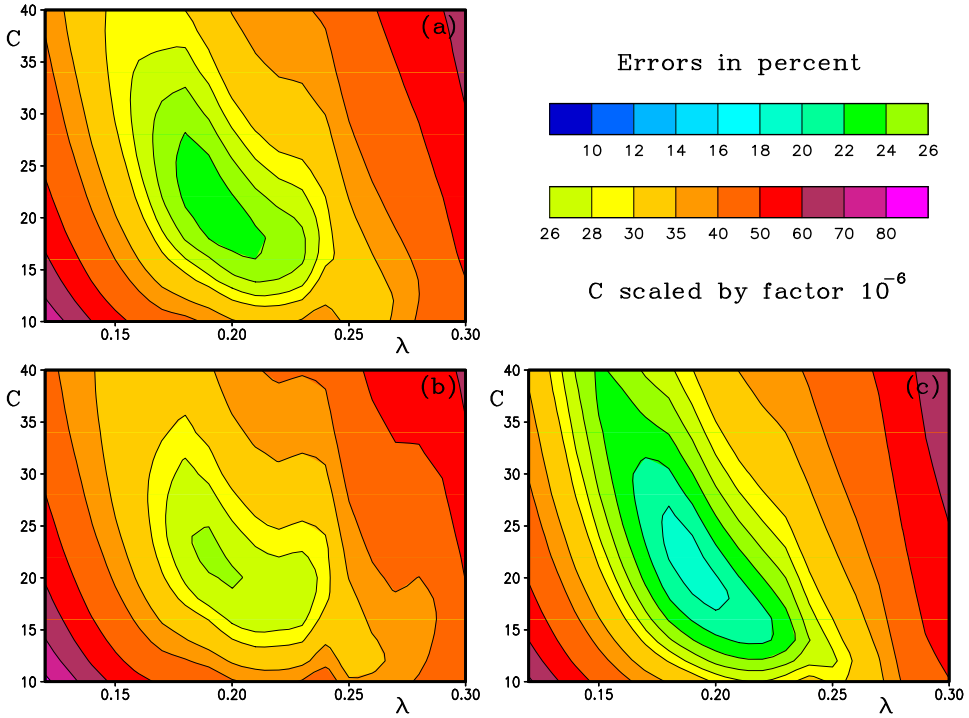

Fig. 7.12 : Cost function ζ of Eq. (7.2) for MDIA with single parameter quadruplet (λ) and $N = 1$ as a function of λ and C using a discrete parameter resolution as in Fig. 6.13. $a_h = 10$, $a_{E1} = a_{E2} = 1$, $a_{s1} = a_{s2} = 0$. (a) All test data. (b) Time limited test only. (c) Fetch limited test only.

the nonlinear nature of the problem. This, however, proved not to be the case for MDIAs with more components. Therefore, additional attention has been paid to the search algorithms employed. Ultimately, the optimization was performed using a combination of genetic and steepest descent methods, as described in some detail in Appendix B.

First, the most simple MDIA based on single parameter quadruplets is considered. Because there appears to be no stability issued with this quadruplet, a consistent set of MDIAs can be developed starting with $N = 1$, and increasing N until no further gain in accuracy can be achieved, or until the behavior of the quadruplets becomes erratic as in the previous section. The results of such optimizations are gathered in Table 7.1.

Results for $N = 1$ in Table 7.1 provide a baseline for all other MDIAs. The optimal cost function for the traditional DIA thus becomes $\zeta = 26.0\%$. Note that both this cost function and the corresponding values of $\lambda = 0.212$ and $C = 1.88\,10^7$ correspond well with the results presented graphically in Fig. 7.13. This tentatively validates the search algorithm(s) as described in Appendix B.

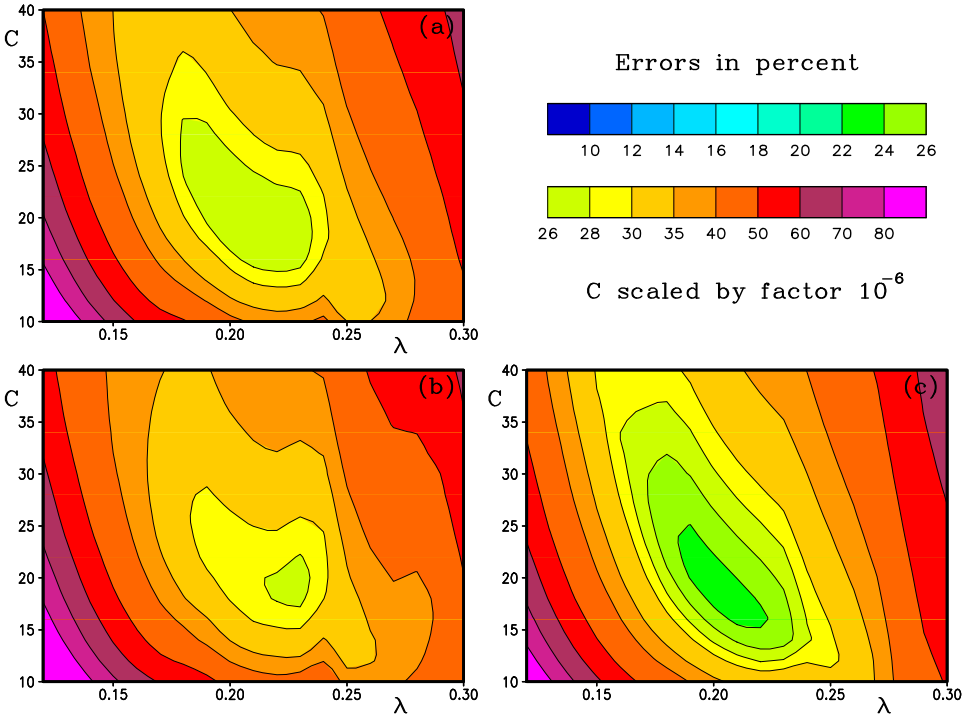

Fig. 7.13 : Like Fig. 7.12 with $a_h = 10$, $a_{E1} = a_{E2} = a_{s1} = a_{s2} = 1$.

Increasing the number of components in this MDIA to $N = 2$ has a dramatic positive impact on the model results (Table 7.1). The cost function ζ is reduced from 26.0% to 16.3%, an error reduction of 37%. The gain in accuracy occurs in all error measures, but is mostly due to an improved description of the steepness spectra (ϵ_{s1} and ϵ_{s2}, error reductions of approximately 50%), and in the energy spectra (ϵ_{E1} and ϵ_{E2}, error reductions of approximately 38%). Note, however, that the errors in the energy and steepness spectra remain at an unacceptable high level. The improvement of the wave height error is more moderate (ϵ_H, error reduction of order of 10 to 15% on average), but this is less relevant, because the wave height errors were already in an acceptable range.

Increasing the number of components in this MDIA further to $N = 3$ has a minute impact on the quality of the MDIA, reducing the overall cost function ζ by only 1.1%. This improvement was mainly obtained by a better description of the wave height, and is accompanied by a small deterioration of the description of the steepness spectra. However, from a practical perspective, all error measures are essentially unchanged when going from $N = 2$ to $N = 3$ for the MDIA with a quadruplet defined by λ only. Increasing the number of components further to $N = 4$ also has no benefit (see Appendix B.4).

Table 7.1: Optimum parameter settings (λ, C), corresponding cost function ζ and errors ϵ as a function of the number of components N for an MDIA based on the one-parameter quadruplet definition. First and second lines of error values correspond to time and fetch limited cases, respectively.

N	ζ (%)	λ (-)	C $\times 10^{-7}$	ϵ_H (%)	ϵ_{E1} (%)	ϵ_{E2} (%)	ϵ_{s1} (%)	ϵ_{s2} (%)
1	26.0	0.212	1.88	4.77	148.	117.	41.2	39.1
				2.23	133.	102.	38.3	36.4
2	16.3	0.127	3.84	4.27	93.2	74.0	19.9	20.3
		0.278	1.83	1.89	80.3	63.5	18.8	19.0
3	16.1	0.024	4.88	3.93	93.8	74.3	21.0	20.7
		0.127	5.60	1.27	79.5	63.0	19.8	19.4
		0.279	2.58					

The next step in refining the MDIA is to increase the complexity of the quadruplet to the two-parameter (λ, μ) definition. As discussed above, this is not a generally stable configuration for $N = 1$. The genetic search algorithm indicates that an MDIA version of this quadruplet nevertheless shows stable model behavior over large parameter ranges. Considering the optimization results for individual spectra, the more complex quadruplet definition is expected to start to provide benefit over the single parameter definition for $N = 3$. The optimization experiments were therefore started with $N = 3$. Results are summarized in Table 7.2. The entry for $N = 1$ in this Table present results for $\mu \equiv 0$ and $N = 1$ for reference purposes only.

Comparing this MDIA to the baseline of the optimized traditional single component MDIA (compare $N = 3$ and $N = 1$ entries in Table 7.2), the improvement is dramatic. The overall cost function ζ and the wave height error ϵ_H are reduced by 55%, the spectral errors are reduced by approximately 60%, and the error s in the steepness spectra are reduced 30 to 50%. More interesting, however, is the comparison between this MDIA based on the (λ, μ) quadruplet with three components, with the MDIA based on the λ-only quadruplet with three components (Compare $N = 3$ entries in Tables 7.2 and 7.2, respectively). Going to the more complicated quadruplet definition with the same number of components in the MDIA reduces the cost function ζ by 28%. The improvement in the spectral errors ϵ_E is even more impressive at 40 to 45%, However, the error in the two-dimensional steepness spectrum ϵ_{E2} increases by 20 to 30%, whereas the errors in the one-dimensional steepness spectra ϵ_{E1} remain largely unchanged. This implies that the definition of the quadruplet influences both the overall cost function ζ, and the distribution of the errors ϵ in the cost function ζ.

Increasing the number of components to $N = 4$ for the MDIA with the two-

Table 7.2: Like Table 7.1 for two-parameter quadruplet (λ, μ). First line of Table 7.1 is reproduced for reference purposes.

N	ζ (%)	λ (-)	μ (-)	C $\times 10^{-7}$	ϵ_H (%)	ϵ_{E1} (%)	ϵ_{E2} (%)	ϵ_{s1} (%)	ϵ_{s2} (%)
1	26.0	0.212	—	1.88	4.77	148.	117.	41.2	39.1
					2.23	133.	102.	38.3	36.4
3	11.6	0.063	0.009	12.1	2.11	58.6	49.4	25.1	19.6
		0.184	0.028	2.40	1.09	46.3	42.2	26.3	21.8
		0.284	0.128	5.33					
4	12.1	0.127	0	5.01	2.62	63.9	54.3	24.0	18.3
		0.133	0.032	0.353	0.74	50.7	43.5	24.8	19.2
		0.253	0	1.55					
		0.278	0.151	6.48					

parameter (λ, μ) quadruplet definition does not result in a lower cost function for the resulting quadruplet layout (see Table 7.2). This suggests that with the present optimization setup, the optimal model behavior has been reached. It furthermore suggests that although the genetic algorithm may sample the optimization space fairly efficiently, there is no guarantee that the absolute optimum setting is found; a 'perfect' algorithm would be able to find the solution that is comparable to the optimum solution for $N = 3$ or better.

The final stage of optimization for the present study considers an MDIA with a quadruplet defined by three parameters, λ, μ and $\Delta\theta$. For reasons of computational economy, only MDIAs with $N = 3$ and $N = 4$ could be considered here. In fact, the most complicated MDIA thus considered required the dedicated use of a 16 processor Linux cluster for nearly two months to complete the genetic search algorithm. The results are summarized in Table 7.3. As with the two parameter quadruplet definition, the experiments are started with $N = 3$.

This quadruplet with $N = 3$ components again provides a notable improvement over the corresponding MDIA with a two parameter quadruplet (12% reduction in ζ), and a large improvement over the single parameter quadruplet with 1 or two components (54% and 37% reduction of ζ, respectively). Compared to the two-parameter quadruplet, the improvement in the error is mostly obtained due to improved behavior for the spectral error measures, with a slight deterioration of the error measures for spectral steepness. Unlike with the previous approaches, adding a fourth component systematically improves the behavior of this MDIA (a reduction of ζ by 6% by going from $N = 3$ to $N = 4$). This improvement is obtained in both spectral and steepness error measures.

Table 7.3: Like Table 7.2 for three-parameter quadruplet $(\lambda, \mu, \Delta\theta)$.

N	ζ (%)	λ (-)	μ (-)	$\Delta\theta$ (°)	C $\times 10^{-7}$	ϵ_H (%)	ϵ_{E1} (%)	ϵ_{E2} (%)	ϵ_{s1} (%)	ϵ_{s2} (%)
1	26.0	0.212	—	—	1.88	4.77	148.	117.	41.2	39.1
						2.23	133.	102.	38.3	36.4
3	10.2	0.108	0.013	24.4	6.21	1.28	45.3	40.5	27.6	23.8
		0.233	0.262	34.5	11.4	0.55	39.0	41.5	26.2	22.6
		0.254	0.106	15.1	4.49					
3	10.3	0.104	0.007	2.7	4.50	1.89	49.1	48.6	23.5	22.2
		0.236	0.270	30.4	12.9	0.76	34.4	39.9	21.8	19.0
		0.252	0.064	21.5	3.03					
4	9.6	0.065	0.167	82.2	8.32	2.19	41.7	43.5	22.6	20.2
		0.111	0.237	52.0	3.74	0.76	30.5	35.6	22.7	19.1
		0.127	0	4.0	5.14					
		0.302	0.195	4.9	3.45					

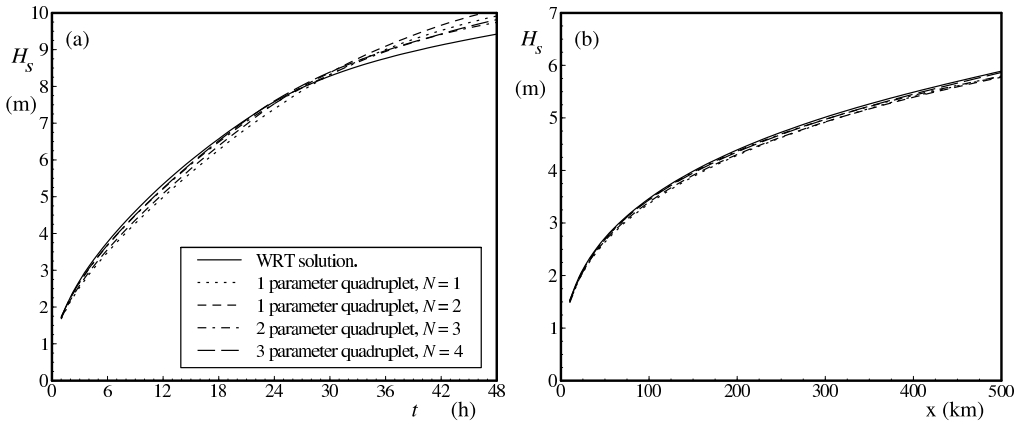

Fig. 7.14 : Wave height H_s for (a) time limited test as a function of time t and (b) for fetch limited test as a function of fetch x for the WRT model solution and various settings of the two parameter DIA as identified in the legend.

7.3 Comparison of approaches.

In the previous (sub) sections, optimized MDIAs are judged only by their cost function ζ. In practical applications, however, the actual behavior of physical parameters like the wave height H_s and the (steepness) spectra are equally important. Therefore, such parameters are compared briefly in the present section, similar to the comparison between various conventional DIAs as presented in Figs. 6.8 through 6.12.

Figure 7.14 shows the resulting wave height for the time and fetch limited test for several optimized MDIA, starting with the optimized conventional DIA (quadruplet based on λ only, single component), and ending with the most complex MDIA (quadruplet based on λ, μ and $\Delta\theta$, four components). The wave heights are excellently represented by all optimized MDIAs. The only notable error occurs with the less complex MDIAs at the later stages in the time limited growth (panel a). The MDIA here tend to overestimate wave growth, more so for the less complicated MDIAs, but still notable for the most complex MDIAs.

Figures 7.15 and 7.16 show the 1-D energy and steepness spectra after 24h in the time limited test, and at 300km in the fetch limited test, respectively. In both cases, the wave heights for all model runs are virtually identical, making differences in the figures purely due to differences in spectra shape. In spite of the close total energy contents (H_s) of the spectra, there are significant differences in the spectral shapes. The most simple DIA available underestimates the spectral peak energy by nearly 40% (a panels in both figures). By increasing the complexity of the MDIA, this deficiency is systematically reduced to less than 10% for the two most complex MDIAs. However, the improvement in the description of the spectral peak is accompanied by a deterioration of the description of the (steepness) spectra at higher frequencies, as is clear from the corresponding lines in the b panels of both figures.

Finally, Figs. 7.17 and 7.18 present the corresponding two-dimensional spectra. These spectra show a systematic improvement with increasing complexity of the spectrum.

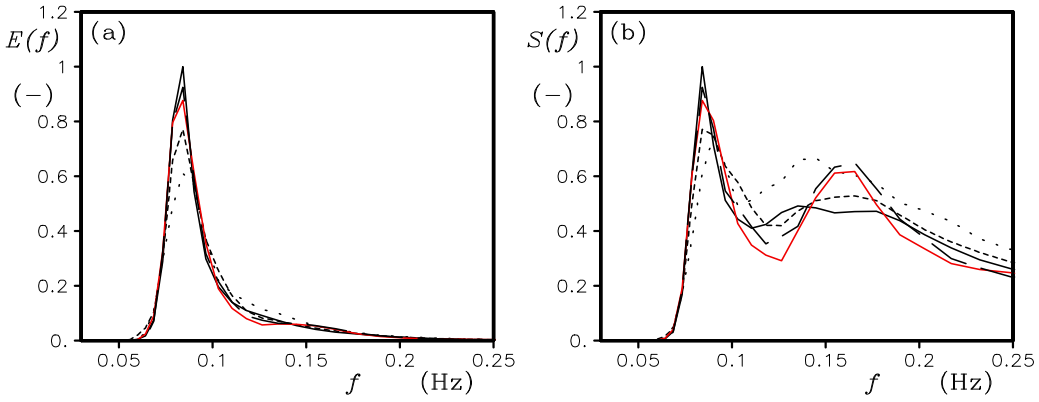

Fig. 7.15 : One dimensional spectrum $E(f)$ (panel a) and steepness spectrum $S(f) = k^2 E(f)$ for the time limited test after 24 h. Legend as in Fig. 7.14. The two-parameter quadruplet with $N = 3$ is replaced by a red line for clarity. Spectra normalized with maximum value for WRT results.

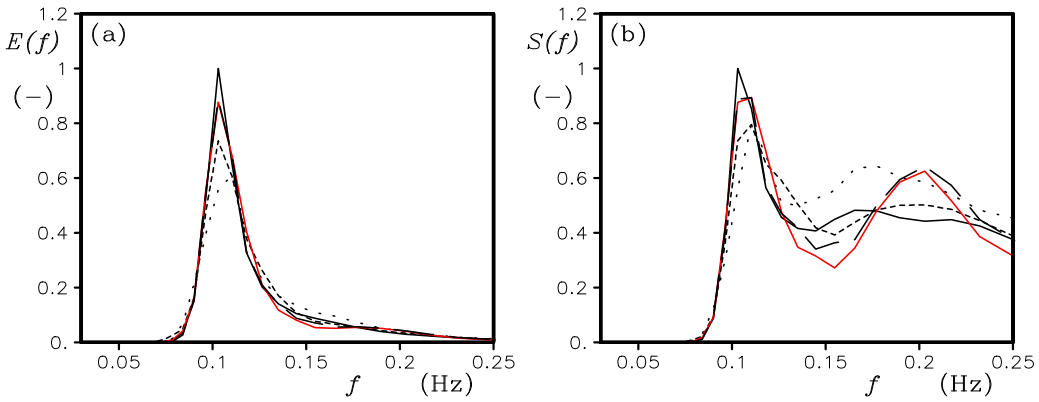

Fig. 7.16 : Like Fig. 7.15 for fetch limited test at 300 km.

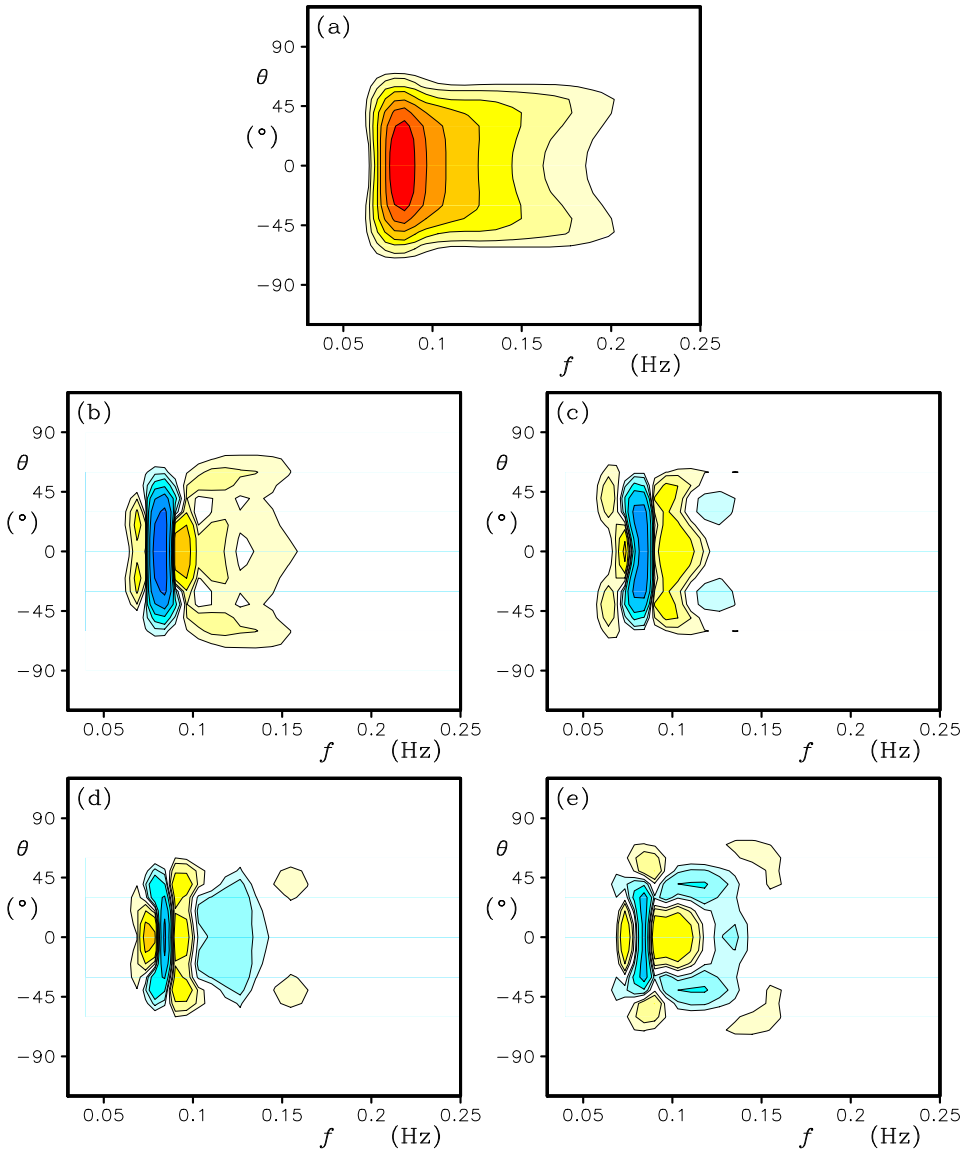

Fig. 7.17 : (a) Reference spectrum (WRT) after 24 from time limited test, and differences with results for (b) HHAB, (c) TC, (d) HK, and (e) 'present' model runs (see Table 6.1). Contours at factor 2 interval with highest contour at 0.5 times the maximum spectral energy density. Blue shading identifies negative differences. Differences defined as WRT - DIA results.

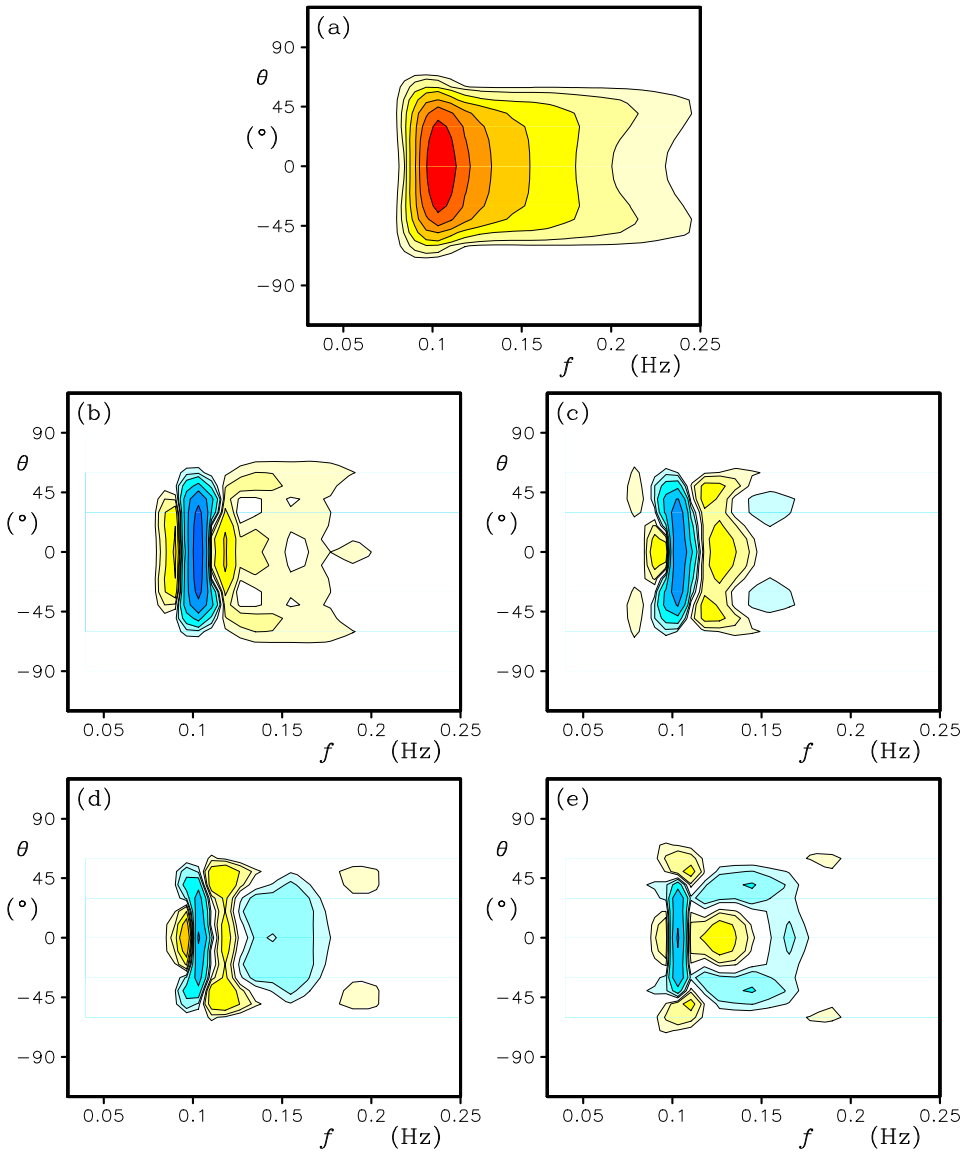

Fig. 7.18 : Like Fig. 7.17 for fetch limited test at 300 km.

7.4 Robustness of approaches.

The robustness of MDIAs with alternative definitions of the quadruplet has been identified as a possible problem in the previous sections. Two observation have been made from the optimization experiments regarding the robustness of such MDIAs.

First, for the two parameter MDIA with $N = 3$ the initial populations in the genetic search algorithm show a large number of unstable solutions. Loosely defining an unstable solution as a solution with $\zeta > 100\%$, the initial generation includes roughly 75% unstable solutions. This rapidly reduces to about 15% in generation 10, and stabilizes between 10 and 15% for later generations. All other MDIAs with the multi-parameter quadruplet definition and $N \geq 3$. Show similar behavior.

Second, in the steepest descent algorithm, unstable solutions never resulted from (small) perturbations to the parameter setting for each MDIA.

Considering that the genetic search algorithm focuses on areas with low costs functions, both observations suggest that there is a sufficiently large area in parameter space of stable solutions around the optimum solution for the stability of these more complicated MDIAs not to be a practical problem. However, this hypothesis will need to be addressed in more detail in upcoming studies.

7.5 Conclusions.

The holistic approach to optimizing interaction parameterizations has resulted in the following conclusions for the multi parameter, multi component MDIA:

1) Increasing the complexity of the quadruplet definition, as well as the number of components N as considered in an MDIA, systematically improves the behavior of such MDIAs.

2) Saturation of improvement occurs at relatively small numbers of components N for the present model and optimization approaches, and is roughly consistent with the results presented in Part 1.

3) Different definitions of the quadruplet do influence individual error measures for wave heights, spectra and steepnesses differently.

4) Robustness is a potential problem for more complex quadruplet definitions, but does not appear to be a practical problem in the present experiments.

5) The genetic algorithm used for the present optimization proved powerful, but also has clear economic and accuracy limitations for the most complex MDIAs considered here.

As a side note, it is interesting to observe that optimization of the MDIA to individual spectra will lead to bifurcation behavior in the optimized parameter values. Such behavior has not been observed explicitly in holistic approach. However, the apparent existence of many local minima of the cost function in parameter space may well be a reflection of this bifurcation behavior.

8 Summary and conclusions

The present study starts with the definition of a general, multiple DIA, which represents the maximum flexibility of previous DIAs presented in literature. The only omission from previous literature is the definition of individual proportionality constants for individual terms in the equation for the interaction strength (Ueno and Ishizaka, 1997; Hashimoto and Kawaguchi, 2001) and the variable DIA (Part 1). The omission of these approaches is based on results presented in Part 1. Because the results published in Part 1 indicate that accurate interactions for an individual spectrum do not guarantee stable or accurate model integration, a basic time and fetch limited growth test are set up. Benchmark results for wave heights and various spectral parameters are obtained by using the exact (Webb-Resio-Tracy) algorithm for S_{nl}. Furthermore, individual spectra from these computations are used occasionally for optimization of individual interactions. Such spectra are expected to be more representative for wave models than previously used parametric spectra.

In Section 3 an attempt is made to understand why some DIAs do not result in stable model integration. A possible explanation is the basic signature of contributions to S_{nl} for a given discrete frequency. The traditional DIA results in a three-lobed structure, that can be an obvious building block for a three-lobed overall interaction. Other quadruplet layouts do not incorporate this basic feature, and may therefore have more problems representing the three-lobed structure of the interactions for more arbitrary spectra. Furthermore, the different sampling characteristics of the spectral space for more complex quadruplets suggests that grid decoupling may occur. However, the results presented in Section 4 prove the latter to be a moot point.

In Section 4 the effects of the quadruplet layout and the way in which the quadruplet is used to sample spectral space are addressed. It is shown that the way in which a quadruplet is used to sample spectral space only influences interaction at the level of the necessary interpolations and redistributions in spectral space. This has negligible impact on interactions for individual spectra, but may have a larger impact on spectra obtained by model integration due to the nonlinearity of the problem. Given the small impact of the sampling on the results, it is advisable to use a symmetric quadruplet layout, as this is most conducive to numerical economy (see Section 4.3).

In Section 5 alternative quadruplets with a three-peaked signature are considered. For this purpose, the Van Vledder (2001) quadruplet is first reformulated in a symmetric form. It is shown that by defining a quadruplet with $\mu \equiv 0$, $\lambda \neq 0$ and $\Delta\theta \neq 0$, such a signature can be achieved. A simple integration test with the WAVEWATCH III model shows promising results. Unfortunately, more rigorous optimization efforts in the following sections show that this approach also often results in unstable model integration.

In Sections 6 and 7 single and multiple DIAs are optimized by optimizing time and fetch limited model results. This holistic optimization approach leads to systematically improved model behavior, unlike optimization techniques based on individual spectra and interactions as used in previous studies and in Part 1. An optimization for each individual model spectrum for the time and fetch limited runs nevertheless shows interesting results. Such optimization leads to bifurcation behavior of optimized model parameters, which at least qualitatively explains why better interactions for individual spectra do not necessarily lead to better model behavior.

Section 6 concentrates on single component MDIAs. It is show that only the conventional quadruplet layout results in unconditionally stable model integration for such MDIAs. The low dimensionality of the optimization process allows for a full mapping of the error behavior of the wave model in parameter space. It is shown that the wave height and the energy spectrum can be optimized simultaneously, but that this always leads to sub-optimal behavior for steepness measures. It is furthermore shown that the wave height can be represented accurately, but that significant errors remain in the spectral shape, even for optimized MDIAs.

In this section, previously suggested parameter settings for the conventional DIA are compared with present optimized settings. Particularly interesting are the settings as used in the default WAVEWATCH III model. Such settings result in the spectral peak to be spuriously moved to higher frequencies, whereas the low frequency flank of the spectrum is relatively well represented (see Figs. 6.11 and 6.12). This explains an apparent paradox that has been observed in WAVEWATCH III results. Initial swell arrival times appears reasonable well represented, whereas peak periods in wind sea conditions appear systematically under estimated by roughly 10%. The latter deficiency has been reported at several conferences, but to the knowledge of the present author has not been published in detail.

Section 7 concentrates on more complex MDIAs. It is show that by increasing the complexity of the MDIA, and by using a holistic optimization technique, it is possible to dramatically improve the quality of the model results when compared similar results obtained with the exact interaction algorithm. Nevertheless, notable errors remain the the present approach. Furthermore, it is clear that different quadruplet definitions lead to different error focuses in the cost function. Finally, it appears that for MDIAs with at least $N = 3$ components, there is no serious robustness issue, in spite of such issues with the underlying MDIAs with $N = 1$ components.

The above results clearly identify the holistically optimized MDIA as a much more accurate alternative for the traditional DIA, although the economy of such approaches has not been adequately addressed yet. In this feasibility study,

the final optimization capabilities have been limited by numerical economy of approaches, an a lack of a detailed analysis of the optimization procedures itself. A significant part of the economical limitations are due to the fact that a non-optimized MDIA implementation was used. Also missing from the present study are a detailed assessment of the robustness of the approaches, and an assessment into errors for more complex / realistic wave conditions. With this in mind, additional studies regarding this MDIA should consider the following issues:

1) Having established the MDIA with the expanded quadruplet layout as a viable alternative to the conventional DIA, a numerically optimized version of this MDIA needs to be developed to facilitate further numerical experiments and optimization. Actual or future incorporation of shallow water effects needs to be considered.

2) Having established the genetic algorithm as a viable method for holistic optimization of the MDIA, a detailed assessment of this optimization procedure appears essential. Eiben and Smith (2003) provide a plethora of avenues to do this. Included in this are the need to re-evaluate the costs function ζ, and the allowed range of parameter values (particularly negative values of C).

3) The resulting MDIA will need to be applied to more realistic wave conditions, to assure that the improvements for idealized conditions carry over to more practical model applications.

4) The robustness of the MDIA needs to be addressed in more detail.

5) The final economy of such MDIAs needs to be addressed. Note that in the context of the dynamic integration scheme in WAVEWATCH III (Tolman, 1992, 2002a) the economy is a function of both the computational costs for individual interactions, and the resulting time steps in the integration scheme.

This page is intentionally left blank.

References

Booij, N., R. C. Ris and L. H. Holthuijsen, 1999: A third-generation wave model for coastal regions, Part I, model description and validation. *J. Geophys. Res.*, **104**, 7649–7666.

Eiben, A. E. and J. E. Smith, 2003: *Introduction to Evolutionary Computing.* Springer, 299 pp.

Fletcher, C. A. J., 1988: *Computational techniques for fluid dynamics, part I and II.* Springer, 409+484 pp.

Hargreaves, J. C. and J. D. Annan, 1998: Integration of source terms in WAM. in *Proceedings of the 5th International Workshop on Wave Forecasting and Hindcasting*, pp. 128–133.

Hargreaves, J. C. and J. D. Annan, 2001: Comments on improvement of the short fetch behavior in the WAM model. *J. Atmos. Oceanic Techn.*, **18**, 711–715.

Hashimoto, N. and K. Kawaguchi, 2001: Extension and modification of Discrete Interaction Approximation (DIA) for computing nonlinear energy transfer of gravity wave spectrum. in *4th International Symposium on Ocean Wave Measurement and Analysis*, pp. 530–539. ASCE.

Hasselmann, K., 1960: Grundgleichungen der seegangsvoraussage. *Schiffstechnik*, **1**, 191–195.

Hasselmann, S., K. Hasselmann, J. H. Allender and T. P. Barnett, 1985: Computations and parameterizations of the nonlinear energy transfer in a gravity-wave spectrum, Part II: parameterizations of the nonlinear energy transfer for application in wave models. *J. Phys. Oceanogr.*, **15**, 1378–1391.

Leonard, B. P., 1979: A stable and accurate convective modelling procedure based on quadratic upstream interpolation. *Comput. Methods Appl. Mech. Engng.*, **18**, 59–98.

Leonard, B. P., 1991: The ULTIMATE conservative difference scheme applied to unsteady one-dimensional advection. *Comput. Methods Appl. Mech. Engng.*, **88**, 17–74.

Phillips, O. M., 1977: *The dynamics of the upper ocean, second edition.* Cambridge Univ. Press, 336 pp.

Resio, D. T. and W. Perrie, 1991: A numerical study of nonlinear energy fluxes due to wave-wave interactions. Part 1: Methodology and basic results. *J. Fluid Mech.*, **223**, 609–629.

Tolman, H. L., 1991: A third-generation model for wind waves on slowly varying, unsteady and inhomogeneous depths and currents. *J. Phys. Oceanogr.*, **21**, 782–797.

Tolman, H. L., 1992: Effects of numerics on the physics in a third-generation wind-wave model. *J. Phys. Oceanogr.*, **22**, 1095–1111.

Tolman, H. L., 2002a: Limiters in third-generation wind wave models. *The Global Atmosphere and Ocean System*, **8**, 67–83.

Tolman, H. L., 2002b: User manual and system documentation of WAVEWATCH III version 2.22. Tech. Note 222, NOAA/NWS/NCEP/MMAB, 133 pp.

Tolman, H. L., 2003: Optimum Discrete Interaction Approximations for wind waves. Part 1: Mapping using inverse modeling. Tech. Note 227, NOAA/NWS/NCEP/MMAB, 57 pp. + Appendices.

Tolman, H. L., 2004: Inverse modeling of Discrete Interaction Approximations for nonlinear interactions in wind waves. *Ocean Mod.*, **6**, 405–422.

Tolman, H. L., B. Balasubramaniyan, L. D. Burroughs, D. V. Chalikov, Y. Y. Chao, H. S. Chen and V. M. Gerald, 2002: Development and implementation of wind generated ocean surface wave models at NCEP. *Wea. Forecasting*, **17**, 311–333.

Tolman, H. L. and D. V. Chalikov, 1996: Source terms in a third-generation wind-wave model. *J. Phys. Oceanogr.*, **26**, 2497–2518.

Tracy, B. and D. T. Resio, 1982: Theory and calculation of the nonlinear energy transfer between sea waves in deep water. WES Report 11, US Army Corps of Engineers.

Ueno, K. and M. Ishizaka, 1997: On an efficient calculation method of the nonlinear energy transfer in wind waves. *Sottukojiho, JMA*, **64**, 75–80, (In Japanese).

Van Vledder, G. Ph., 1990: Directional response of wind waves to turning winds. Communications on Hydraulic and Geotechnical Engineering 90-2, Delft Universtity of Technology, ISSN 0169–6548, 255 pp. (Doctoral Thesis).

Van Vledder, G. Ph., 2001: Extension of the Discrete Interaction Approximation for computing nonlinear quadruplet wave-wave interactions in operational wave prediction models. in *4th International Symposium on Ocean Wave Measurement and Analysis*, pp. 540–549. ASCE.

Van Vledder, G. Ph., 2002a: Improved parameterizations of nonlinear four wave interactions for application in operational wave prediction models. Report 151a, Alkyon, The Netherlands.

Van Vledder, G. Ph., 2002b: A subroutine version of the Webb/Resio/Tracy method for the computation of nonlinear quadruplet interactions in a wind-wave spectrum. Report 151b, Alkyon, The Netherlands.

WAMDIG, 1988: The WAM model – a third generation ocean wave prediction model. *J. Phys. Oceanogr.*, **18**, 1775–1809.

Webb, D. J., 1978: Non-linear transfers between sea waves. *Deep-Sea Res.*, **25**, 279–298.

Young, I. R. and G. Ph. Van Vledder, 1993: A review of the central role of nonlinear interactions in wind-wave evolution. *Trans. Roy. Soc. London*, **342**, 505–524.

APPENDICES

This page is intentionally left blank.

A Quadruplet layout

A.1 General considerations

In the present study, the (deep water) quadruplet with unlimited versatility is defined from Eqs. 2.2 through 2.4 and the bottom line in Table 2.1 as

$$\left.\begin{array}{rcl} \sigma_1 & = & (1+\mu)\sigma \\ \sigma_2 & = & (1-\mu)\sigma \\ \sigma_3 & = & (1+\lambda)\sigma \\ \sigma_4 & = & (1-\lambda)\sigma \\ \boldsymbol{k}_1+\boldsymbol{k}_2 & = & \boldsymbol{k}_3+\boldsymbol{k}_4 \\ \theta_2 & = & \theta_1 \pm \Delta\theta \end{array}\right\} \quad , \tag{A.1}$$

where the definition of $\Delta\theta$ depends on the actual quadruplet layout selected. Furthermore, the wavenumber $k = ||\boldsymbol{k}||$ and the frequency σ satisfy the (deep water) dispersion relation

$$\sigma^2 = gk \quad . \tag{A.2}$$

Symmetric sampling of frequency space furthermore suggests that $\boldsymbol{k}_1+\boldsymbol{k}_2$ are lined up in direction with a discrete spectral wavenumber for which the contributions are computed. Thus, the quadruplet angles θ_1 through θ_4 are given relative to the corresponding discrete spectral direction. From Eqs. (A.1) and (A.2), the wavenumbers of the quadruplet become

$$\left.\begin{array}{rcl} k_1 & = & (1+\mu)^2\,\sigma^2 g^{-1} \\ k_2 & = & (1-\mu)^2\,\sigma^2 g^{-1} \\ k_3 & = & (1+\lambda)^2\,\sigma^2 g^{-1} \\ k_4 & = & (1-\lambda)^2\,\sigma^2 g^{-1} \end{array}\right\} \quad , \tag{A.3}$$

which in nondimensional form, defining $\tilde{k}_i = gk_i\sigma^{-2}$, becomes

$$\left.\begin{array}{rcl} \tilde{k}_1 & = & (1+\mu)^2 \\ \tilde{k}_2 & = & (1-\mu)^2 \\ \tilde{k}_3 & = & (1+\lambda)^2 \\ \tilde{k}_4 & = & (1-\lambda)^2 \end{array}\right\} \quad . \tag{A.4}$$

For convenience, $\tilde{k}_c$ is defined as

$$\tilde{k}_c = g\,||\boldsymbol{k}_1+\boldsymbol{k}_2||\,\sigma^{-2} = g\,||\boldsymbol{k}_3+\boldsymbol{k}_4||\,\sigma^{-2} \quad . \tag{A.5}$$

The internal quadruplet angles θ_1 through θ_4 are needed to compute discrete interaction contributions. These angles are defined by the two triangles, with sides $(\tilde{k}_1, \tilde{k}_2, \tilde{k}_c)$ and $(\tilde{k}_c, \tilde{k}_3, \tilde{k}_4)$, respectively. The actual quadruplet layout chosen

(one, two or three parameters versions) define $\tilde{k}_1$, $\tilde{k}_2$ and $\Delta\theta$, and hence $\tilde{k}_c$. From this the angles θ_3 ad θ_4 always follow as

$$\theta_3 = \pm \arccos\left(\frac{\tilde{k}_3^2 + \tilde{k}_c^2 - \tilde{k}_4^2}{2\,\tilde{k}_c\,\tilde{k}_3}\right) \quad , \tag{A.6}$$

$$\theta_4 = \mp \arccos\left(\frac{\tilde{k}_4^2 + \tilde{k}_c^2 - \tilde{k}_3^2}{2\,\tilde{k}_c\,\tilde{k}_4}\right) \quad . \tag{A.7}$$

Not every value of λ results in a valid quadruplet configuration. First, identical quadruplet layouts are found for λ and $-\lambda$ (or μ and $-\mu$). Therefore, it is sufficient to consider $\lambda > 0$, $\mu > 0$ and $\theta > 0$ only. Considering, furthermore, that $\tilde{k}_3 + \tilde{k}_4$ is a monotonically increasing function of λ, upper and lower bounds of λ are defined by

$$\left.\begin{array}{rcl} (1+\lambda)^2 + (1-\lambda)^2 & \geq & \tilde{k}_c \\ (1+\lambda)^2 - (1-\lambda)^2 & \leq & \tilde{k}_c \end{array}\right\} \quad , \tag{A.8}$$

which corresponds to

$$\sqrt{\max\left(0., \frac{1}{2}\tilde{k}_c - 1\right)} \leq \lambda \leq \frac{1}{4}\tilde{k}_c \quad . \tag{A.9}$$

These general considerations will be used in the following section to define several practical quadruplets

A.2 Practical quadruplets

Four practical quadruplets will be considered here in some more detail. These are the conventional DIA quadruplet, the two parameter quadruplet from Part 1, the two parameter quadruplet from Section 5, and the three parameter quadruplet.

The DIA quadruplet is defined by $\mu \equiv 0$ and $\Delta\theta \equiv 0$. With this, $\tilde{k}_c = 2$, and the internal angles of the quadruplet become

$$\theta_1 = \theta_2 = 0 \quad , \tag{A.10}$$

$$\theta_3 = \pm \arccos\left(\frac{(1+\lambda)^4 + 4 - (1-\lambda)^4}{4\,(1+\lambda)^2}\right) \quad , \tag{A.11}$$

$$\theta_4 = \mp \arccos\left(\frac{(1-\lambda)^4 + 4 - (1+\lambda)^4}{4\,(1-\lambda)^2}\right) \quad , \tag{A.12}$$

and valid quadruplet configurations can be found for

$$0 \leq \lambda \leq 0.5 \quad . \tag{A.13}$$

The quadruplet from Part 1 is defined by λ and μ, whereas $\Delta\theta$ follows from the assumption that $\tilde{k}_c \equiv 2$. With this the internal angles of the quadruplet become

$$\theta_1 = \pm \arccos\left(\frac{(1+\mu)^4 + 4 - (1-\mu)^4}{4\,(1+\mu)^2}\right) \quad , \tag{A.14}$$

$$\theta_2 = \mp \arccos\left(\frac{(1-\mu)^4 + 4 - (1+\mu)^4}{4\,(1-\mu)^2}\right) \quad , \tag{A.15}$$

$$\theta_3 = \pm \arccos\left(\frac{(1+\lambda)^4 + 4 - (1-\lambda)^4}{4\,(1+\lambda)^2}\right) \quad , \tag{A.16}$$

$$\theta_4 = \mp \arccos\left(\frac{(1-\lambda)^4 + 4 - (1+\lambda)^4}{4\,(1-\lambda)^2}\right) \quad . \tag{A.17}$$

Note that close correspondence to the layout of the DIA quadruplet above. Note, furthermore, that the signs of θ_1 and θ_2 are opposite, as are the signs of θ_3 and θ_4, resulting in four possible quadruplet configurations. Cyclic exchange of λ and μ results in the same quadruplet, so that unique quadruplets exist for

$$0 \leq \mu \leq \lambda \leq 0.5 \quad . \tag{A.18}$$

The two parameter quadruplet from Section 5 is defined by $\mu \equiv 0$, and λ and $\Delta\theta$ used defined. With this,

$$\tilde{k}_c = 2\cos(0.5\Delta\theta) \quad , \tag{A.19}$$

and the internal quadruplet angles become

$$\theta_1 = \pm\frac{1}{2}\Delta\theta \quad , \tag{A.20}$$

$$\theta_2 = \mp\frac{1}{2}\Delta\theta \quad , \tag{A.21}$$

$$\theta_3 = \pm \arccos\left(\frac{(1+\lambda)^4 + 4\cos^2(0.5\Delta\theta) - (1-\lambda)^4}{4\ \cos(0.5\Delta\theta)\ (1+\lambda)^2}\right) \quad , \tag{A.22}$$

$$\theta_4 = \mp \arccos\left(\frac{(1-\lambda)^4 + 4\cos^2(0.5\Delta\theta) - (1+\lambda)^4}{4\ \cos(0.5\Delta\theta)\ (1-\lambda)^2}\right) \quad . \tag{A.23}$$

The addition of $\Delta\theta$ to the DIA quadruplet does not change the lower limit of valid values for λ, but it does change the upper limit. Valid values for λ are given as

$$0 \leq \lambda \leq 0.5\cos(0.5\Delta\theta) \quad . \tag{A.24}$$

For the full three parameter quadruplet layout, $\tilde{k}_c$ becomes

$$\tilde{k}_c = \left[(1+\mu)^4 + 2(1+\mu)^2(1-\mu)^2\cos(\Delta\theta) + (1-\mu)^4\right]^{1/2} \quad , \tag{A.25}$$

The corresponding internal angles become

$$\theta_1 = \pm \arccos\left(\frac{(1+\mu)^4 + \tilde{k}_c^2 - (1-\mu)^4}{2\,\tilde{k}_c\,(1+\mu)^2}\right) \quad , \tag{A.26}$$

$$\theta_2 = \mp \arccos\left(\frac{(1-\mu)^4 + \tilde{k}_c^2 - (1+\mu)^4}{2\,\tilde{k}_c\,(1-\mu)^2}\right) \quad , \tag{A.27}$$

$$\theta_3 = \pm \arccos\left(\frac{(1+\lambda)^4 + \tilde{k}_c^2 - (1-\lambda)^4}{2\,\tilde{k}_c\,(1+\lambda)^2}\right) \quad , \tag{A.28}$$

$$\theta_4 = \mp \arccos\left(\frac{(1-\lambda)^4 + \tilde{k}_c^2 - (1+\lambda)^4}{2\,\tilde{k}_c\,(1-\lambda)^2}\right) \quad . \tag{A.29}$$

For reasons of symmetry, the values of μ and $\Delta\theta$ are limited to

$$0 \le \Delta\theta \le 180^\circ \quad , \tag{A.30}$$

$$0 \le \mu < 1 \quad . \tag{A.31}$$

The limits of λ then follow from Eqs. (A.9) and (A.25). Note that, depending on the values of μ and $\Delta\theta$, the lower limit for λ can be much larger than 0. Furthermore, there is no symmetry that commands that μ is always smaller than λ or vise versa.

B Growth curve optimization

B.1 Error measures

An integral way of tuning and testing parameterizations for the nonlinear interactions is to optimize the results of model integration, rather than the approximation to the interactions for given spectra. The most detailed and basic predicted parameter of a third generation wave model is the energy density spectrum $E(f,\theta)$ as it evolves in space and time. More robust and integrated parameters obtained from this spectrum are the one dimensional frequency spectrum $E(f)$ and the significant wave height H_s

$$E(f) = \int E(f,\theta)\, d\theta \quad , \tag{B.1}$$

$$H_s = 4\left[\int\int E(f,\theta)\, df\, d\theta\right]^{1/2} = 4\sqrt{E_t} \quad , \tag{B.2}$$

where E_t is the total wave energy. These three parameters could all form the basis of the optimization of model results. If the wave height is considered, only the total energy is considered. If the one dimensional spectrum is considered, the focus is on both the integral energy, and the location of the spectral peak. With the full spectrum, directional properties of the spectrum also become important. These three measures, however, concentrate on the peak of the wave spectrum. Particularly the high frequency flank of the spectrum, however, is important for many processes governing air-sea interactions. This part of the spectrum is not well represented in the above error measures. Additional error measures that focus more on the high frequency part of the spectrum would be the one and two dimensional steepness spectra, which for deep water can be defined as $k^2E(f) = (2\pi)^4 g^{-2} f^4 E(f)$ and its one dimensional form integrated over the directions.

Ideally, the optimization gives equal wight to model behavior during the entire model evolution. To assure such behavior of the error measure, errors should be normalized on a spectrum by spectrum basis. With this in mind, the following five root mean square error measures have been defined in the present study

$$\epsilon_H = \left[\frac{1}{N}\sum_1^N \frac{\left(H_{s,x} - H_{s,a}\right)^2}{H_{s,x}^2}\right]^{1/2} \quad , \tag{B.3}$$

$$\epsilon_{E1} = \left[\frac{1}{N}\sum_1^N \frac{\int \left\{E_x(f) - E_a(f)\right\}^2 df}{E_{t,x}^2}\right]^{1/2} \quad , \tag{B.4}$$

$$\epsilon_{E2} = \left[\frac{1}{N} \sum_{1}^{N} \frac{\int\int \{E_x(f,\theta) - E_a(f,\theta)\}^2 \, df d\theta}{E_{t,x}^2} \right]^{1/2} , \tag{B.5}$$

$$\epsilon_{s1} = \left[\frac{1}{N} \sum_{1}^{N} \frac{\int f^8 \{E_x(f) - E_a(f)\}^2 \, df}{S_{t,x}^2} \right]^{1/2} , \tag{B.6}$$

$$\epsilon_{s2} = \left[\frac{1}{N} \sum_{1}^{N} \frac{\int\int f^8 \{E_x(f,\theta) - E_a(f,\theta)\}^2 \, df d\theta}{S_{t,x}^2} \right]^{1/2} , \tag{B.7}$$

Where N is the number of output points considered in the optimization, where the suffices x and a denote the exact and approximated solutions, respectively, and where

$$S_t = \int\int f^4 E(f,\theta) \, df d\theta \tag{B.8}$$

is the integral steepness, computed over the discrete spectral domain only (ignoring the constant factor $(2\pi)^4 g^{-2}$ as in the remainder of the error computation). Because all these error parameters are internally normalized for each spectral data point, the errors are in fact relative errors. Ideally, such errors should be in the percentile range, or even better.

The error measures are computed separately for the time and fetch limited cases, which contain 48 and 50 reference spectra, respectively. For each of the five error measures the composite error ϵ_c can be computed from the errors of the time and fetch limited cases (ϵ_t and ϵ_f, respectively) as

$$\epsilon_c = \left[\frac{48\epsilon_t^2 + 50\epsilon_f^2}{98} \right]^{1/2} . \tag{B.9}$$

In order to obtain an optimum MDIA, these errors need to be evaluated in a subset of one ($N = 1$) or more ($N > 1$) $(\lambda, \mu, \Delta\theta, C)$-spaces. If this parameter space is of sufficiently low dimensionality, it is possible to map errors by a brute force method in discretized parameter spaces. This is useful for nonlinear problems like the one considered here, because such nonlinear problems potentially have several local error minima in parameters space, which poses problems for conventional optimization algorithms.

For many MDIAs, the number of free parameters in the parameterization prohibits full mapping of the errors in parameter space. Hence, search algorithms need to be employed. In such search algorithms, a composite error or cost function needs to be defined and minimized. In the present study, this cost function ζ is defined as a weighted average of the five previously defined errors in Eq. (7.2). In the following section, the two optimization techniques utilized here are discussed.

B.2 Optimization by steepest descent

The first optimization technique utilized is a straightforward steepest descent method, similar to the one used in optimizing the MDIA for individual spectra and their exact interactions. The following search strategy is employed.

First, the quadruplet layout and the number of quadruplets is selected. Second, the the quadruplets are initialized by choosing initial values for each parameter defining the quadruplet, and the corresponding cost function ζ is computed. After initialization, all parameters defining a single component of the MDIA are perturbed to estimate the partial derivatives of the cost function with respect to all the parameters defining this component of the MDIA. From these partial derivatives, a steepest descent path is estimated, and a single discrete search of the minimum cost function along this path is performed. The parameter settings with the overall lowest cost functions from the initial MDIA settings, or from individual parameter perturbations and or from the descent path search is then retained. A single search step is performed for each individual quadruplet of the MDIA in succession, after which the procedure is repeated for each quadruplet. After no further convergence can be achieved in this way, the search increments in parameter space are incrementally reduced.

This optimization differs from the optimization for individual spectra and sources in two major ways. First, for the optimization of individual sources, a best fit for all values of C can be found explicitly by matrix inversion, directly giving a best fit solution for each (set of) quadruplet configuration(s). In the optimization of model results, C needs to be found iteratively, like all other parameters of the MDIA. Furthermore, the procedure employed for individual sources allows C to vary freely. In the model optimization, the increment procedure is set up such that the quadruplet parameters always result in valid quadruplets, and that C will always remain positive.

Initial experiments with this optimization technique indicated that its results may be sensitive to initial conditions, particularly for MDIAs with several components. This implies that there are multiple local minima of the cost function ζ in the parameter space of the MDIA, making a descent method less suitable to find the global minimum of the cost function, and hence the global best parameter settings of the MDIA. To provide an objective way to sample the entire parameter space for minima in the cost function in an economical way, a genetic search algorithm was employed. This algorithm is described in the following section.

B.3 Optimization by genetic algorithm

As an alternative to a steepest descent algorithm, a so-called genetic algorithm has been constructed (e.g., Eiben and Smith, 2003). Genetic algorithms loosely take their search strategy from natural selection in biology. Some advantages of such an algorithm for the present study are

1) Genetic algorithms sample the entire parameters space for local and global minima of the cost function, and are therefore in principle less (or not) sensitive to initial conditions.

2) They do not depend on the cost function to be differentiable in parameter space. Figure 6.6a indicates that particularly ϵ_H is not particularly smooth in λ space, which will hamper the efficiency of a descent algorithm.

3) Such algorithms are more efficient than random search or full mapping of the cost function in parameter space.

A disadvantage of a genetic algorithm is that it is efficient to approximate the optimal choice, but that the final convergence may be slow. Furthermore, the genetic algorithm (as adopted here) features a built-in discrete resolution, whereas a steepest descent algorithm can provide the results at arbitrary resolution. For this reason, the genetic and steepest descent algorithms are used here in tandem. The genetic algorithm is used to map the general optimum behavior of the MDIA in full parameter space, and is used to provide near-optimal initial conditions for a subsequent steepest descent method. The remainder of this section will be used to describe the genetic algorithm used here.

In a genetic algorithm, a set of parameters to be optimized is described as a single string of bits. For the present application, a single component of the MDIA is described with λ and C, and optionally with μ and $\Delta\theta$. To convert this into a single bit string, these parameters are described discretely with a minimum value, a maximum value, and an increment. The binary description makes it convenient to define the increment indirectly from a predefined number of bits and the minimum and maximum values of the parameter. For instance, setting the minimum and maximum values of λ at 0 and 0.5, respectively, and describing λ with 6 bits results in $2^6 = 64$ discrete values, and a linear increment of 0.0079. μ and $\Delta\theta$ are discretized similarly, whereas C is discretized logarithmically, with a constant increment factor between consecutive discrete values. The actual discretizations used here are gathered in Table B.1. Note that the discretization is fairly coarse. This will speed up the convergence of the search algorithm, and is justified by the fact that the genetic algorithm is used here only to find areas in parameter space close to the global optimum settings. If such points cannot be found with relatively coarsely discretized parameter space, this probably implies that the optimum settings are very sensitive. This suggests that such settings will probably be specific for spectral resolutions, and is generally not conducive for accurate practical applications.

Having the individual parameters described as bit strings, the entire set of parameters needs to be transformed into a single bit string. For a single com-

Table B.1: Discrete description of parameters in the genetic algorithm for optimization of MDIAs. Increments are linear, except for the factor increment for C.

parameter	minimum	maximum	bits	increment
λ	0	0.5	6	0.0079
μ	0	0.5	6	0.0079
$\Delta\theta$	0°	180°	6	1.43°
C	$1\,10^6$	$2\,10^8$	7	1.043

ponent of the MDIA, the order of the parameters in the bit string is always set as

$$\lambda - [\mu - [\Delta\theta]] - C$$

where the square brackets indicate the inclusion of the parameters for the appropriate quadruplet configuration. For an MDIA with more than one quadruplet configuration, the corresponding bit strings are combined in a single string. This is done randomly, without sorting individual quadruplets in any way. In this way, an MDIA with a single component and a quadruplet defined by λ only is described with a string of 13 bits. For instance, the bit string

$$0011000111110$$

translates into an MDIA defined approximately by

$$\lambda = 0.095 \quad , \quad C = 1.33\,10^7$$

With this configuration, $2^{13} = 8192$ discrete values of (λ, C) are distinguished, which could all be tested by brute force as in Section 7. Extending this MDIA to two components extends the length of the bit string to 26 bits. For instance, the bit string

$$01101110110100011000111110$$

translates into an MDIA defined approximately by

$$\lambda_1 = 0.214 \quad , \quad C_1 = 4.27\,10^7$$
$$\lambda_2 = 0.095 \quad , \quad C_2 = 1.33\,10^7$$

With this configuration, $2^{13} \approx 67\,10^6$ discrete options exist, which cannot practically be assessed by brute force. For more complicated quadruplet configurations, or larger numbers of components, the number of options to be considered obviously becomes even more untenable from a brute force perspective.

After an individual MDIA can be described as a bit string, the next step in the present genetic algorithm is to define a population size M. Each member of this population is then initialized randomly. For each member the cost function ζ according to Eq. (7.2) is then evaluated. For each member of the population a 'score' is then defined as $1/\zeta$. This completes the processing of the initial population.

From the initial or subsequent generations new generations are generated, together with there scores. After experimentation with an MDIA with two components and a quadruplet defined by λ only, the following 'procreation' strategy was developed:

1) After sorting the population by the score $1/\zeta$, a fraction of the population with the best scores is transferred to the next generation without modification. This fraction is set here to 1/6.

2) Members of the present generation are allowed to become 'parent' in the new generation if their cost function ζ is less then $2\zeta_{\min}$, where $\zeta_{\min}$ is the cost of the best scoring member of the present population. At least 1/4 of the present population, but no more than 1/2 of the present population are allowed to become parents.

3) Pairs of two parent are chosen from the thus established group of parents. Pairs are selected with a probability proportional to $1/\zeta - 1/\zeta_{\max}$, where $\zeta_{\max}$ corresponds to the cost function for the allowed parent with the highest cost function.

4) For each pair of parents two offspring are generated by randomly choosing a part of the bit string for each separate component of the MDIA, using each part of each parent exactly once. Within the part of the string representing one component of the MDIA, the 'genes' are allowed to cross over 0, 1 or 2 times, with probabilities of 0.5, 0.25 and 0.25 respectively. Furthermore, each bit of each child is allowed to mutate to its opposite value with a probability of 0.1. New MDIA configurations thus generated are added to the new population unless one of the following criteria is met:

   - The quadruplet configuration does not satisfy the resonance conditions.
   - The bit string is identical to a bit string that has already been put in the new population.
   - The MDIA configuration is identical to one already included in the population. Note that this requirement differs from the previous as it includes sorting of parameters, and combination of components with identical quadruplet configurations.

Table B.2: Population sizes M and number of generations L as used in the genetic search algorithm for various quadruplet layouts and number of components N. Table displays pairs (M, L). Empty slots in table consider configurations that have not been analyzed.

N	(λ)	(λ, μ)	$(\lambda, \mu, \Delta\theta)$
1	(60,6)		
2	(180,20)		
3	(300,50)	(300,80)	(900,75)
4	(300,50)	(600,75)	(900,75)

5) For all new members of the population the cost function ζ is evaluated, and the population is sorted with respect to ζ.

Population size and number of populations to be evaluated are determined subjectively, and are gathered in Table B.2. The case of $N = 1$ for a quadruplet based on λ is trivial, and is considered for basic testing of the algorithm only. The corresponding case with $N = 2$ has been used here to experiment with the algorithm, and will furthermore be used to illustrate the behavior of the genetic algorithm.

This example MDIA has four free parameters; λ_1, C_1, λ_2 and C_2. It is therefore impossible to visualize the entire parameter space at once. Instead, the evolution of generations will be illustrated here with the evolution of (λ_1, λ_2), which are presented in Fig. B.1 for selected generations. All 180 members of each generation are presented, using color coding to identify the lowest cost functions in each generation. Note that in the bit string, a distinction is made between MDIAs where the first and second component are exchanged, but that such MDIA in a physical sense are identical. Therefore, the components in Fig. B.1 are sorted so that $\lambda_1 < \lambda_2$. Degenerated MDIAs with $\lambda_1 = \lambda_2$ and hence $N = 1$ in physical space are not shown in the figure. Such MDIAs make up a negligible part of each population, with more frequent occurrences in earlier generations.

In the first generation (Fig. B.1a), the generation more or less evenly occupies the (λ_1, λ_2) space, with no clearly preferred areas with better cost functions (see rank legend in the figure). After three to six generations (Figs. B.1b,c), members of the population with better scores start to cluster in (λ_1, λ_2) space, particularly preferring combination where either λ_1 or λ_2 is close to the optimum value for a single component MDIA (i.e., $\lambda \approx 0.21$). In generation 6, the first members with low cost functions are found near the eventual optimum solution with $\lambda_1 \approx 0.13$ and $\lambda_2 \approx 0.27$. With subsequent generations, the members of the population with the lowest cost functions cluster more and more in this part of (λ_1, λ_2) space, abandoning earlier preferred locations.

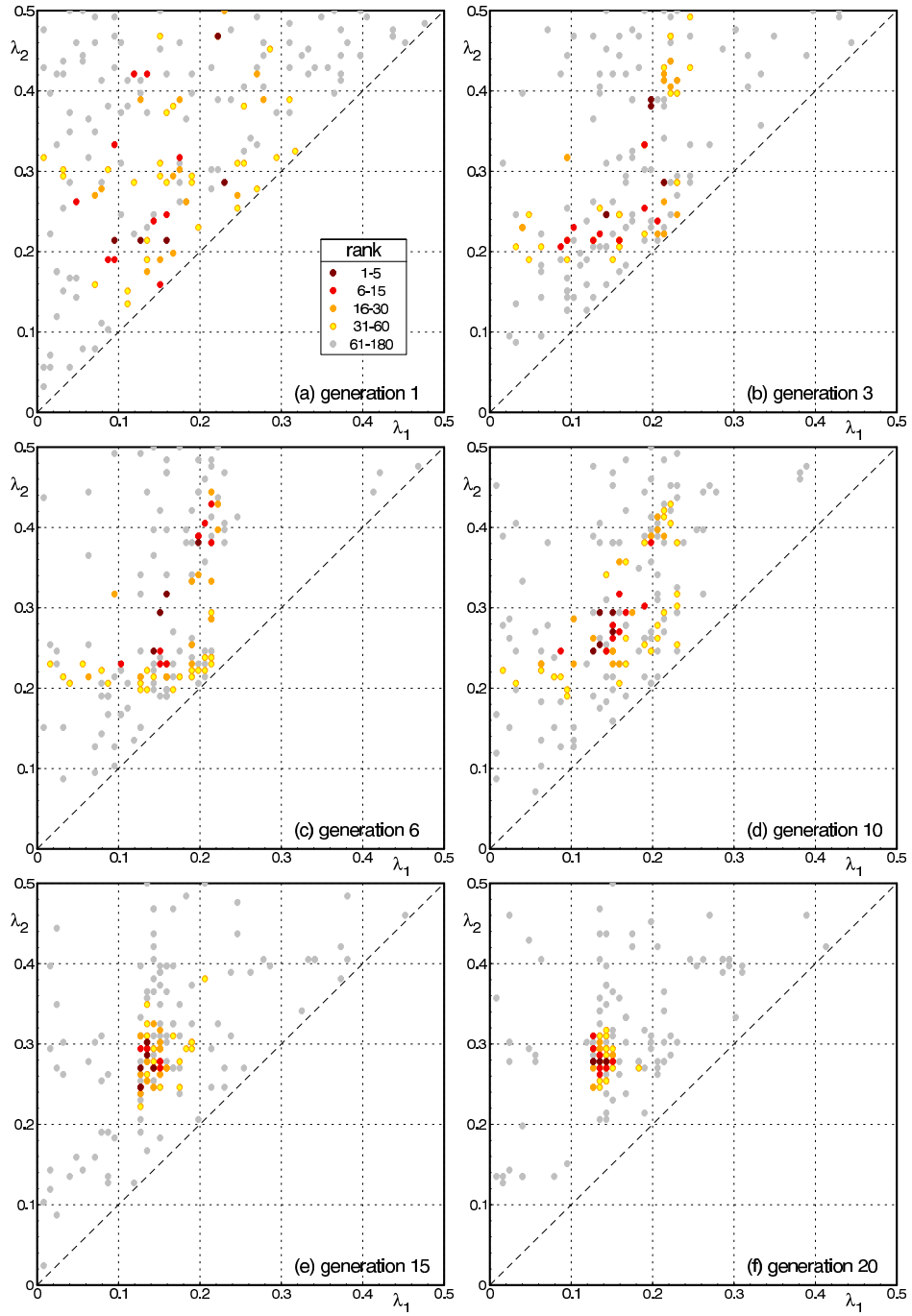

Fig. B.1 : λ_2 as a function of λ_1 for selected generations of the genetic search algorithm for an MDIA with two components ($N = 2$) and a quadruplet defined by λ only. The rank number is based on the value of the cost function ζ of each member of the population, rank number 1 being the member with the lowest cost function.

The 'final solution' of generation 20 (Fig. B.1f) is the ultimate goal of the optimization procedure, It is, however, instructive to look at previous generations in some detail. As already mentioned above, it is clear that the initial preferred configurations mimic the single component MDIA. Furthermore, around generation 10 (Fig. B.1d), good solutions also cluster around $\lambda_1 \approx 0.2$ and $\lambda_2 = 0.4$. This suggest that there might be a local minimum in the cost function for such configurations of the MDIA. Inspection of the corresponding costs functions shows that $\zeta \approx 0.22$ in this region, which is much larger than for the 'final' optimum results ($\zeta \approx 0.17$). Hence there appears to be no reason to further investigate this area in parameter space. The example nevertheless indicates that the genetic algorithm can identify multiple near-optimal solutions, and that it is prudent to follow the evolution of the generations through time to identify these. In this context it is also prudent to map the evolution of MDIA configurations as a function of the cost function ζ, and will be done in the following section.

B.4 Composite search results

The hybrid method to find the optimum parameter setting for several MDIAs consists of three steps:

1) Run a genetic search algorithm to identify promising initial estimated of parameter settings for each MDIA.

2) Use such settings as initial conditions for a descent search algorithm for the corresponding minimum in the cost function ζ, and the corresponding MDIA settings. This procedure can be repeated with different initial conditions as indicated by the results of step 1.

3) Re-establish errors and ζ with rounded values of the parameters settings to assure that the optimization is not overly sensitive to the exact parameter values.

In the main report, the main attention is focused on the final MDIA settings obtained with this method. In this appendix, some more attention will be given to the results of the genetic optimization procedure. In Table B.2, some additional information on the genetic optimization procedure has already been presented. In Table B.3 the initial conditions as used in the final descent optimization are gathered. In the remainder of this appendix, these initial conditions will be discussed in more detail. Finally, Table B.4 presents the final cost functions of the best initial condition as determined from the genetic algorithm, the final score of the descent algorithm, and the final score of the rounded parameter settings. The improvement of the first score to the second score indicates the accuracy of the genetic algorithm, which is limited by the limited number of generations considered (convergence), and the relatively poor discrete resolution used. The

Table B.3: Initial conditions used in the steepest descent MDIA optimization procedures corresponding to the results presented in Tables 7.1, 7.2 and 7.3. Columns represent 1, 2 and 3 parameter quadruplet, respectively. Initial conditions for $N = 1$ not based on genetic algorithm.

N (-)	λ (-)	C $\times 10^{-7}$	λ (-)	μ (-)	C $\times 10^{-7}$	λ (-)	μ (-)	$\Delta\theta$ (°)	C $\times 10^{-7}$
1	0.250	2.00							
2	0.127	4.27							
	0.278	1.93							
3	0.024	6.48	0.063	0.008	10.7	0.103	0.008	24	5.97
	0.127	5.49	0.175	0.040	2.48	0.230	0.262	36	11.6
	0.278	2.38	0.278	0.151	5.97	0.262	0.111	14	4.84
			0.127	0	3.93	0.095	0.008	4	4.84
			0.246	0.032	1.12	0.230	0.279	34	11.6
			0.270	0.143	5.97	0.254	0.056	19	2.59
			0.127	0.008	3.77				
			0.262	0.016	1.22				
			0.262	0.151	6.48				
4			0.127	0	5.49	0.071	0.127	81	8.68
			0.143	0.008	0.272	0.111	0.230	53	2.38
			0.254	0.008	1.51	0.135	0	1	5.72
			0.278	0.151	6.48	0.302	0.183	9	3.19

increase of the cost function from the second to the the third value provides an indication of the sensitivity of the cost function to the actual parameter settings of the MDIA.

In the optimization experiments, MDIAs with increasing complexity are considered, The experiments started with the single parameter quadruplet definition, defining the entire MDIA by λ and C. Such an MDIA with a single component ($N = 1$) is added for completeness, and to provide a baseline of performance for more complicated MDIAs. Due to the simplicity of this MDIA, and the well documented behavior of its errors in the full parameter space, only a single arbitrary initial condition has been used for the descent algorithm (see Table B.3). This explains the large drop in cost function from the initial conditions (33.4%) to the optimized values (26.0%). The effects of the round off of the optimized parameter valued are negligible (a difference of 0.003%), as would be hoped for. For all other settings, the initial settings result in errors that are relatively close to the results of the steepest descent methods, and the round off has little impact.

The MDIA based on λ and C only benefits greatly form adding a second component ($N = 2$). The genetic algorithms shows convergence to a single

Table B.4: Optimum cost functions ζ in % for optimized MDIAs with various numbers of components N and quadruplets defined by 1, 2 or three parameters. Cost functions from left to right per table entry correspond to initial conditions taken from the genetic search algorithm, the corresponding final result of descent algorithm, and cost function for MDIA after rounding off of parameters as found by the descent algorithm.

N	quadruplet definition								
	(λ)			(λ, μ)			$(\lambda, \mu, \Delta\theta)$		
1	33.4	26.0	26.0						
2	16.8	16.3	16.3						
3	16.3	16.0	16.1	12.4	11.5	11.6	12.5	10.1	10.2
				12.8	12.1	12.1	12.7	10.2	10.3
				12.8	12.2	12.3			
4	16.2	—	—	12.4	12.0	12.1	12.0	9.6	9.6

dominant minimum of the cost function ζ, as discussed in the context of Fig. B.1. Adding a third and fourth component adds little to quality of the MDIA. This is illustrated in Fig. B.2 with the values of λ for the highest ranked (lowest ζ) members of generation 50 of each experiment. Note that convergence behavior of the genetic search algorithm with the population size and number of generations as identified in Table B.2 suggest that the algorithm has come close to the optimal solution. This is tentatively confirmed by the small additional improvement as achieved by the descent algorithm (see Table B.4).

For this MDIA with 3 components (Fig. B.2a), several near-optimal solution types can be identified. The three best members of the population ($\zeta < 16.35$) combine the optimum MDIA with $N = 2$ with third component with $\lambda \approx 0.02$. Such an MDIA has a cost function that is only marginally better than the corresponding optimal MDIA with $N = 2$, both in the genetic search procedure, and in the descent method (see Table B.4, note that the second and third cost function for the MDIA differ by only 0.04%). A second near-optimal solution type identified in Fig. B.2a corresponds to the optimum two-component MDIA with the third component extremely close to either $\lambda = 0.127$ or 0.278. In essence, these can be considered as degenerated two-component solution, particularly because the score of such MDIAs are not improved compared to the scored of the corresponding three component MDIAs. A third near-optimal solution adds the third component more balanced between $\lambda = 0.127$ and 0.278. Additional steepest descent experiments starting from such initial conditions indicate that such solution also do not improve upon the first type of solution identified here, always resulting in $\zeta > 16.3$ (figures not presented here). More importantly, none of these solutions provide results that improve upon the two component MDIA.

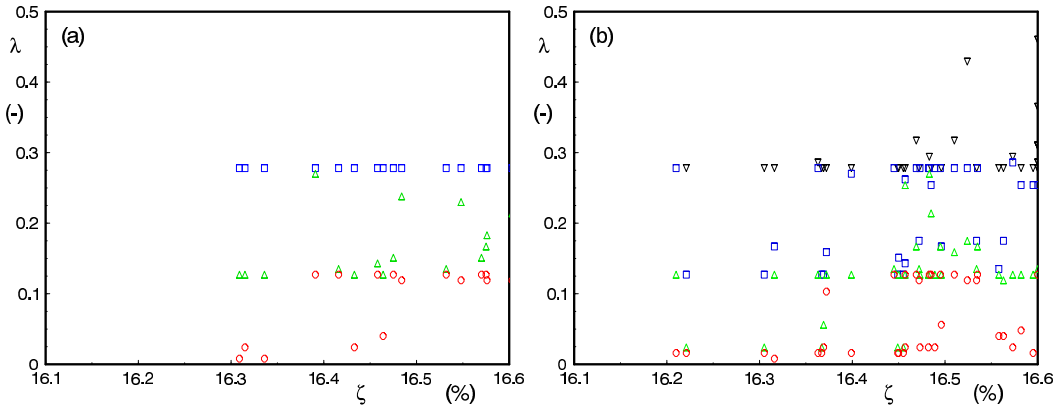

Fig. B.2 : λ as a function of ζ for the highest ranked members of generation 50 of the genetic search algorithm for an MDIA with the quadruplet defined by λ only for (a) $N = 3$ and (b) $N = 4$. Symbols and colors identify λ_1 through λ_4, as sorted by value.

The initial conditions presented in Table B.3 for this MDIA represent the first type of solution as identified in Fig. B.2a.

Adding a fourth component to this MDIA (Fig. B.2b) produces results that are very similar to those of this MDIA with $N = 3$ (Fig. B.2a); the additional component has a value of λ that generally lies close to a previously established value of λ, hence producing near-degenerated MDIAs with effectively $N = 3$ or $N = 2$. This is convincingly demonstrated by the fact that the highest ranked member of this population actually represents a truly degenerated MDIA with $N = 3$, that is, two of the components have identical λ and can therefore be combined in a single MDIA component. Because this highest scoring MDIA has a cost function ζ that is consistent with the optimal results for the corresponding MDIA with $N = 3$ (see Table B.4), it was not deemed necessary to investigate this MDIA with $N = 4$ further.

Next, the MDIA with a quadruplet defined by λ and μ will be addressed. The investigation starts with $N = 3$, as described in the main body of the report. The genetic search algorithm identifies several potentially optimal solutions that have been used as initial conditions for the steepest descent algorithm. This is illustrated in Fig. B.3 with the values of λ and μ for the highest ranking members of population number 80. The three different initial conditions are identified as A through C in the figure.

Initial conditions A in Fig. B.3 consist of three distinctly different values of λ. For the MDIA components with the lowest λ, the values of μ are generally low. For the third component, however, μ is substantial. Initial conditions B have similar general characteristics, with the second and third value of λ more similar, and with generally distinctly different from the values of initial conditions A. Initial conditions C are similar to B in character and values, with the

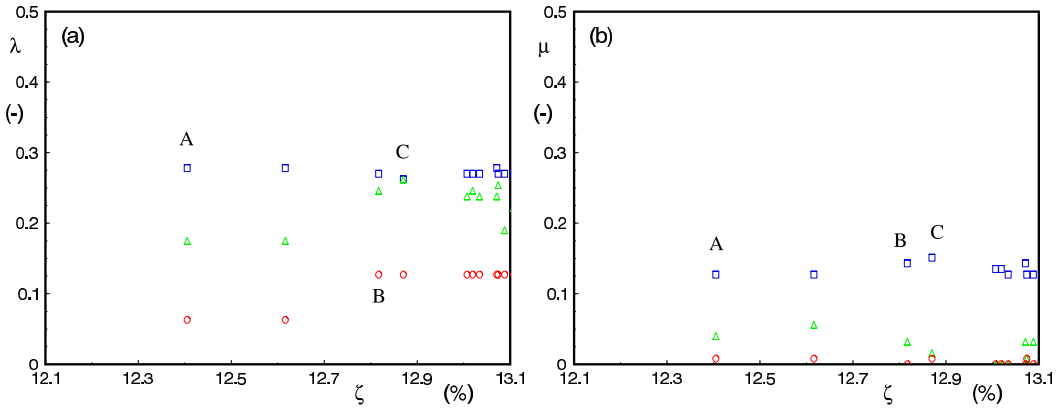

Fig. B.3 : λ (panel a) and μ (panel b) as a function of ζ for the highest ranked members of generation 80 of the genetic search algorithm for an MDIA with $N = 3$ and the quadruplet defined by λ and μ. Symbols and colors identify λ_1 through λ_3, as sorted by value.

distinction that $\lambda_2 = \lambda_3$, whereas μ_2 is small and μ_3 is substantial. Although this initial condition in many ways is similar to conditions B, it has been considered separately for the sake of completeness. The optimization results from the three initial conditions after the steepest descent method and the rounding off of the parameter settings are gathered in Table B.5.

Several interesting observations can be made from the data presented in Table B.5. First, the best initial conditions do result in the best optimized MDIA following the three step approach used here. Second, the three different initial conditions lead to different optimized MDIAs, confirming the fact that a straightforward descent algorithm is highly unlikely to find the global optimum settings for an MDIA, and that it is essential to use the genetic search algorithm to find suitable initial conditions for a descent algorithm. This is even true for the fairly similar initial conditions B and C, which converge to similar but not identical final optimized MDIAs. Third, the three optimized MDIAs do share a similar structure of the errors ϵ underlying the cost function ζ, suggesting the the distribution of errors ϵ in the cost function ζ is less sensitive to the final layout of this MDIA, than the actual cost function ζ. Considering the above, only the optimized MDIA A has been used in the body of this report.

Note that the difference of the errors in Table B.4 between the initial conditions and the final results are substantial. This might be due to insufficient convergences in the genetic algorithm. To test this, the number of generations was increased from 50 to 80 (Table B.2). However, this has no impact on the best scores used as initial conditions, which, in fact, all had been found at generation 50. This could mean two things; first, this may be due to the impact of the relatively course discretization of parameter space in the genetic algorithm. Second, it may identify a lack of diversity in the populations in the genetic algorithm.

Table B.5: Like Table 7.2 for two-parameter quadruplet (λ, μ) with $N = 3$ for initial conditions A through C. in Fig. B.3.

initial cond.	ζ (%)	λ (-)	μ (-)	C $\times 10^{-7}$	ϵ_H (%)	ϵ_{E1} (%)	ϵ_{E2} (%)	ϵ_{s1} (%)	ϵ_{s2} (%)
A	11.6	0.063	0.009	12.1	2.11	58.6	49.4	25.1	19.6
		0.184	0.028	2.40	1.09	46.3	42.2	26.3	21.8
		0.284	0.128	5.33					
B	12.1	0.127	0	3.83	2.52	64.1	54.2	24.8	18.8
		0.248	0	1.12	0.64	50.8	43.4	25.6	19.6
		0.275	0.146	5.19					
C	12.3	0.127	0.006	3.86	2.51	64.7	54.4	25.3	19.8
		0.261	0	1.22	0.64	52.0	43.7	26.0	20.0
		0.270	0.153	5.61					

The latter would require a larger population. Considering the large cost involved with the genetic algorithm, the experiment has not been rerun with a larger population, but the population size has been increased for similar experiment with larger N (see Table B.2).

The logical next step is to consider the MDIA with the (λ, μ) quadruplet definition and with $N = 4$ components. Figure B.4 presents the best performing members of population 75 for the corresponding genetic experiment. A comparison with the results presented in Fig. B.3 shows two things. First, the highest ranking members of both generations have very similar scores ζ. Second, the quadruplet layout for $N = 3$ and $N = 4$ with the lowest costs are significantly different, with the $N = 4$ solution not appearing to degenerate into a $N = 3$ solution. This suggest that there may be more accurate solutions for $N = 4$ that have not yet been found. However, with the present model setup, the genetic experiments already become prohibitively expensive. Because the present study is, furthermore, still to be considered a feasibility study, it will presently be assumed that no significant progress can be made for $N \geq 4$. This assessment will need to be reconsidered in the followup studies.

Figure B.4 shows a single best initial condition to be used. These initial conditions are presented in Table B.3, the resulting errors (ζ) of the three step optimization are presented in Table B.4. As already observed, the results are very similar to those for $N = 3$, and in fact represent a deterioration compared to the case with $N = 3$. Hence, further complications by increasing N further will not be considered at this stage.

The final step is to consider the three parameter $(\lambda, \mu, \Delta\theta)$ quadruplet, again starting with $N = 3$. The population size and number of generations (Table B.2) are now fully governed by the economics of the computations. In fact, the com-

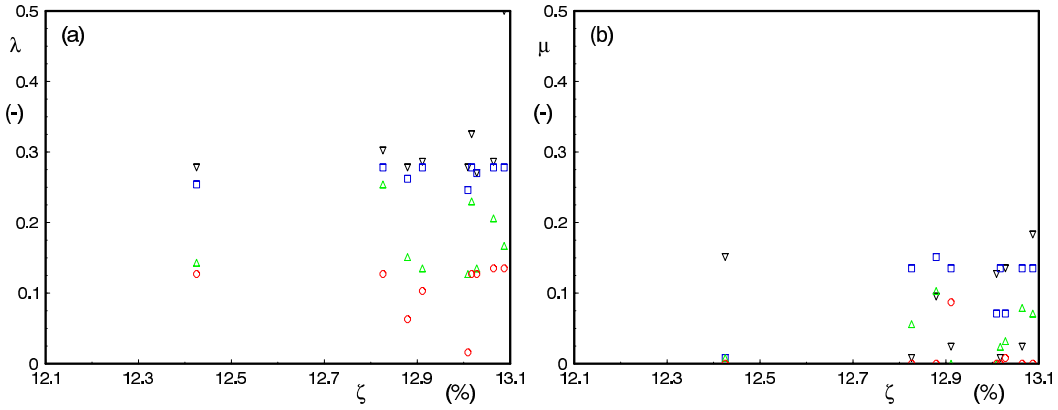

Fig. B.4 : Like Fig. B.3 for generation 75 and $N = 4$.

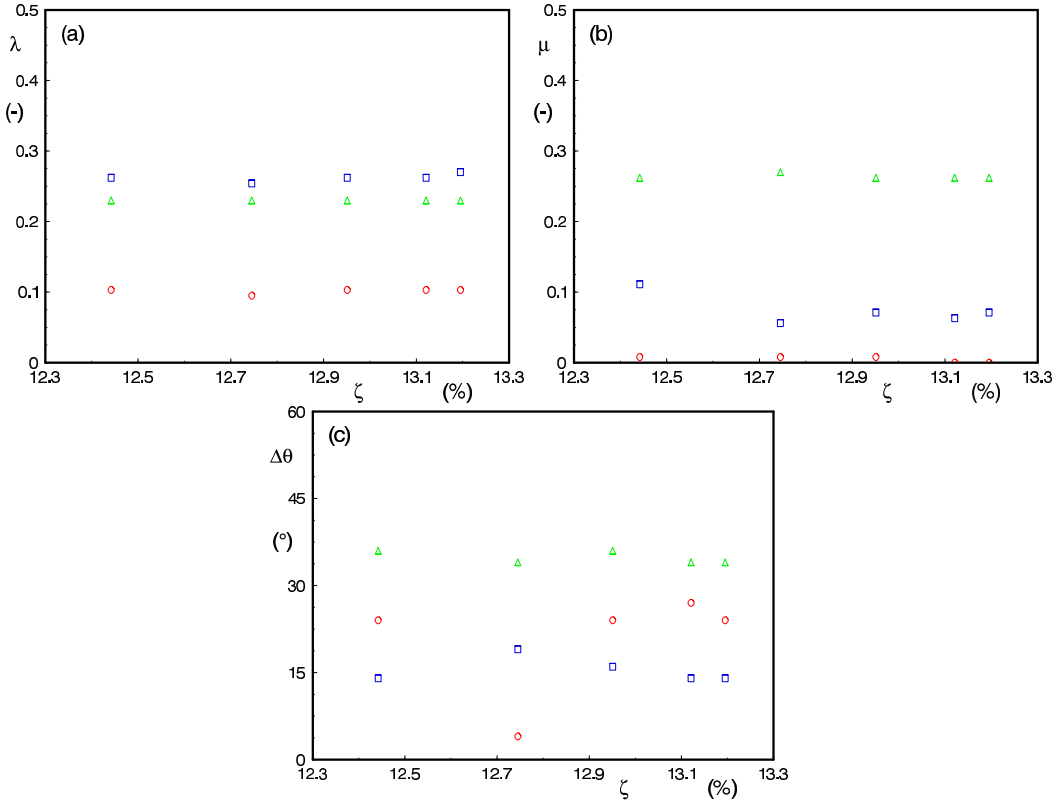

Fig. B.5 : λ (panel a), μ (panel b) and $\Delta\theta$ (panel c) as a function of ζ for the highest ranked members of generation 75 of the genetic search algorithm for an MDIA with $N = 3$ and the quadruplet defined by λ, μ and $\Delta\theta$. Symbols and colors identify λ_1 through λ_3, as sorted by value.

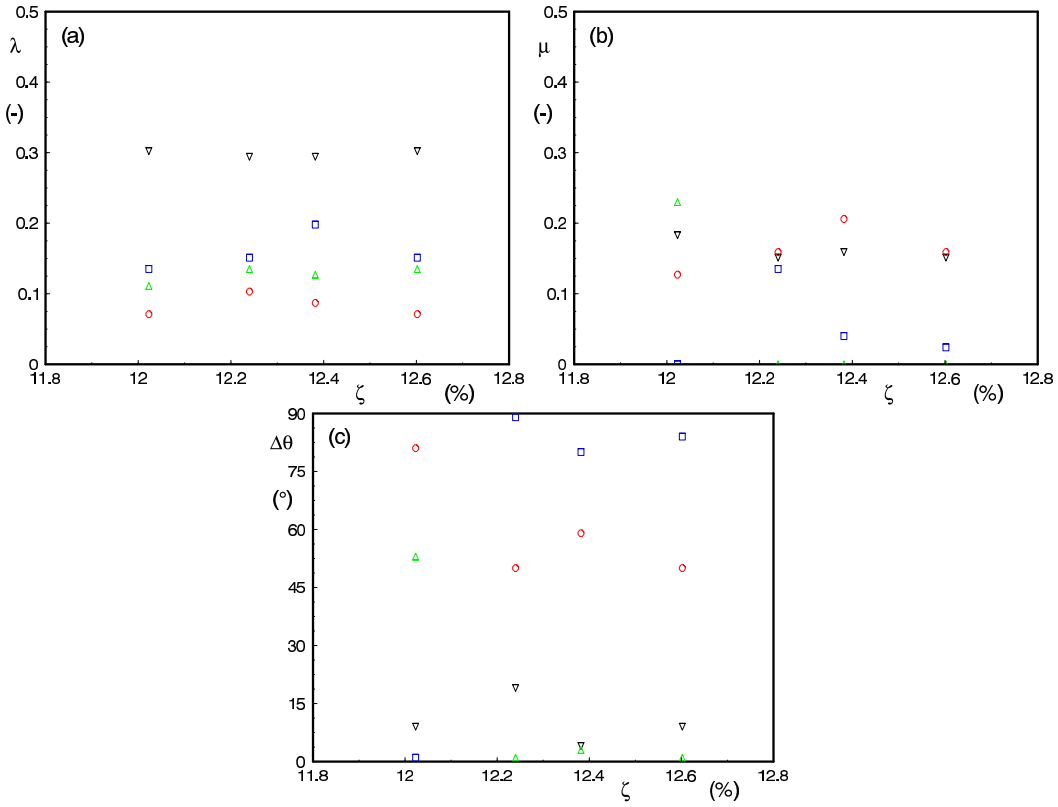

Fig. B.6 : Like Fig. B.5 for generation 75 and $N = 4$.

putations for the genetic experiments with $N = 4$ took two months two complete on a 16 processor Linux cluster, clearly pushing the limits of practical feasibility.

Figure B.5 shows λ, μ and $\Delta\theta$ of the highest scoring members of generation 75 for the corresponding MDIA with $N = 3$ components. The five highest scoring members of the population show near-identical distributions of λ, and very similar distributions of μ. The second ranked member, however, shows clearly different behavior of the angles $\Delta\theta$ when compared to the other four members displayed in this figure. Considering this, two different initial conditions have been used for the steepest descent algorithm. These two initial conditions are presented in Table. B.3 and the resulting minimum cost functions ζ in the three step optimization procedure are presented in Table B.4. The two initial conditions both lead to much more accurate DIAs after the steepest descent optimization, suggesting a limited accuracy of the genetic search. Both initial conditions furthermore lead to nearly identical cost functions ζ, although the way in which the low cost function is achieved is somewhat different ways, as discussed in the connection with Table 7.3.

Figure B.6 shows λ, μ and $\Delta\theta$ of the highest scoring members of generation 75 for the corresponding MDIA with $N = 4$ components. The four highest scoring

members of the population all show clearly different parameter settings. Only the best initial conditions have been used here. As with the case of $N = 3$, the steepest descent method greatly improves the cost function of the optimum MDIA. Furthermore, the addition of the fourth component adds additional accuracy, and the rounding off has of the parameter values has no discernible impact on the results.